

Alma Mater Studiorum – Università di Bologna

Dipartimento di Ingegneria dell'Energia Elettrica e dell'Informazione
" *Giuglielmo Marconi* " - DEI

DOTTORATO DI RICERCA IN

Ingegneria Biomedica, Elettrica e dei Sistemi (IBES)

Ciclo XXXI

Settore Concorsuale di afferenza: 09/E2

Settore Scientifico disciplinare: ING-IND/33

ENERGY MANAGEMENT SYSTEMS OF MICROGRIDS

Presentata da: *Ing. Stefano Lilla*

Coordinatore Dottorato

Prof. Daniele Vigo

Supervisore

Prof. Alberto Borghetti

Co-Supervisore

Prof. Carlo Alberto Nucci

Esame finale anno 2019

"If you think education is expensive, try ignorance"

Derek Bok

(President of Harvard University)

Acknowledgements

I would like to thank and dedicate this Thesis to my family.

A very special thanks to my supervisors, Prof. Alberto Borghetti and Prof. Carlo Alberto Nucci, who supported me in each step of my research activities.

Special thanks go also to the Power Systems group of the University of Bologna, Department of Electrical, Electronic and Information Engineering "G. Marconi": Fabio Napolitano, Fabio Tossani, Camilo Orozco Corredor, Juan Diego Rios Penaloza, Giorgia Pulazza and James Amankwah Adu.

A special acknowledgment to Prof. Dominique Gabioud and Prof. Davide Pavanello and all the group of the GridLab for their generous support and continues encouragement during the period spent at the HES-SO Valais-Wallis, University of Western Switzerland.

Abstract

Conventional distribution networks were designed to be operated as passive networks, but with the increasing penetration of renewable energy sources new opportunities and new issues have been appeared. The distributed operation of parts of the system denoted as microgrids or, more generally, as local energy communities could be an effective answer to the issues posed by the increasing complexity of the modern power distribution systems scenarios.

The research carried out during this Ph.D. project can be divided into three main parts. The first one deals with the modeling and analysis of low voltage power distribution networks feeding residential, commercial and small-scale industrial consumers including distributed generation units and storage systems. It focuses on an optimization model that has been applied to the energy management system of the experimental microgrid built at the University of Applied Sciences and Arts of Western Switzerland, HES-SO Valais-Wallis, Sion. For this purpose, a mixed integer linear programming model is developed and presented, which takes into account the unbalanced operation of the LV network and the presence of the neutral wire. The validation of the accuracy of the model through the mentioned experimental microgrid and an analysis of some simulation results for a 24 hours horizon are presented too.

The second part focuses on the day-ahead operational planning of a microgrid with the presence of several prosumers equipped with generating units, local loads and battery storage systems, which are assumed able to implement transactive energy control actions. This type of grid-connected microgrids are often referred to as local energy communities (LEC). The day-ahead optimization is important indeed for the scheduling of the batteries, since we assume that the distributed generation is mainly not dispatchable, as is the case for photovoltaic units. The problem has been addressed by means of two different optimization procedures, namely a centralized mathematical programming model and a specific distributed optimization procedure based on the adoption of the alternating direction method of multipliers (ADMM). Both approaches, centralized and distributed, provide the scheduling of the batteries in order to limit the balancing action of the external grid and allocate the power losses in the local network to the various transactions. The distributed procedure is characterized by novel aspects with respect to the approaches already presented in the

literature: the application of the ADMM for the case of a local energy community with various energy storage systems and the inclusion of the power loss of the local network without the need of a central coordinator. The results obtained for various case studies by means of the distributed approach are compared with those obtained by using the centralized model.

The third part deals with the day-ahead optimization of the operation of a local energy system consisting of photovoltaic units, energy storage systems and loads aimed at minimizing the electricity procurement cost considering the uncertainties in the load and generation forecasts. The local energy system may refer either to a small industrial site or to a residential neighborhood. Two mixed integer linear programming models are adopted, each for a different representation of the battery: a simple energy balance constraint and the Kinetic Battery Model. The chapter describes the generation of the scenarios, the construction of the scenario tree and the intraday decision-making procedure based on the solution of the multistage stochastic programming. Moreover, the daily energy procurement costs calculated by using the stochastic programming approach are compared with those calculated by using the Monte Carlo method. The comparison is repeated for two different sizes of the battery and for two load profiles.

The final chapter of the thesis is devoted to the conclusions and to the definition of some research objectives for the continuation of the activities.

Keywords: Alternating Direction Method of Multipliers (ADMM); Distributed Optimization; Energy Management; Energy Scheduling; Kinetic Battery Model; Local Energy Community; Low Voltage Network; Microgrid; Monte Carlo Method; Renewable Energy; Mixed Integer Linear Programming (MILP); Network Power Loss; Stochastic Programming.

Contents

1.	Introduction	9
1.1.	Toward Smart Grids	9
1.1.1.	Power Distribution Systems Evolution	9
1.1.2.	Micro-Grids as a key	10
1.1.3.	Local Energy Community (LEC)	12
1.1.4.	Energy Management Systems	13
1.2.	Description of the structure of the thesis	16
1.3.	Literature review.....	17
1.4.	Specific contribution of the thesis.....	19
2.	Energy management system for the real time operation of a low voltage network.....	21
2.1.	Introduction.....	21
2.2.	Description of the experimental microgrid	21
2.3.	Tuning and preliminary measurements of the experimental microgrid	23
2.4.	Description of the Optimization Model.....	24
2.5.	Model Validation.....	29
2.6.	Simulation Results	31
2.7.	Conclusions of chapter 2	35
3.	Day-ahead scheduling of a local energy community	36
3.1.	Introduction.....	36
3.2.	Problem formulation – centralized approach.....	37
3.2.1.	First stage: ideal network.....	39
3.2.2.	Second stage: network with losses	43
3.3.	Problem formulation – distributed approach.....	45
3.3.1.	First stage: ideal network.....	45
3.3.2.	Second stage: network with losses	47

3.4.	Implementation and test results.....	48
3.4.1.	Scenario 1: prosumers without batteries.....	50
3.4.2.	Scenario 2: prosumers with batteries.....	52
3.5.	Conclusions of chapter 3	55
4.	Multi-stage stochastic optimization for the operation of local energy systems.....	57
4.1.	Introduction.....	57
4.2.	Model of the local energy system	58
4.2.1.	Model with a simple representation of the battery state of charge.....	58
4.2.2.	Model with the kinetic battery model.....	60
4.3.	Multi-stage stochastic optimization procedure	62
4.3.1.	Generation of scenarios	63
4.3.2.	Construction of the scenario tree	64
4.3.3.	Intraday decision-making procedure	65
4.4.	Numerical tests.....	67
4.5.	Conclusions of chapter 4	72
5.	Conclusions.....	73
Appendix A:	Energy storage systems in distribution networks.....	75
A.1.	Introduction.....	75
A.2.	Technologies.....	77
A.3.	Applications	78
Appendix B:	GridLab	81
B.1.	Configuration	81
B.2.	Preliminary operation.....	81
B.3.	GridLab Laboratory	85
Appendix C:	Optimization Tools and Algorithms	87
C.1.	AIMMS and the mathematical programming.....	87
C.2.	Algorithms.....	88

References..... 96

Acronyms..... 101

1. Introduction

1.1. Toward Smart Grids

1.1.1. *Power Distribution Systems Evolution*

The electrical power distribution system was designed to meet the needs of users and few large producers in a slow-changing regime. The liberalization of the electricity markets in the last decade and the proliferation of prosumers, have produced a rapid evolution by introducing elements of novelty as well as many new issues for the Distribution System Operators (DSOs). Therefore, the electrical power networks are evolving to respond dynamically, efficiently and flexibly to the increased demand (also due to the rise of the use of heat pumps and electric vehicles) and to the growing penetration of renewable energies (active users have exceeded 800,000 units in Italy, mostly equipped with solar generators). It is necessary to develop new operating strategies and smart network management algorithms in order to allow and support the complete integration of distributed generation (DG) technologies. The benefits of the DG penetration growth are:

- the diversifications of energy sources;
- the reduction of greenhouse gas emissions;
- the power quality and reliability improvement;
- the increase of the flexibility of electricity market.

The new grid architecture, known by the name of Smart Grid (SG) or intelligent grid, will benefit from the progress in control theory, and information - communication technologies. Two-way flows of electricity and information will be enabled to provide enhanced energy efficiency and power delivery stability (*Wang et al., 2015*). The progress of the system must integrate several functions, e.g., monitoring, control/optimization, communication, and protection, taking into account the operational security, the technical sustainability, and costs, with the implementation of hierarchical control strategies, targeted for the various voltage levels, and modern energy management techniques. One of the SG biggest potentials is to

allow a more flexible power system management, opening new business opportunities and operational possibilities specially regarding the integration of renewable energy sources (RES) into distribution systems. The new generation of power distribution systems is designed to obtain higher efficiency of control and operation with respect to conventional ones. They will be capable to:

- safely integrate more RES and in general DGs into the network, i.e., enhancing the hosting capacity of the distribution systems;
- deliver power more efficiently and reliably through demand response and comprehensive control and monitoring capabilities;
- use automatic reconfiguration of the network to prevent outages or quickly restore (self-healing capabilities);
- enable consumers to have larger control over their electricity consumption and to actively participate in the electricity market.

1.1.2. *Micro-Grids as a key*

In this context, the development of a small power grid, constituted by users and producers connected to the same low voltage network, which perform a synergic interaction with the external grid, is expected to produce significant benefits. This kind of small power grid is known as microgrid (MG). In Figure 1-1 a general scheme of a MG is represented. On the one hand, producers and users would become more independent, can maximize self-consumption and minimize the exchange with the utility network (in order to minimize the procurement costs); on the other hand, the DSO could mitigate the effects of intermittent and fluctuating production of RES, postpone the network reinforcement and the installation of centralized storage systems, increase the system reliability and resiliency, and decrease the network losses.

More precisely, a MG can be defined as a part of an electric power distribution system that is located downstream of the distribution substation. It includes an assortment of DGs, distributed storage units and different end users, e.g., residential buildings, commercial centers, and industrial sites (*Katiraei, F. , Iravani, R., Hatziargyriou N., and Dimeas, 2008*). The electrical connection point of the microgrid to the utility system constitutes the microgrid point of common coupling (PCC).

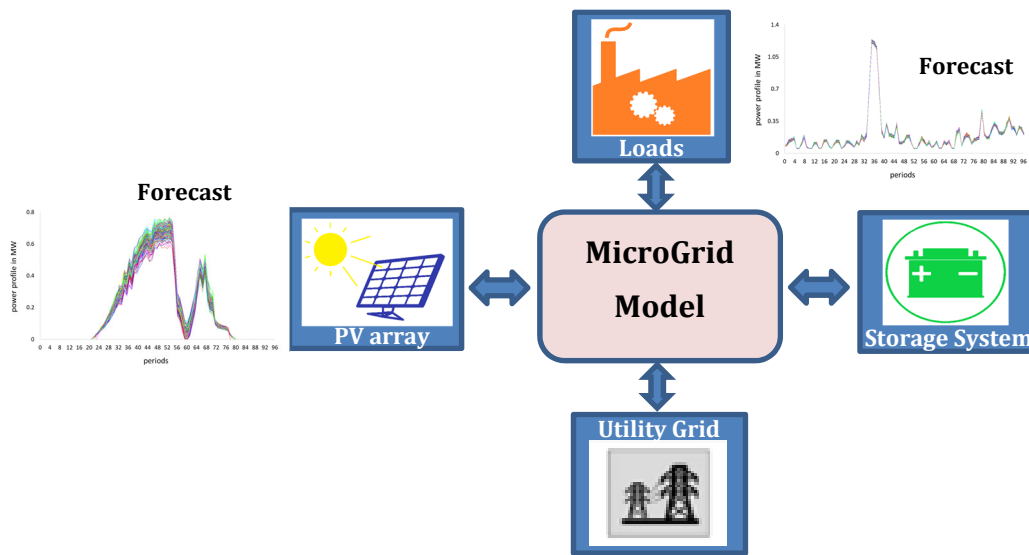


Figure 1-1. General scheme of a MG.

Some of the major benefits associated with MGs include:

- providing energy services tailored to end users' requirements;
- allowing the operations with the utility grid for the energy exchange and ancillary services;
- enabling an improved reliability through coordinated response during emergency situations to serve critical loads and to reduce outage impacts;
- deferring capital investments for grid assets;
- allowing the adoption of new energy technologies and services;
- reducing grid usage with the help of energy storage.

Recently, many initiatives have been carried out in the field of MGs, as documented in e.g., *Mengelkamp et al., 2018* and *Hossain et al., 2014*.

MGs can work in two different ways: grid connected through the PCC and off-grid in which the MG is disconnected and operates in islanded conditions. In some cases, MG does not provide PCC for connection to the main network and works stand-alone (*Ippolito et al., 2014*). This thesis focuses on grid-connected MGs.

In MGs, the adoption of Energy Storage System (ESS) is crucial. A short description of the advantages of ESSs is the following (*Wang et al., 2015*).

- Support of RES penetration: since RES production cannot always match power demand, the reliability of MGs increases if the extra power produced during off-peak times is saved for usage in peak demand.
- Reduction of peak demand and the levelling of grid load profile: the use of ESS can improve the utilization factor of the system by reducing the differences of the demand in different hours.
- Improvement of the performances of existing power system: the use of ESSs may reduce line-congestion and power loss in peak times, thus alleviating the need of grid expansion.
- Support of the electrification of urban transportation: the ESS use can provide the mean to meet the demand requirements of a large number of concurrent charging of electric vehicles (EVs).
- Increase of the overall grid resilience, also in the occasion of extreme environmental conditions and emergencies.

In the past, the commercial development of ESSs was hindered from the cost and efficiency restrictions. However, as described in Appendix A, the rapid technological improvement in recent years (especially for electrochemical storage units) has significantly improved the efficiency and the costs. Consequently, there is an exponential increase in the applications.

1.1.3. Local Energy Community

A prosumer (producer and user at the same time) operates its available units with the aim to reduce its dependence on the main grid and to minimize the energy bill. The enhancement of the self-consumption of the energy produced is becoming a very important topic and in this regard a patent has been developed by myself (*Lilla, 2015*). In this framework, a study on residential prosumers in the European Union is available in *European Commission, 2017*.

Prosumers are actively engaged in producing more energy than they would utilize in order to trade the excess to others. Prosumers can act either on their own or collectively through aggregators, as energy service companies, contractors or cooperatives. It is possible for a prosumer to optimize financial returns by directly trading with other prosumers through an energy exchange platform. Energy trading and sharing among prosumers could also improve the balance of energy supply and demand (*Jogunola et al., 2017*). Thus, the concept of Local Energy Community (LEC) systems has recently started to gain attention.

It is possible to define a LEC as the economic and operational participation and/or ownership of DGs and ESSs by citizens or members of the community. From the organization point of view, a LEC is any combination of at least two of the following elements:

- local stakeholders own the majority or all the resources;
- voting control keep on a community-based organization;
- the majority of social and economic benefits are distributed locally.

The benefits of a LEC system include increased efficiency and reduced operating costs, due to economies of scale, increased reliability, reduced emissions and a broader choice of fuels (including RES and low-grade heat) (Teotia & Bhakar, 2016). In Van Der Schoor & Scholtens, 2015 others social aspects are investigated.

1.1.4. Energy Management Systems

The design of the control and management structures of MGs is a difficult engineering task. This is due to the different types of variables to be monitored (active power, reactive power, dispatching, voltage deviations, limitation of currents, etc.), to the complexity of the optimization problem, the large number of units, and the extension of the grid. A general overview of Energy Management Systems (EMS) objective functions and optimization models is represented in Figure 1-2.

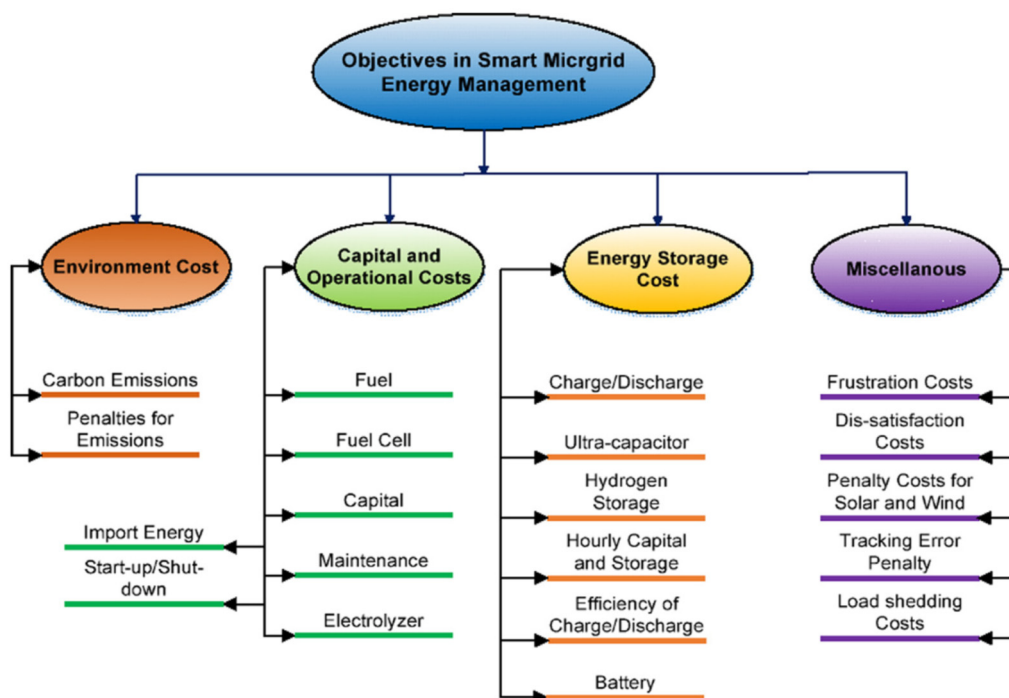


Figure 1-2. EMS objective functions. Adapted by Ahmad Khan et al., 2016

Figure 1-3 presents a general overview about MGs control with hierarchical structure (Olivares *et al.*, 2014).

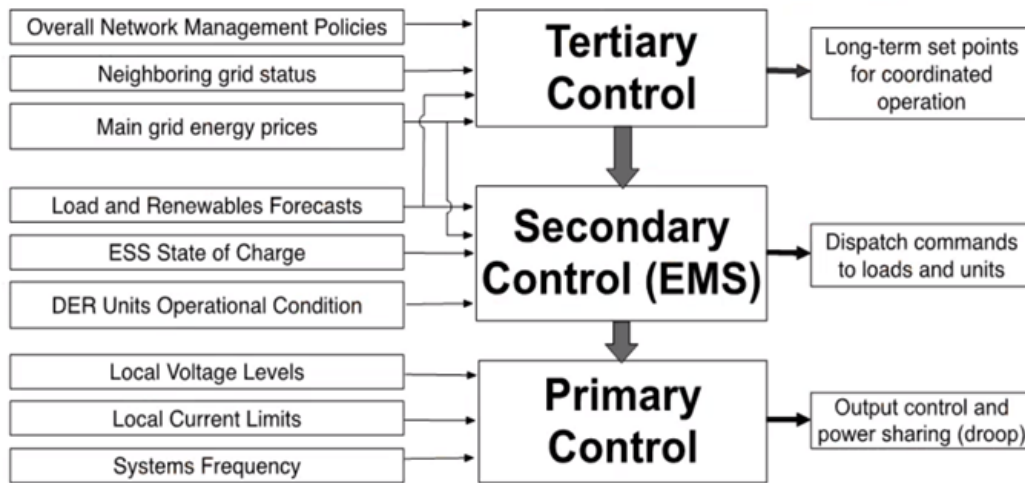


Figure 1-3. General overview MG control.

This thesis is mainly concerned with the energy management of MGs, therefore it is framed in the secondary control. Generally, loads and DG forecast, ESS state of charge (*SoC*) and DGs operational condition are the input of the system, meanwhile dispatch commands to loads and DG are the output.

The MG Energy Management System (EMS) is responsible for the reliable, secure and economical operation. The objective of the EMS consists of finding the optimal (or near optimal) Unit Commitment and the scheduling of the available DG units so that prefixed objectives are reached. In MGs, the EMS functions must be performed by an automatic system.

About the EMS architecture, two main methods can be identified:

- hierarchical centralized structure (analogous to those used in large grid);
- distributed structure (agent base control, distributed optimal power flow, etc.).

A centralized architecture (Figure 1-4) is composed of a central unit that collects the appropriate information from every DG unit, loads, and the utility grid (e.g., costs, limitations, parameters, etc.), as well as the forecast (e.g., load and solar irradiance) to determine an appropriate UC and dispatch of the resources according to the designated objectives. The central controller can make decisions using either real-time calculations of the optimal operation, or pre-defined and continuously-updated databases that contain the information

relevant to the suitable operating conditions provided by offline calculations (e.g. day-ahead scheduling) or other approaches.

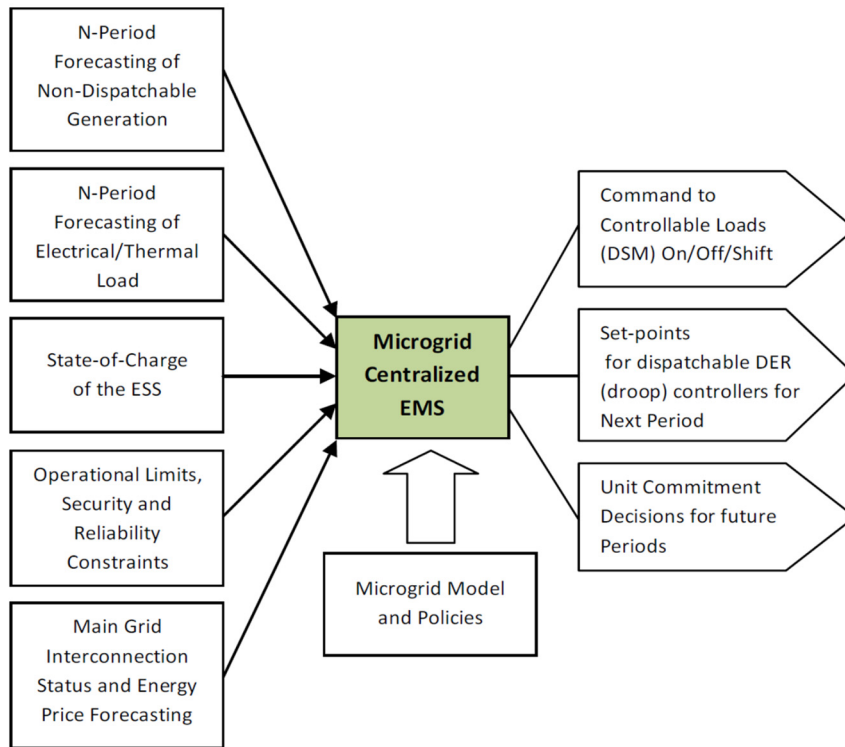


Figure 1-4. Centralized architecture of MG. Adapted by *Olivares et al., 2014*.

The centralized control method requires data collection from users by the MG control center. All the computing and control tasks are performed in the control center. Centralized control method may lead to user privacy issues and delayed operations in MGs with many prosumers. A decentralized control carries out the energy management function by a decomposition into subproblems to be solved locally by each user, to achieve utility exchange minimization, load smoothing, and privacy protection, while providing the highest possible autonomy for DG units and loads (*Olivares et al., 2014*). Distributed approach grants the following advantages:

- it solves the problem in a distributed manner with local information;
- it does not require disclosure of the user's utility function and its parameters;
- each user behaves independently in the power grid;
- each user can individually take part to the market;
- possible use of blockchain methods to trade energy (as shown in e.g., *Munsing et al., 2017*, and *Zizzo et al., 2018*).

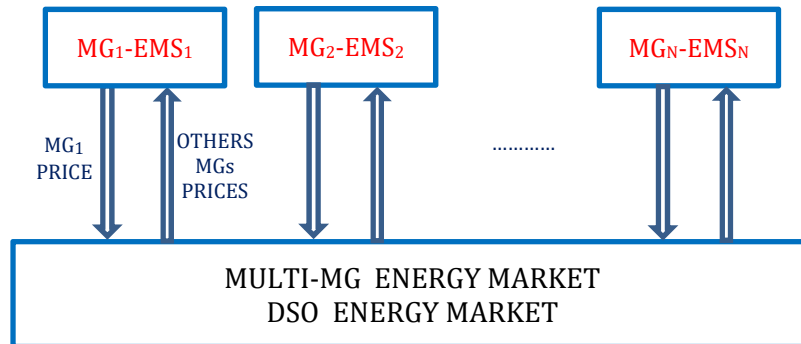


Figure 1-5. Decentralized ADMM architecture of MG.

One of the most adopted methods of decomposition is the Alternating Direction Method of Multipliers (ADMM), used in Chapter 3.

A further classification of the EMS function is based on the inclusion of the uncertainties of the generation and load forecast. We can distinguish between deterministic and stochastic approaches. The first part of the thesis presents deterministic models, which implicitly consider that the forecast is reliable. In chapter 4 the thesis presents a stochastic model to incorporate renewable source and loads uncertainties in the analysis.

1.2. Description of the structure of the thesis

Chapter one introduces the topic with the general description of the processed issues and the specific contributions.

Chapter two deals with the modeling and analysis of low voltage (LV) power distribution networks feeding residential, commercial and small-scale industrial consumers including distributed generation units and storage systems. It focuses on real-time optimization model to be included in the EMS for the experimental microgrid built at the University of Applied Sciences and Arts of Western Switzerland, HES-SO Valais-Wallis, Sion. For this purpose, a mixed integer linear programming (MILP) model is presented, which takes into account the unbalanced operation of the LV network and the presence of the neutral wire. The validation of the accuracy of the model through the mentioned experimental microgrid and an analysis of some simulation results for a 24 hours horizon are presented too.

Chapter three is focused on the day-ahead operational planning of a microgrid with the presence of several prosumers equipped with generating units, local load and battery storage systems able to implement transactive energy control actions. This type of grid-connected microgrids are often referred to as LEC. In these communities, the day-ahead optimization is very important for the scheduling of the use of the batteries, particularly when the distributed generation (DG) is mainly not dispatchable, as in the case of small-size PV units. The problem has been addressed with both the solution of a centralized mathematical programming model and with the design of a specific distributed optimization procedure based on the adoption of the ADMM.

Chapter four deals with the day-ahead optimization of the operation of a local energy system consisting of PV units, ESSs and loads aimed at minimizing the electricity procurement cost. The local energy system may refer either to a small industrial site or to a residential neighborhood. Two MILP models are adopted, each for a different representation of the battery: a simple energy balance constraint and the Kinetic Battery Model. The chapter describes the generation of the scenarios, the construction of the scenario tree and the intraday decision-making procedure based on the solution of the multistage stochastic programming. Moreover, the daily energy procurement costs calculated by using the stochastic programming approach are compared with those calculated by using the Monte Carlo method. The comparison is repeated for two different sizes of the battery and for two load profiles.

Chapter five concludes the thesis and summarizes the main results.

1.3. Literature review

In the following, we provide a review of previous contributions relevant to each chapter of the thesis.

As mentioned, Chapter 2 deals with the real time management of the experimental platform developed at the University of Western Switzerland. The optimization model of a low voltage (LV) distribution network to be included in the energy management system is conceived to improve the use of energy resources for the minimization of the power exchange with the external utility network and voltage control. With respect to other solution approaches, the

use of a MILP model in the case of LV networks, has been used e.g., in *Zhu et al.*, 1998 for load balancing, in *Bahramirad & Daneshi*, 2012 for planning purposes, in *Liu et al.*, 2013 for the definition of electric vehicles charging strategy. In *Parisio et al.*, 2014 a model predictive control (MPC) approach based on a MILP optimization is applied to the operation of a system with storage units. Quadratic programming models are proposed in e.g. *Ratnam et al.*, 2015a, *Ratnam et al.*, 2015b for the coordination of ESS with PV generators in order to minimize the impact of the residential system on the grid, by reducing the network peak demand and non-compliant voltage deviations. Other approaches have been also investigated in the literature (see e.g., *Schweickardt et al.*, 2016 and *Bennett et al.*, 2015 and the references therein).

The MILP model presented in chapter 2 takes into account the unbalanced operation of the LV network and the presence of the neutral wire to reduce the degree of unbalance, as dealt with in e.g., *Caldon et al.*, 2014 in order to exploit the capability of inverter-interfaced units to reduce the degree of unbalance.

Chapter 3 analyzes the implementation of an EMS function for the optimal use of the available resources in a local energy community (LEC). There are several studies regarding real implementation of the LEC concept, e.g. the Brooklyn microgrid project (*Mengelkamp et al.*, 2018). As mentioned, chapter 3 focuses on the centralized optimization approach based on a MILP model and on the distributed one based on the ADMM. ADMM is one of the most frequently adopted consensus algorithms (*Boyd et al.*, 2011) and it has been recently investigated for the solution of scheduling problems in microgrids (e.g., *Zheng et al.*, 2018, *Liu et al.*, 2018, and references therein). In particular, both *Zheng et al.*, 2018 and *Liu et al.*, 2018 deals with similar multi-microgrid systems as the one considered in this work, with the presence of local generation and battery energy storage (BES) systems and the possibility to exchange energy with an external utility grid. Moreover, *Liu et al.*, 2018 addresses the uncertainty of renewable energy, load consumption, and energy prices through a robust optimization approach. In *Ma et al.*, 2018 the uncertainty is addressed by using regret minimization. In *Zhao et al.*, 2018b the use of a primal Benders decomposition approach instead of Lagrangian-based dual decomposition, such as the ADMM, has been presented.

Other approaches adopt hierarchical architectures with a central controller that coordinates the power exchange among microgrids and the trading with the utility grid, as described in, e.g., *Zhao et al.*, 2018a and references therein.

In chapter 4, the considered MG includes a PV unit capable to provide a significant part of the local energy consumption and it is also equipped with an energy storage unit to fully exploit the available renewable energy source even for the case of a limited capability of the external utility network which the system is connected to. This scenario is realistic in many actual situations, as shown in *Graditi et al., 2016, van Leeuwen et al., 2017* and references therein.

In chapter 4, we focus on the solution of the day-ahead scheduling, which is in general associated with a real time control of the integrated PV-ESS, as dealt with in e.g., *Conte et al., 2017* and *Lilla et al., 2017*.

Since the forecasts of both PV production and load consumption are affected by significant uncertainties, either stochastic optimization approaches or Monte Carlo simulations are typically adopted to solve this kind of problems (e.g., *Reddy et al., 2017; Lazaroiu et al., 2016; Yuan et al., 2011*). In chapter 4 both approaches are used and compared.

Moreover, two different ESS models are compared: a simple energy balance and the kinetic battery model (KiBaM) as indicated in *Manwell & McGowan, 1993; Daniil et al., 2015; Bordin et al., 2017* (also adopted in the Homer Energy software) for the representation of the battery state of charge. Other detailed models have been proposed in e.g. *Sakti et al., 2017*.

1.4. Specific contribution of the thesis

With regard to the EMS for the real time operation, a MILP model of a low voltage network, specifically developed for the Energy Management Systems of the experimental network, has been implemented as described in Chapter 2. It is able to control active and reactive power of the dispatchable resource (DG and BSS) and takes into account the unbalanced operation of the LV network. The work also includes the implementation of the optimization algorithm in the supervisory control and data acquisition (SCADA) architecture of the experimental system and the execution of the tests.

For day-ahead scheduling of a LEC presented in Chapter 3, with centralized and distributed (ADMM-based) approaches, the specific contributions are:

- the proposed method allocates the losses in the local network to each energy transaction;
- the ADMM approach provides results close to those obtained by using a MILP centralized approach that includes the same constraints and the power loss allocation;

- the structure of the proposed scheduling functions is consistent with the billing procedure and the metering units installed in the LEC.

As presented in Chapter 4, multistage stochastic programming (SP) based on *k*-means clustering method for the day-ahead and intraday scheduling in local energy systems provides improved results with respect to the application of the Monte Carlo method. The SP approach is also applicable to models that include a detailed representation of the battery under the assumption that the MILP characteristics of the model are preserved.

2. Energy management system for the real time operation of a low voltage network

2.1. Introduction

The chapter deals with an optimization model of a LV distribution network to be included in the EMS of the GridLab district experimental platform¹ developed at the HES-SO Valais-Wallis in Sion, Switzerland. The optimization model is conceived to improve the use of energy resources for both the minimization of the power exchange with the external utility network and voltage control.

With respect to other solution approaches, the use of a MILP model can benefit from the existence of very efficient solvers (such as those available in Cplex and Gurobi), which allow for the solution of problems of considerable size with limited computation time.

The MILP model presented in this chapter takes into account the unbalanced operation of the LV network and the presence of the neutral wire.

2.2. Description of the experimental microgrid

Within the features installed in the GridLab laboratory at the HES-SO Valais-Wallis in Sion, the so-called GridLab District is a 400-V modular platform which allows developing and assessing intelligent solutions in order to operate more efficiently a distribution network in presence of prosumers, i.e., sites that can both absorb or inject active and reactive power in the LV network, through local generation and storage systems. The GridLab district reproduces a simplified residential distribution network composed of four LV feeders as shown in Figure 2-1.

¹ The GridLab of the HES-SO Valais-Wallis is the Swiss member of DERlab (www.der-lab.net), the European network of laboratories dedicated to the study of integration of renewables into grid.

The behavior of each prosumer (12 in total) is reproduced by means of 15-kVA three-phase AC bidirectional static converters (ABB ACS800-11 series) with power outputs that can be monitored and changed in real time via an Ethernet link.

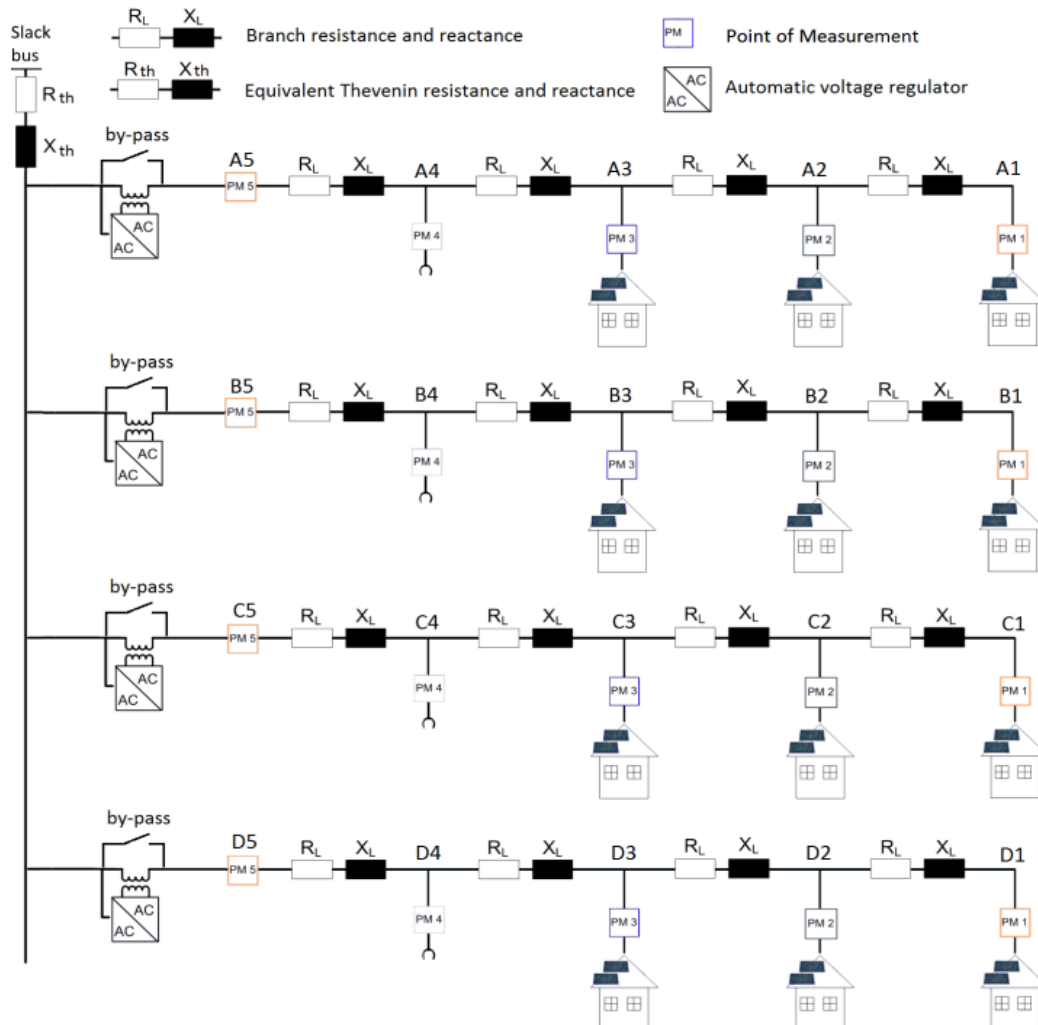


Figure 2-1. Schematic view of the GridLab District.

Of the four feeders, feeder B reproduces a buried line (UG) whereas feeders A, C and D reproduce overhead distribution lines (OH). As shown in Figure 2-1, a feeder is composed by four 95 mm^2 500 m-long line models each represented by a pair R_L - X_L realized by resistors and inductors with $R_L = 150 \text{ m}\Omega$ and $X_L = 141.4 \text{ m}\Omega$ for feeders A, C, D and $X_L = 40.2 \text{ m}\Omega$ for feeder B.

In addition, each feeder includes a series power electronic AVR (Automatic Voltage Regulator), developed at the HES-SO Valais-Wallis in Sion, which are all assumed by-passed in this work.

In order to allow equipment testing, or to compare the effectiveness of different technical solutions, each feeder can host an external connection in correspondence of the measurement points PM4 shown in Figure 2-1.

The modular concept of the GridLab District allows validating numerous optimization strategies by acting on the reactive power of each prosumer, by defining the share of local storage, or by acting on each feeder with the corresponding AVR. The general architecture of the GridLab for Supervisory Control and Data Acquisition (SCADA) system is shown in Figure 2-2.

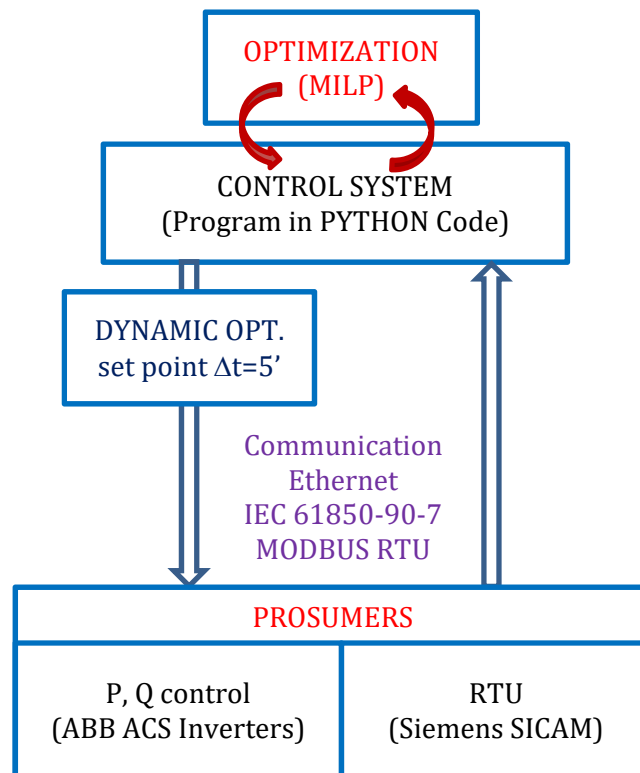


Figure 2-2. GridLab SCADA: general block diagram.

2.3. Tuning and preliminary measurements of the experimental microgrid

The GridLab is only a small part of the LV network of the school. A Thévenin equivalent is introduced in the model. The equivalent impedance (R_{th}, X_{th}) has been derived from the following equations:

$$R_{th}I^{re} - X_{th}I^{im} - V_{th} \cos \delta + V_L = 0 \quad (2.1)$$

$$R_{th}I^{im} + X_{th}I^{re} - V_{th} \sin \delta = 0 \quad (2.2)$$

where V_{th} is the no-load voltage, V_L is the voltage in last accessible bus (e.g. A5 for feeder A) and δ is the angle between V_{th} and V_L . R_{th} and X_{th} are inferred by the least-square optimization for a system of equations (2.1) and (2.2) for different measurement tests.

Preliminary validation of the optimization model has been carried out using a single feeder of the GridLab. Difference between calculated end measured values of V (at the buses) and I (injected/withdrawn by prosumers) results in reasonably good agreement with particular reference to the voltage values. More details are reported in Appendix B.

2.4. Description of the Optimization Model

The MILP model of the LV voltage network is based on the models presented in *Borghetti, 2012, 2013* and *Borghetti et al., 2015* for the case of medium voltage (MV) feeders.

The voltages of each node and the currents of each branch are represented by the Cartesian coordinates of their phasors: (V^{re}, V^{im}) and (I^{re}, I^{im}) , respectively. All the equations are written in per unit (p.u.). Let $N = \{1, 2, \dots, n_{end}\}$ the set of buses of the network, the Cartesian coordinates of the voltages between the bus k and the bus j , for each phase (phase a), are:

$$V_k^{re} - V_j^{re} = R_{k,j}I_{k,j}^{re} - X_{k,j}I_{k,j}^{im} \quad \forall k, j \in N \quad (2.3)$$

$$V_k^{im} - V_j^{im} = X_{k,j}I_{k,j}^{re} - R_{k,j}I_{k,j}^{im} \quad \forall k, j \in N \quad (2.4)$$

and the Cartesian coordinates of the current in the bus k are:

$$\sum_{j \in N} I_{k,j}^{re} - \sum_{j \in N} I_{j,k}^{re} = I_k^{re} \quad \forall k, j \in N \quad (2.5)$$

$$\sum_{j \in N} I_{k,j}^{im} - \sum_{j \in N} I_{j,k}^{im} = I_k^{im} \quad \forall k, j \in N \quad (2.6)$$

The corresponding relations for the phases b and c include the $2/3\pi$ phase shift.

The model aims at minimizing the production costs associate with DGs and storage units, the power exchange with the external network and the voltage deviations with respect to the

rated values in a time horizon T (24 periods, Δt of one hour in the simulations shown in this chapter).

Two different thresholds below and above the rated voltage value V_n are introduced in the objective function with different penalty coefficients, namely

- first range threshold: $V^{max1} = 1.03 V_n$ and $V^{min1} = 0.97 V_n$ (Std. D-A-CH-CZ working group, 2007);
- second range threshold: $V^{max2} = 1.1 V_n$ and $V^{min2} = 0.85 V_n$ (Std. EN 50438:2013/IS1, 2015).

The objective function is:

$$OF = \sum_t C_{DG,B}^P + \sum_t C_{DG,B}^Q + \sum_t (p^{imp} E^{imp} - p^{exp} E^{exp}) + \sum_{t,k} p_V^{max1} \Delta V_k^{up,1} + \sum_{t,k} p_V^{min1} \Delta V_k^{down,1} + \sum_{t,k} p_V^{max2} \Delta V_k^{up,2} + \sum_{t,k} p_V^{min2} \Delta V_k^{down,2} \quad (2.7)$$

where:

- $C_{DG,B}^P$ and $C_{DG,B}^Q$ are the global cost associated with active and reactive energy production by dispatchable DG units and charging/discharging operation of storage systems (€);
- p^{imp} and p^{exp} are the prices (€/kWh) relevant to the active energy imported and exported;
- E^{imp} , E^{exp} , are the active energies absorbed and injected into the grid (kWh);
- p_V^{max1} , p_V^{max2} and p_V^{min1} , p_V^{min2} are the penalty coefficients (€/V) for maximum and minimum voltage violation (first and second limit);
- ΔV_k^{up1} , ΔV_k^{up2} and ΔV_k^{down1} , ΔV_k^{down2} are the nonnegative values of the violations (first and second limit) of the voltage RMS value at bus k with respect to V^{max1} , V^{max2} and V^{min1} , V^{min2} .

Both real and imaginary parts of the bus k voltages are represented as the sum of the corresponding p.u. values at the slack bus (V_0^{re} , V_0^{im}) and their respective deviations

$$V_k^{re} = V_0^{re} + \Delta V_k^{re} \quad \text{and} \quad V_k^{im} = V_0^{im} + \Delta V_k^{im} \quad (2.8)$$

As mentioned in the Introduction, the model takes into consideration the presence of the neutral conductor, grounded at the secondary side of the MV/LV transformer. A three-phase symmetrical system of voltages characterizes the slack bus, which represents the connection

to the external grid. The voltage phasor of phase a at the slack bus is assumed to lay on the real axis. The model includes the linear constraints of voltage drops in all the phase conductors and the neutral, as well as the current balances in all the network nodes.

The model allows handling both active and reactive power injection of dispatchable units as optimization variables. For the active and reactive power outputs (P and Q) of the dispatchable resources, the MILP model includes the following constraints:

- P and Q capability curves of DG units are assumed rectangular;
- for PV units, only Q is assumed to be dispatchable;
- the on-off state of DGs, associated with binary variables, is an optimization variable of the model;
- a limited number of on-off operations is allowed.

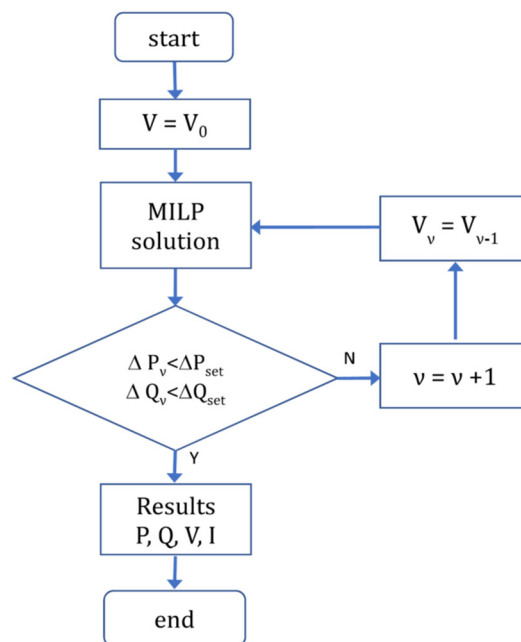


Figure 2-3. Iterative procedure to calculate the dispatchable variables P and Q .

In the dispatchable constraints units, the non-linear relationships between powers, voltages and currents are iteratively approximated by using the voltage values obtained in the previous iteration. The first calculation is performed by assuming the rated value (Figure 2-3).

In order to improve convergence, starting from the second iteration, the OF includes two additional terms that prevents the change of the power set points of the DGs, if a significant improvement of the OF is not expected:

$$\begin{aligned}\Delta P_\nu &= k_\nu \sum_{k,t} |P_{k,t,\nu} - P_{k,t,\nu-1}| \\ \Delta Q_\nu &= k_\nu \sum_{k,t} |Q_{k,t,\nu} - Q_{k,t,\nu-1}|\end{aligned}\quad (2.9)$$

where ΔP_ν and ΔQ_ν are the differences between the active and reactive power set points of dispatchable DGs at the ν -th iteration with respect to the previous one and k_ν is a coefficient progressively increased at each iteration. The procedure (Figure 2-3) ends when all the powers changes fall below a defined threshold (typically few watts or vars).

The calculation of the state of charge of the storage units takes into account a simplified linear representation of batteries and converters losses. Active and reactive powers P_b and Q_b provided by the batteries at the AC side are dispatchable variables and are constrained by the relevant rectangular capabilities.

The model of the batteries is represented by

$$E_{max} SoC_t = \begin{cases} E_{max} SoC_0 - (P_b + L_b^{imp} + L_b^{exp}) \Delta t & \forall b, t = 1 \\ (1 - \delta) E_{max} SoC_{t-1} - (P_b + L_b^{imp} + L_b^{exp}) \Delta t & \forall b, t > 1 \end{cases} \quad (2.10)$$

where E_{max} is the battery storage capacity (kWh), SoC_t is the state of charge at the period t (in p.u.), SoC_0 is the initial state of charge (in p.u.), and δ is the self-discharging rate (in p.u.).

L_b^{imp} and L_b^{exp} are variables that account for the battery's losses, during charges and discharges, respectively,

$$\begin{aligned}L_b^{imp} &= (1 - \eta_c) P_b^- \\ L_b^{exp} &= \frac{1 - \eta_d}{\eta_d} P_b^+ \quad \forall b, t\end{aligned}\quad (2.11)$$

where η_c and η_d are the batteries efficiency factor (p.u.) for charges and discharges, P_b^- and P_b^+ are nonnegative variables that represent the active power during charges and discharges, respectively. The use of both P_b^- and P_b^+ is introduced in order to avoid binary variables *Dabbagh et al., 2016*, hence: $P_b = P_b^+ - P_b^-$.

Further constraints are introduced for representing the behavior of the batteries: initial and final *SoC* values are defined and power outputs are limited by the rated values.

The representation of the non-dispatchable loads and generators is adapted from *Borghetti et al., 2015*. The constant power behavior is approximated by using a linear model (for phase a)

$$I_k^{re} = \frac{P_k^0}{V_0^{re}} - \frac{P_k^0}{V_0^2} \Delta V_k^{re} - \frac{Q_k^0}{V_0^2} \Delta V_k^{im} \quad (2.12)$$

$$I_k^{im} = -\frac{Q_k^0}{V_0^{re}} + \frac{P_k^0}{V_0^2} \Delta V_k^{im} + \frac{Q_k^0}{V_0^2} \Delta V_k^{re} \quad (2.13)$$

where I_k^{re} and I_k^{im} are the current Cartesian coordinates at each bus k and for each phase, P_k^0 and Q_k^0 are the active and reactive power consumed/generated at rated voltage V_0 . In *Borghetti et al., 2015* the linear approximated representations relevant to constant current and constant impedance behavior are also reported.

The minimum and maximum branch current constraints are defined by using the method described in e.g. *Borghetti, 2013* that makes use of polygons for representing the feasible regions for voltages and currents.

A regular polygon with \bar{z}_l sides is adopted for the linear representation of the maximum current limit in branch b (Figure 2-4-a). Each of the vertices of the polygon has coordinates

$$I_b^{re} \cos[(i-1/2)\alpha], \quad I_b^{im} \sin[(i-1/2)\alpha] \quad (2.14)$$

with $i = 1, 2, \dots, \bar{z}_l$ and $\alpha = 2\pi/\bar{z}_l$.

As the polygon should be inscribed in the circle with equation $I_b^{re^2} + I_b^{im^2} = I_b^{\max^2}$ then the radius of the circle inscribed in the polygon is equal to $I_b^{\max} \cos(\alpha/2)$. The set of linear constraints that represent the polygon are given by the equations of lines tangent to the inscribed circle. The model enforces the phasor coordinates to be inside all the linear constraints, i.e.

$$\cos(i\alpha)I_b^{re} + \sin(i\alpha)I_b^{im} \leq I_b^{\max} \cos(\alpha/2) \quad \forall i = 1, 2, \dots, \bar{z}_l \quad (2.15)$$

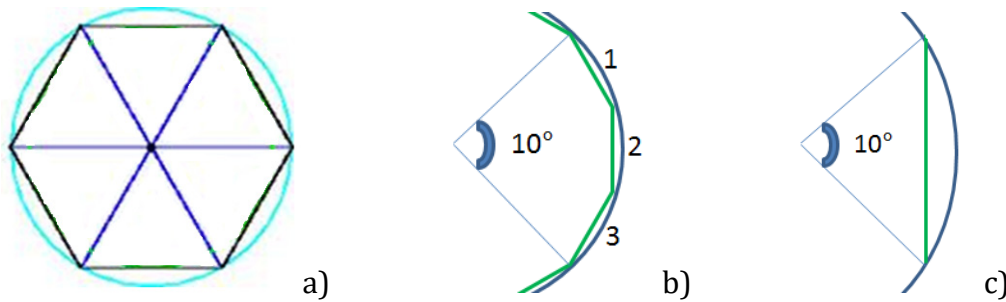


Figure 2-4. a) Minimum and maximum branch current constraints approach – b, Maximum voltage constraints and c) minimum voltage constraints approaches.

A similar model is adopted for violations ΔV_k^{up} of the voltage RMS value at bus k with respect to V^{max} (Figure 2-4-b). Assuming that the maximum voltage phase difference between a bus and the slack bus is lower than $\pi/18$ (i.e. 10 degrees), angle α is now defined as $\alpha = \pi/9(z_V - 1)$, being z_V the odd number of sides of the polygon considered in the model. The set of constraints that define ΔV_k^{up} for phase a is

$$\cos\left[\left(i - \frac{\bar{z}_V - 1}{2}\right)\alpha\right]V_k^{re} + \sin\left[\left(i - \frac{\bar{z}_V - 1}{2}\right)\alpha\right]V_k^{im} - \Delta V_k^{up} \leq V^{max} \cos(\alpha/2) \quad \forall i = 1, 2, \dots, \bar{z}_V \quad (2.16)$$

For the case of ΔV_k^{down} , as shown in *Borghetti, 2013*, the constraint would require the introduction of additional binary values. In this treatment we have simplified the constraint (Figure 2-4-c) and we impose for phase a that

$$V_k^{re} + \Delta V_k^{down} \geq V^{min} \quad (2.17)$$

The corresponding constraints for the other two phases (b and c) include the $2/3\pi$ phase shift.

The model has been implemented in AIMMS (Advanced Interactive Multidimensional Modelling System) optimization environment and the CPLEX solver has been used.

2.5. Model Validation

The validation of the model has been carried out reproducing different scenarios in the full configuration of the GridLab District illustrated in Figure 2-1, with the AVRs by-passed.

The results obtained by the MILP algorithm in terms of P , Q profiles of the dispatchable resources are sent to the prosumers of the GridLab District. Each prosumer is able to exchange active and reactive power with the feeder in a programmable way. Several 24-h scenarios have been reproduced on an accelerated time scale in the GridLab. The monitoring system performs the measurements of powers, voltages, and currents at the connection point of each prosumer.

As an example, the comparison between measured and calculated values for the active and reactive power outputs of prosumer 1 connected to feeder B are shown in Figure 2-5 and Figure 2-6, whilst in Figure 2-7 shows the comparison of the voltage behavior measured and calculated at bus A3.

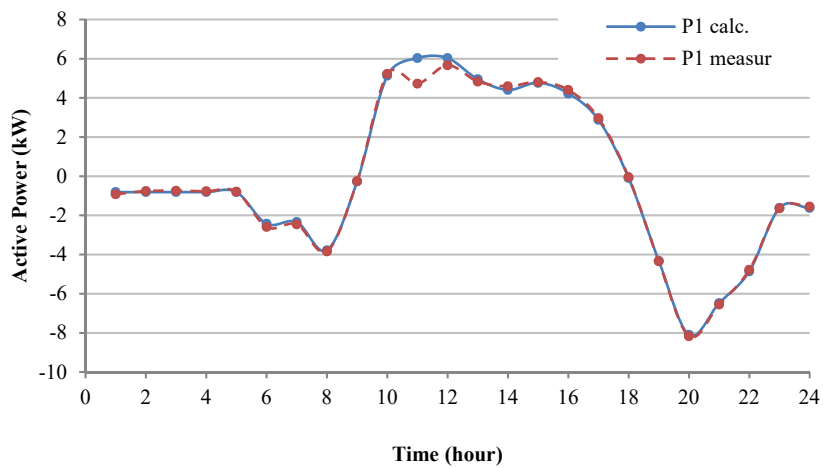


Figure 2-5. Comparison between measured and calculated values of the active power output of prosumer B1.

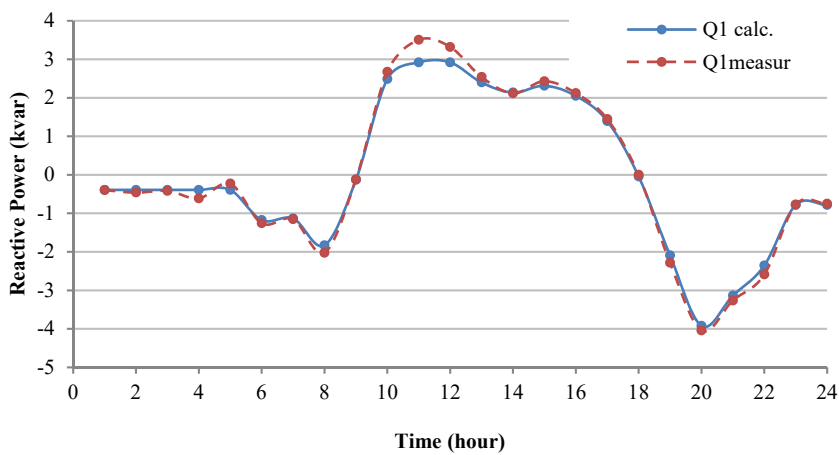


Figure 2-6. Comparison between measured and calculated values of the reactive power output of prosumer B1.

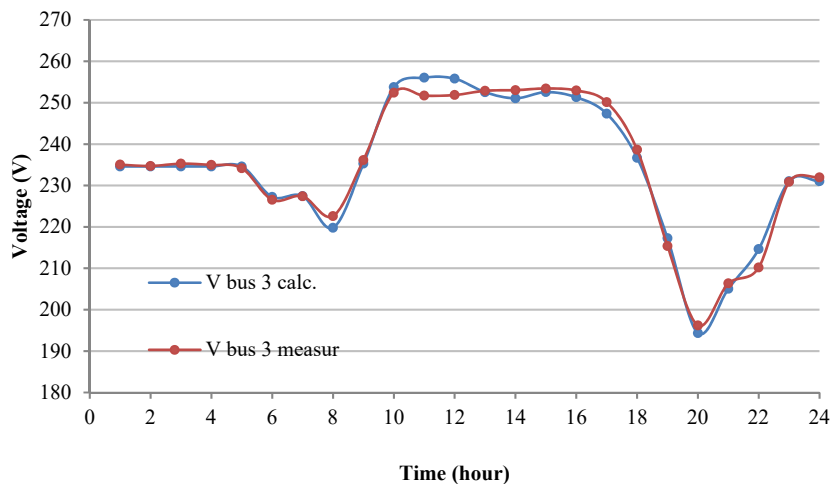


Figure 2-7. Comparison between measured and calculated values of the voltage at bus A3.

In Table 2-1, the deviations between measured and calculated data for the two considered tests are reported. The table shows the mean values for the 24 periods. In each of the four

feeders the configuration is characterized by the presence of the following units: a 10 kVA non-dispatchable generator, two dispatchable 12 kVA generators, three 9 kVA loads. The same configuration is assumed in the second test that includes also a three-phase battery connected to feeder A, prosumer 3.

TABLE 2-1 – DEVIATIONS BETWEEN MEASURED AND CALCULATED VALUES

Buses	Configuration 1			Configuration 2		
	P %	Q %	V %	P %	Q %	V %
A1	3.46	8.07	1.03	1.64	1.89	1.05
A2	5.68	4.91	1	3.38	6.6	1.08
A3	4.52	6.72	1.13	4.19	6.24	0.79
B1	4.57	8.44	0.66	3.61	4.57	0.67
B2	3.14	4.83	0.57	3.23	3.76	0.7
B3	2.45	7.01	0.62	4	10.39	0.72
C1	5.54	3.47	1.08	3.6	5.25	1.25
C2	3.98	3.27	1.1	4.87	6.41	1.39
C3	3.64	3.81	1.2	4.05	5.88	1.57
D1	6.9	6.4	1.27	3.98	8.37	1.14
D2	3.83	5.68	1.09	6.61	4.02	1.37
D3	3.17	7.78	1	4.6	8.55	1.57

For small power values (less than 1 kW or 1 kvar) some deviations are noticed, mainly due to harmonics produced by the ABB ACS converters. Moreover, the converters activate an automatic power limitation when the voltage exceeds the inside threshold (as shown in Figure 2-5 and Figure 2-6 between hour 10 to hour 12). However, in general, the measurements are in reasonably good agreement with the calculated values, as also confirmed by further comparison performed with different loads, DGs and batteries.

2.6. Simulation Results

Several simulations have been performed with different load configurations, with and without the presence of dispatchable generators and batteries.

In Table 2-2, the prices and penalty coefficients used in the simulations are reported whilst Table 2-3 describes the various configurations considered in this work. The first configuration is characterized by the presence of both dispatchable and non-dispatchable units. The second

one is identical to the previous but with the presence of distributed three-phase batteries. The PF for non-dispatchable units has been chosen equal to 0.9. The initial and final SoC of the batteries are equal to 1.

TABLE 2-2 – PRICES AND PENALTY COEFFICIENTS

Quantity	Price
Active energy imported	0.1 (€/kWh)
Active energy exported	0.05 (€/kWh)
Active energy produced by dispatchable generators and exchanged by batteries	0.08 (€/kWh)
Reactive energy produced by dispatchable generators and exchanged by batteries	0.08 (€/kvarh)
Voltage violation (second limit)	1 (€/V)
Voltage violation (first limit)	0.1 (€/V)

TABLE 2-3 – DESCRIPTION OF THE CONFIGURATIONS

Input Data	Bus connection	Rate
<i>Configuration 1</i>		
Loads	A1, A2, A3, B1, B2, B3, C1, C2, C3, D1, D2, D3	9 kVA
Non-dispatchable DG	A3, B3, C3, D3	10 kVA
Dispatchable DG	A1(PV), A2, B1(PV), B2, C1(PV), C2, D1(PV), D2	12 kVA
Batteries	none	
<i>Configuration 2</i>		
Loads	A1, A2, A3, B1, B2, B3, C1, C2, C3, D1, D2, D3	9 kVA
Non-dispatchable DG	A3, B3, C3, D3	10 kVA
Dispatchable DG	A1(PV), A2, B1(PV), B2, C1(PV), C2, D1(PV), D2	12 kVA
Batteries	A1, A2, A3, B1, B2, B3, C1, C2, C3, D1, D2, D3	8 kW / 8 kWh

In order to avoid the inclusion of a constraint enforcing a minimum value of the power factor at the connection to the external grid, also the reactive power exchange is penalized in the objective function.

The profiles of the total active and reactive power relevant to the first configuration are reported in Figure 2-8 and Figure 2-9, respectively, whilst the ones relevant to configuration 2 are shown in Figure 2-10 and Figure 2-11. The comparison between Figure 2-8 and Figure 2-10 shows that the presence of distributed batteries provides a significant contribution to the reduction (peak and mean value) of the power exchanged with the grid. The incidence of

the batteries also results in a reduction of the power supplied by dispatchable generators. The same considerations apply for the case of reactive power (Figure 2-9 and Figure 2-11).

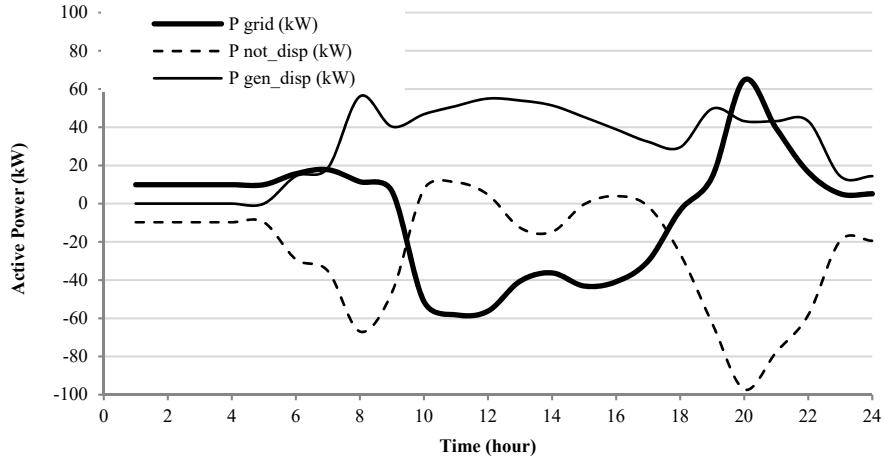


Figure 2-8. Configuration 1: overall active power profiles.

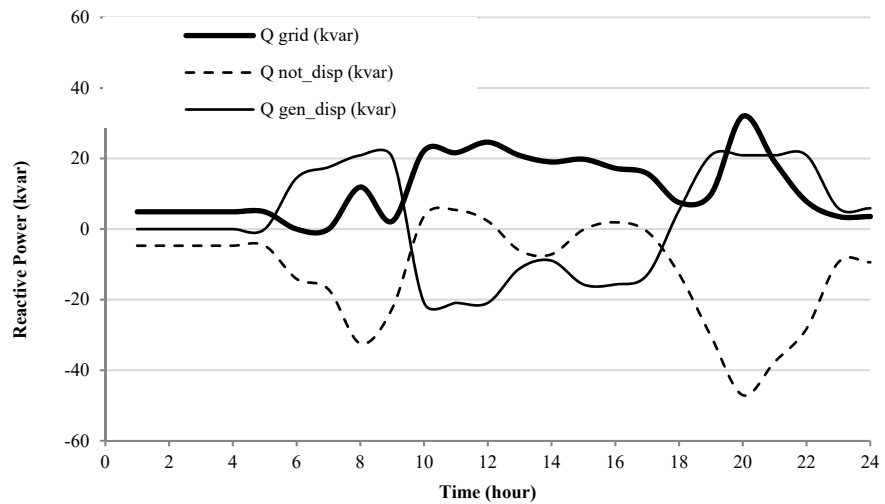


Figure 2-9. Configuration 1: overall reactive power profiles.

The results of the simulations are summarized in Table 2-4, where the values of the energy exchanged with the grid indicates the sum of both the imported energy and the exported one, whilst the cost of active energy exchanged with the network indicates the difference between the cost associated with the imported energy and the revenue due to the exported energy,

namely $\sum_t (p^{imp} E^{imp} - p^{exp} E^{exp})$ in (2.7).

The presence of the batteries decreases the active and reactive energy exchanged with the grid by 21% and 58%, respectively. The corresponding reduction of active and reactive energy produced by dispatchable DG is 30% and 81%, respectively. Due to the significant cost associated with the operation of the batteries (assumed here equal to the prices of the dispatchable DGs), their presence does not decrease the energy procurement costs but has a significant impact on the voltage profile: the costs due to voltage violations in configuration 2 are 67% lower than in configuration 1.

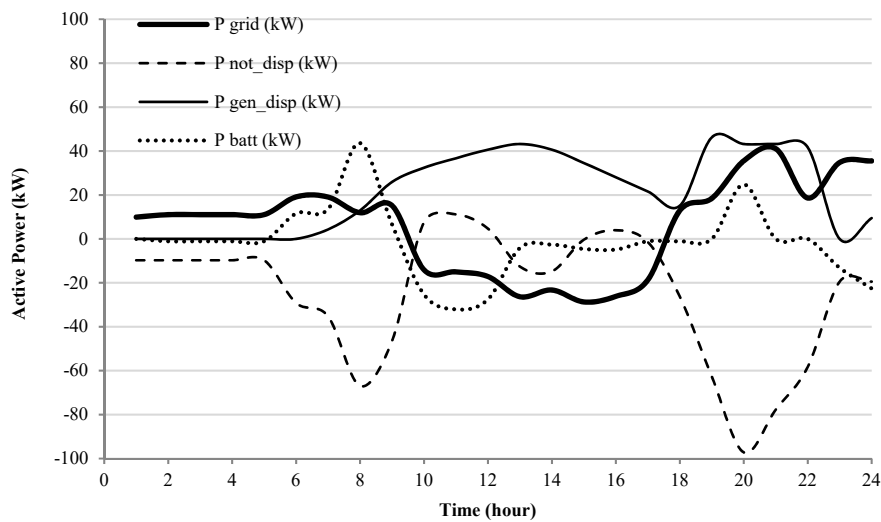


Figure 2-10. Configuration 2: overall active power profiles.

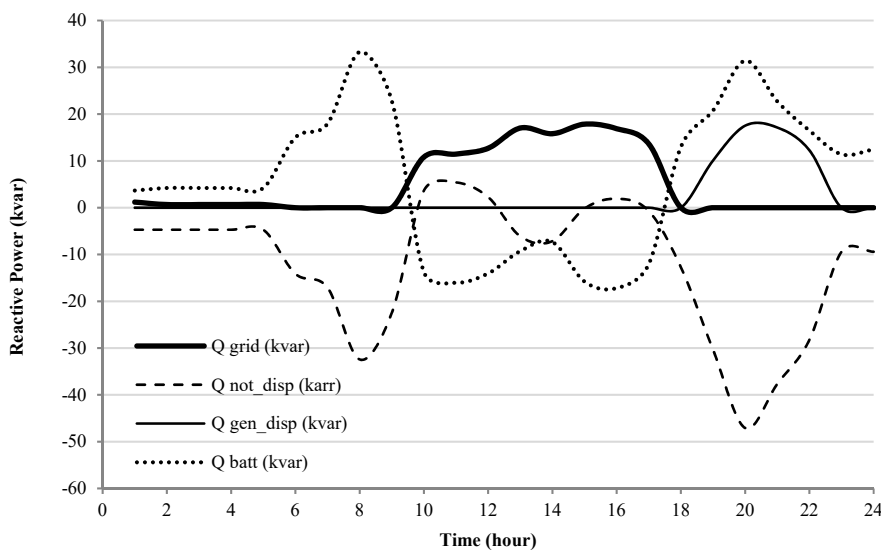


Figure 2-11. Configuration 2: overall reactive power profiles.

TABLE 2-4 – RESULTS OF THE SIMULATIONS

Results	Config. 1	Config. 2
Iterations	3	2
Solving time (s)	65.81	31.31
Active Energy exchanged with the grid (kWh)	616.99	486.32
Reactive Energy exchanged with the grid (kvarh)	283.2	120.14
Active energy produced by disp. DGs (kWh)	742.17	519.89
Reactive energy produced by disp. DGs (kvarh)	301.39	57.04
Batteries active energy exchange (kWh)	0	243.43
Batteries reactive energy exchange (kvarh)	0	343.41
Batteries losses (kW)	0	25.45
Network losses (kW)	35.63	34.44
Cost of active energy exchanged with the grid (€)	6.86	23.17
Cost of active and reactive energy of DGs (€)	83.48	46.15
Cost of active and reactive energy of batteries (€)	0	46.94
Cost of bus voltage violation (€)	129.76	42.42

2.7. Conclusions of chapter 2

A MILP model for the operation of a low voltage network, specifically developed to be computationally compatible with its use in energy management systems, has been presented and validated. In particular, the MILP model has been conceived in order to be integrated in the energy management of the experimental network GridLab district of the HES-SO Valais-Wallis in Sion, Switzerland.

The MILP model represents single-phase and three-phase small loads, distributed generation units, and storage systems. It takes into account the unbalanced operation of the LV network and the presence of the neutral wire.

The comparison between the model results and the measurements gathered by means of the GridLab experimental network shows that the accuracy of the implemented model is reasonably adequate.

Appendix C describes the general characteristics of the AIMMS modelling language and the developed algorithms.

3. Day-ahead scheduling of a local energy community

3.1. Introduction

We consider a local energy community (LEC), i.e., a set of residential or small industrial sites each acting as a prosumer, including, in general, generation and battery energy storage (BES) units other than loads. All the prosumers are connected to the same low-voltage (LV) distribution network, which is the internal network of the LEC and it is connected to the external utility grid. In a LEC, each prosumer uses the available energy resources in cooperation with the others to minimize the energy procurement cost of the LEC.

The economic justification for the formation of a LEC is mainly due to the difference between the price of the energy supplied by the utility grid and the price of the energy provided to the utility grid. This difference can be significant, e.g. due to the costs of the ancillary services.

The operation of a LEC requires the implementation of an energy management system (EMS) for the optimal exploitation of the available resources (*Pandzic & Bobanac, 2018*), with particular reference to the storage units.

This chapter focuses on an algorithm for the day-ahead scheduling of the BES units, by assuming that all the generation units of the LEC are photovoltaic (PV) systems. The algorithm is based on the alternating direction method of multipliers (ADMM). The EMS scheduling is based on the forecast of PV production and load of each prosumer during the following day. This chapter does not address the issues of the uncertainty associated with these forecasts, as accomplished, for instance, in *Orozco et al., 2018* and references therein.

The EMS function can be structured as a centralized optimization problem or as a distributed procedure. The centralized approach is the classical one. The central control unit needs to know all the operating characteristics of the prosumers and their forecasts. With respect to a centralized approach, distributed approaches, as the ADMM, are considered more reliable and reduce the need for each prosumer to communicate all characteristics and forecasts of their own units and loads to the other prosumers or to a coordinating unit. Moreover, a distributed

procedure is more appropriate for implementing new transaction methods based on, e.g., blockchain, or, more generally, on distributed ledger technologies.

We describe first the centralized optimization approach based on a mixed integer linear programming (MILP) model and then we focus on the distributed one. The ADMM approach is one of the most frequently adopted consensus algorithms and it is proposed for the day-ahead scheduling of a LEC and power loss in the distribution network are taken into account.

The specific characteristics of the distributed procedure proposed in this chapter are:

- it aims at minimizing the energy procurement cost of the LEC, considering the power loss in the internal network;
- the internal network losses are allocated to each energy transaction;
- the ADMM distributed algorithm is compared with a MILP centralized model that includes the same constraints and the power loss allocation;
- the structure of the proposed scheduling procedure is consistent with the billing procedure and the metering units installed in the LEC.

The structure of the chapter is the following. Section 3.2 is devoted to the formulation of the problem and the description of a centralized approach based on a MILP model. Section 3.3 presents the formulation of the proposed distributed procedure based on the ADMM algorithm. Section 3.4 illustrates the results of numerical tests obtained by using both the abovementioned approaches. Section 3.5 concludes the chapter.

3.2. Problem formulation – centralized approach

Figure 3-1 illustrates the scheme of a typical LEC. The point of common coupling (PCC) with the medium voltage (MV) utility grid is represented by the low voltage (LV) side of the distribution transformer. The grid meter M_g , positioned at the PCC, is bidirectional and measures the energy exchanged by the LEC with the utility grid in each time interval.

Aim of the LEC is to minimize the need to buy or sell energy to the utility grid and to balance local generation and load. Each prosumer trades energy with other prosumers and the utility grid, according to a peer to peer trading scheme without intermediation.

For the implementation of the distributed optimization approach, each prosumer i is equipped with a local bidirectional meter M_i that measures the energy that the specific prosumer exchanges (sell or buy) with the internal network in the time interval. A prosumer cannot act as producer and a consumer in the same time interval.

The day ahead scheduling dealt with in this chapter provides a plan of the optimal use of the LEC energy resources during the next day, with particular reference to the BES units, and calculates the prices of the energy transactions between prosumers. The prices of the exchanges with the utility grid are assumed to be predefined, though varying based on the time of the day.

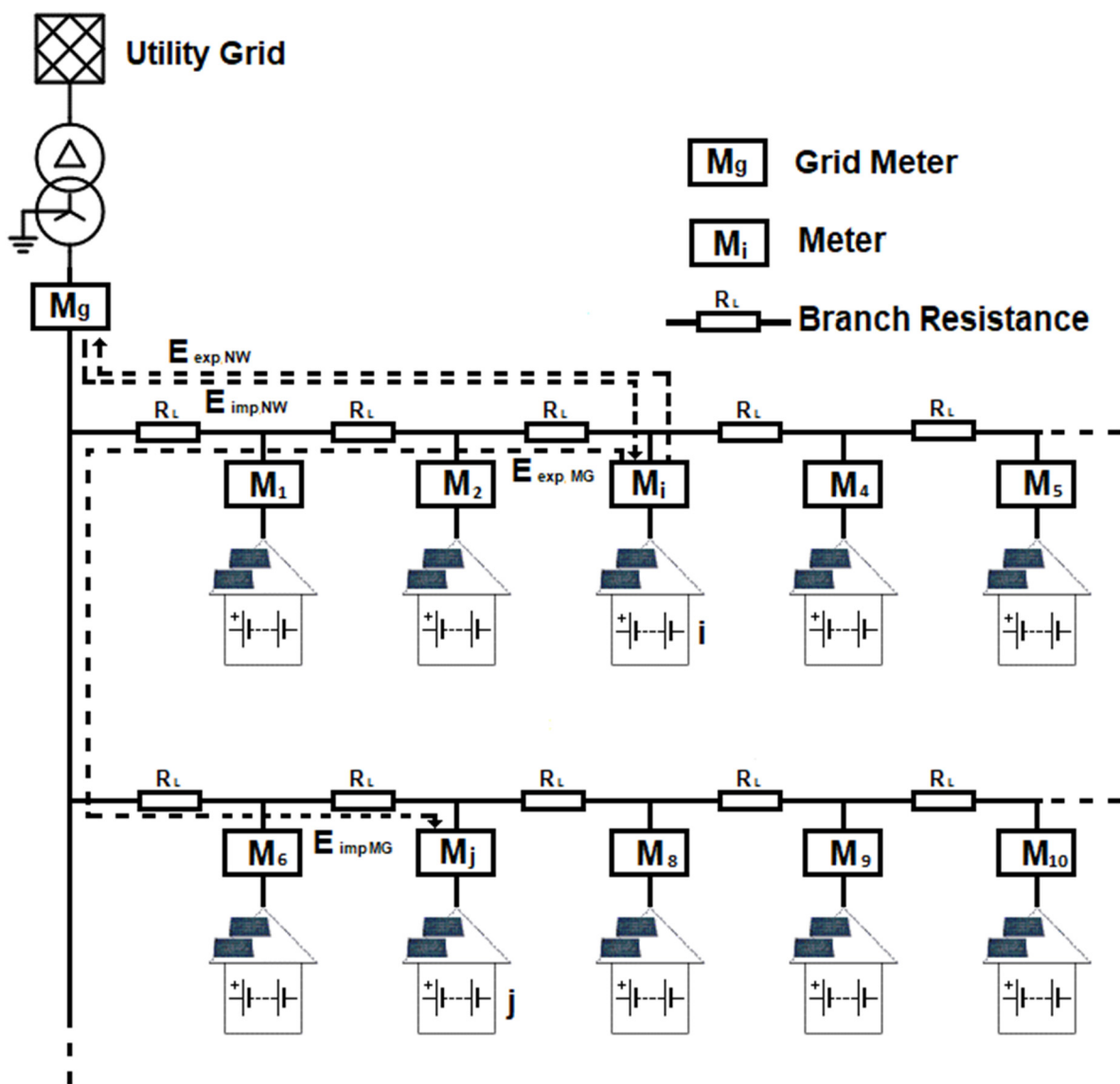


Figure 3-1. Scheme of a LEC with the internal network, prosumers, and meters.

The electricity billing procedure, for each time interval, can be described as follows:

- a) in each time interval, if the LEC buys energy from the utility grid (measured by M_g), the relevant cost is allocated to each consumer i (i.e., a prosumer that consume energy in excess of the local generation in that time interval) proportionally to the ratio of its consumption measured by M_i and the total consumption in the LEC, i.e., the sum of the measured energies of all the prosumers acting as consumers;
- b) if the LEC sells energy to the utility grid (measured by M_g), the relevant revenue is allocated to each producer j (i.e., a prosumer that produces energy in excess of the local load in that time interval) proportionally to the contribution of j to the total LEC production, i.e., the ratio between the energy measured by M_j and the sum of the measurements of all the prosumers acting as producers;
- c) each consumer i is also charged for the energy bought from the producers of the LEC, i.e., the energy given by the difference between the measurement of M_i and the energy allocated to consumer i in step a). The corresponding revenue of producer j is estimated proportionally to the contribution of j to the total LEC production as in step b). The day ahead scheduling procedure calculates the prices of each prosumer j that produces energy.

Both the centralized and the distributed approach of the day-ahead scheduling procedure are divided in two stages. Initially the optimization is carried out without considering the power loss in the internal network. Then, the network power loss is calculated and allocated to each power transaction between two prosumers or between a prosumer and the utility grid.

3.2.1. First stage: ideal network

By denoting as $\Omega = \{1, 2, \dots, N\}$ the set of prosumers i and as $T = \{1, 2, \dots, t_{end}\}$ the set of periods t of the optimization time horizon, the centralized LEC scheduling, without considering the network power loss, is described by the following mixed integer linear programming (MILP) model.

Objective function (*OF*) (3.1) minimizes the total cost associated with the power exchanges with the utility grid in time horizon T : parameters π_{buy}^t and π_{sell}^t are the prices (in €/kWh) of the energy that the LEC buys from and sells to the utility grid, respectively; $P_{buy_Grid\ i}^t$ and $P_{sell_Grid\ i}^t$ are the power bought from and the power sold to the utility grid (in kW), respectively; parameter Δt is the time step (in h).

$$OF = \min \sum_{\substack{t \in T \\ i \in \Omega}} \left(\pi_{\text{buy}}^t P_{\text{buy_Grid } i}^t - \pi_{\text{sell}}^t P_{\text{sell_Grid } i}^t \right) \Delta t \quad (3.1)$$

The constraints are:

$$\sum_{\substack{j \in \Omega \\ j \neq i}} \left(P_{\text{buy } j, i}^t - P_{\text{sell } i, j}^t \right) = 0 \quad t \in T \quad i \in \Omega \quad (3.2)$$

$$P_{G_i}^t + P_{\text{BES_dis } i}^t + P_{\text{buy_Grid } i}^t + \sum_{\substack{j \in \Omega \\ j \neq i}} P_{\text{buy } i, j}^t = P_{D_i}^t + P_{\text{BES_ch } i}^t + P_{\text{sell_Grid } i}^t + \sum_{\substack{j \in \Omega \\ j \neq i}} P_{\text{sell } i, j}^t \quad t \in T, i \in \Omega \quad (3.3)$$

$$\begin{cases} P_{\text{buy_Grid } i}^t = 0 \text{ and } P_{\text{buy } i, j}^t = 0 \text{ if } u_i^t = 0 & u_i^t \in \{1, 0\} \\ P_{\text{sell_Grid } i}^t = 0 \text{ and } P_{\text{sell } i, j}^t = 0 \text{ if } u_i^t = 1 & i \text{ and } j \in \Omega \end{cases} \quad (3.4)$$

$$0 \leq P_{\text{buy_Grid } i}^t \leq P_{\text{buy } i}^{\max} \quad 0 \leq P_{\text{sell_Grid } i}^t \leq P_{\text{sell } i}^{\max} \quad t \in T, i \in \Omega \quad (3.5)$$

$$0 \leq P_{\text{buy } i, j}^t \leq P_{\text{buy } i}^{\max} \quad 0 \leq P_{\text{sell } i, j}^t \leq P_{\text{sell } i}^{\max} \quad t \in T, i \text{ and } j \in \Omega \quad (3.6)$$

$$E_{\text{BES } i}^t = E_{\text{BES } i}^{t-1} + (P_{\text{ch } i}^t \eta_{\text{ch}} - P_{\text{dis } i}^t / \eta_{\text{dis}}) \Delta t \quad i \in \Omega \quad t \in T, t > 1 \quad (3.7)$$

$$\begin{cases} E_{\text{BES } i}^{t-1} = E_{\text{max}, i} + (P_{\text{BES } i}^{t-1} \eta_{\text{ch}} - P_{\text{BES } i}^{t-1} / \eta_{\text{dis}}) \Delta t & i \in \Omega \\ E_{\text{BES } i}^{\text{end}} = E_{\text{BES } i}^{\max} & i \in \Omega \end{cases} \quad (3.8)$$

$$\begin{cases} P_{\text{ch } i}^t = 0 \text{ if } u_{\text{BES } i}^t = 0 & u_{\text{BES } i}^t \in \{1, 0\} \\ P_{\text{dis } i}^t = 0 \text{ if } u_{\text{BES } i}^t = 1 & i \in \Omega \end{cases} \quad (3.9)$$

$$0 \leq P_{\text{BES_dis } i}^t \leq P_{\text{BES } i}^{\max} \quad 0 \leq P_{\text{BES_ch } i}^t \leq P_{\text{BES } i}^{\max} \quad t \in T, i \in \Omega \quad (3.10)$$

$$E_{\text{BES } i}^{\min} \leq E_{\text{BES } i}^t \leq E_{\text{BES } i}^{\max} \quad t \in T, i \in \Omega \quad (3.11)$$

Constraint (3.2) represents the equilibrium between the total power bought by the other prosumers from producer i and the power sold by producer i to the other prosumers. The Lagrangian multiplier λ_i^t associated to (3.2) is the price of producer i in time interval t (the price is independent of the buying prosumer).

Constraint (3.3) represents the power balance for the i -th prosumer: parameters $P_{G_i}^t$ and $P_{D_i}^t$ are the PV power generation and the demand of i (in kW), respectively; non-negative

variables $P_{ch\ i}^t, P_{dis\ i}^t$ are the charging and discharging power of the BES of prosumer i (in kW); non-negative variable $P_{buy\ i,j}^t$ is the power bought by i from j (in kW); non-negative variable $P_{sell\ i,j}^t$ is the power sold by i to j (in kW).

Indicator constraints (3.4), with binary variable u_i^t , are used to avoid concurrent purchase and selling by the same prosumer.

The possibility of prosumer i to buy or sell energy is limited by constraints (3.5) and (3.6) where $P_{sell\ i}^{\max}$ is the largest value between 0 and $P_{G\ i}^t - P_{D\ i}^t + P_{BES\ i}^{\max}$, and $P_{buy\ i}^{\max}$ is the largest value between 0 and $P_{D\ i}^t - P_{G\ i}^t + P_{BES\ i}^{\max}$. $P_{BES\ i}^{\max}$ is the maximum power output of the BES of i .

The state of the energy (*SoE*) of each storage is defined by (3.7) and (3.8), where $E_{BES\ i}^t$ is the *SoE* at time t (in kWh) and η_{ch}, η_{dis} are the battery efficiencies during charge and discharge, to take power loss into account. In (3.8) we assume that BES system is fully charged at the beginning and at the end of the day, where $E_{BES\ i}^{\max}$ is the capacity of the i -th storage.

The power during charge and discharge is limited through parameter P_{BES}^{\max} by constraint (3.10). The *SoE* ($E_{BES\ i}^t$) is bounded between the minimum level $E_{BES\ i}^{\min}$ and the maximum level $E_{BES\ i}^{\max}$ by constraint (3.11). In order to prevent simultaneous charge and discharge of the batteries, indicator constraints (3.9) with a binary variable u_{BES}^t are included.

In the literature accurate MILP models of the BES are described (e.g., in *Orozco et al., 2018, Pandzic & Bobanac, 2018, Sakti et al., 2017* and *Bordin et al., 2017*) that can replace the simpler model represented by (3.7)-(3.11).

The second stage considers the power loss in the internal network by using coefficients K that represent the contribution of each power transaction to the power loss in each branch. To calculate these coefficients, the rms bus voltage values are assumed to be equal to the rated value, the network is assumed to be balanced, and reactive power flows are neglected. Let $B = \{1, 2, \dots, b_{end}\}$ be the set of branches of the network, the power loss in the branch b is:

$$L_{b,i}^t = \left(\frac{R_b}{3V_n^2} \right) (F_b^t)^2 \quad (3.12)$$

where R_b is the resistance of branch b , V_n is the line-to-line rated voltage value and F_b^t is the three-phase power flow in branch b .

The power flow F_b^t in each branch b is positive when the power is directed from the substation to the end of the feeder. F_b^t is calculated as follows:

$$F_b^t = \sum_{i \in \Omega} P_{\text{buy_Grid } i}^t A_{\text{Grid } b, i} - \sum_{i \in \Omega} P_{\text{sell_Grid } i}^t A_{\text{Grid } b, i} + \sum_{i \in \Omega} \sum_{j \in \Omega} P_{\text{buy } i, j}^t A_{b, i, j} \quad (3.13)$$

where $A_{\text{Grid } b, i}$ and $A_{b, i, j}$ are the matrices that describe the network configuration: $A_{\text{Grid } b, i}$ elements are 1 for the branches interested by the power flow exchanged with the external network and 0 otherwise; $A_{b, i, j}$ elements are 1 for the branches in which $P_{\text{buy } i, j}^t$ flows in the positive and -1 in the negative directions, and 0 if branch b is not linked with flow $P_{\text{buy } i, j}^t$.

For the configuration of Figure 3-1, where the nodes are numbered in ascending order along the feeders, when branch b is linked with $P_{\text{buy } i, j}^t$, then $A_{b, i, j}$ elements are 1 for $i < j$ and -1 for $i > j$.

For the power loss allocation, the power flow in branch b is proportionally attributed to each power exchange that has the same direction of the total-flow in the branch. The total net flow $F_{\text{TOT } b}^t$ in branch b at time interval t is defined as:

$$F_{\text{TOT } b}^t = F_{\text{buy_Grid } b}^t - F_{\text{sell_Grid } b}^t + F_{\text{Pros } b}^t \quad (3.14)$$

where

$$F_{\text{buy_Grid } b}^t = \begin{cases} \sum_{i \in \Omega} P_{\text{buy_Grid } i}^t A_{\text{Grid } b, i} & \text{if } F_b^t > 0 \\ 0 & \text{otherwise} \end{cases} \quad (3.15)$$

$$F_{\text{sell_Grid } b}^t = \begin{cases} \sum_{i \in \Omega} P_{\text{sell_Grid } i}^t A_{\text{Grid } b, i} & \text{if } F_b^t < 0 \\ 0 & \text{otherwise} \end{cases} \quad (3.16)$$

$$F_{\text{Pros } b}^t = \begin{cases} \sum_{i, j \in \Omega} P_{\text{buy } i, j}^t A_{b, i, j} & \text{if } \text{sign}(F_b^t) = A_{b, i, j} \\ 0 & \text{otherwise} \end{cases} \quad (3.17)$$

are the contribution to the total net flow of the power exchanged by the prosumers with the external network (bought and sold) and the contribution of the power exchanged among the various prosumers.

As proposed in, e.g., *Conejo et al., 2002* and *Zizzo et al., 2018*, the power loss in branch b is allocated to each power transaction according the corresponding coefficient K defined as the ratio between the power exchanged between prosumer i and the grid, or between prosumer i and j , at time interval t and the total net flow $F_{TOT\ b}^t$ in branch b :

$$K_{buy_Grid\ b,i}^t = \begin{cases} \left| P_{buy_Grid\ i}^t A_{Grid\ b,i} / F_{TOT\ b}^t \right| & \text{if } F_b^t > 0 \\ 0 & \text{otherwise} \end{cases} \quad (3.18)$$

$$K_{sell_Grid\ b,i}^t = \begin{cases} \left| P_{sell_Grid\ i}^t A_{Grid\ b,i} / F_{TOT\ b}^t \right| & \text{if } F_b^t < 0 \\ 0 & \text{otherwise} \end{cases} \quad (3.19)$$

$$K_{buy\ b,i,j}^t = \begin{cases} \left| P_{buy\ i,j}^t A_{b,i,j} / F_{TOT\ b}^t \right| & \text{if } sign(F_b^t) = A_{b,i,j} \\ 0 & \text{otherwise} \end{cases} \quad (3.20)$$

Stage 2 relies on the assumption that the power flows in the real network (with losses) are not much different from those already calculated for the ideal case.

3.2.2. Second stage: network with losses

The MILP model of the second stage includes the losses of each power exchange. Therefore constraints (3.3) is replaced by

$$\begin{aligned} P_{G\ i}^t + P_{BES_dis\ i}^t + P_{buy_Grid\ i}^t - \sum_{b \in B} L_{buy_Grid\ b,i}^t + \sum_{\substack{j \in \Omega \\ j \neq i}} P_{buy\ i,j}^t = \\ P_{D\ i}^t + P_{BES_ch\ i}^t + P_{sell_Grid\ i}^t + \sum_{b \in B} L_{sell_Grid\ b,i}^t + \sum_{\substack{j \in \Omega \\ j \neq i}} P_{sell\ i,j}^t + \sum_{\substack{j \in \Omega \\ j \neq i}} \sum_{b \in B} L_{buy\ b,j,i}^t \end{aligned} \quad (3.21)$$

$t \in T, i \in \Omega$

where $L_{buy_Grid\ b,i}^t$, $L_{sell_Grid\ b,i}^t$, and $L_{buy\ b,j,i}^t$ are the losses in branch b attributed to the power bought by prosumer i from the utility grid, to the power sold by i to the utility grid, and to the power sold by i to j , respectively. For each power transaction, the losses attributed to each transaction are obtained by the product of the corresponding coefficient K and the total value of the power loss L_b^t in branch b :

$$L_{\text{buy_Grid } b,i}^t = K_{\text{buy_Grid } b,i}^t L_b^t \quad t \in T, i \in \Omega, b \in B \quad (3.22)$$

$$L_{\text{buy_Grid } b,i}^t = K_{\text{buy_Grid } b,i}^t L_b^t \quad t \in T, i \in \Omega, b \in B \quad (3.23)$$

$$L_{\text{buy } b,i,j}^t = K_{\text{buy } b,i,j}^t L_b^t \quad t \in T, i \text{ and } j \in \Omega, b \in B \quad (3.24)$$

According to (3.21), prosumer i should compensate the power loss due to the power exchange with the utility grid. Moreover, we assume that both $P_{\text{buy } i,j}^t$ and $P_{\text{sell } i,j}^t$, which correspond to $P_{\text{buy } j,i}^t$, are measured at the connection of the buying prosumer with the internal network. Therefore, according to (3.21) when i sells energy to j , losses are ascribed to prosumer i .

With respect to the first stage, the model of the second stage includes additional constraints to avoid transactions not present in the first stage solution, under the assumption that the power flow distribution in the network is not significantly affected by the losses. These constraints are

$$\begin{cases} P_{\text{sell_Grid } i}^t T_{\text{sell_Grid } i}^t = 0 & t \in T, i \in \Omega \\ P_{\text{buy_Grid } i}^t T_{\text{buy_Grid } i}^t = 0 & t \in T, i \in \Omega \\ P_{\text{buy } i,j}^t T_{\text{buy } i,j}^t = 0 & t \in T, i \text{ and } j \in \Omega, i \neq j \end{cases} \quad (3.25)$$

where parameters $T_{\text{buy_Grid } i}$, $T_{\text{sell_Grid } i}$, and $T_{\text{buy } i,j}$ are equal to 0 if in the first stage solution i buys from the utility grid, sells to the utility grid, and buys from j , respectively; otherwise, these parameters are equal to 1.

Moreover, the second stage model includes the constraints for the piecewise linear approximation of L_b^t , i.e. the power loss in each branch b (Williams, 1990). A set L of segments for the linearization is created and constraints (3.13) are included, for each branch b and time interval t . The allowed range of the power flow in the various branches is divided in N intervals with $N + 1$ breakpoints $H_{\text{Flow } b,l}^t$. The corresponding breakpoints for the losses $H_{\text{Loss } b,l}^t$ are given by (3.12). The piecewise linear approximation of L_b^t is given by

$$F_b^t = \sum_{l \in L} a_{b,l}^t H_{\text{Flow } b,l}^t \quad t \in T, b \in B \quad (3.26)$$

$$L_b^t = \sum_{l \in L} a_{b,l}^t H_{\text{Loss } b,l}^t \quad t \in T, b \in B \quad (3.27)$$

$$\sum_{l \in L} a_{b,l}^t = 1 \quad t \in T, l \in L \quad (3.28)$$

where $a_{b,l}^t$ are SOS2 variables, i.e., they are linked with special ordered set of type 2 constraints so that force at most two and consecutive variables can be non-zero.

3.3. Problem formulation – distributed approach

As mentioned, the distributed approach is based on the ADMM. The optimization is iteratively carried out by each prosumer k . At each ADMM iteration, the power bought or sold by each prosumer calculated in the previous iteration is made known to all the prosumers. These values are considered as parameters in the optimization problem solved by prosumer k at the current iteration and they are denoted by a hat in the model described in this section.

3.3.1. First stage: ideal network

The objective function to minimize by prosumer k is

$$OF_k = \min \sum_{t \in T} [(\pi_{\text{buy}}^t P_{\text{buy_Grid } k}^t \Delta t - \pi_{\text{sell}}^t P_{\text{sell_Grid } k}^t \Delta t) + \sum_{\substack{j \in \Omega \\ j \neq k}} \lambda_j^t P_{\text{buy } k,j}^t \Delta t - \lambda_k^t \sum_{\substack{j \in \Omega \\ j \neq k}} P_{\text{sell } k,j}^t \Delta t + \ell_k^t] \quad (3.29)$$

$$\ell_k^t = m \cdot \rho \left(\sum_{\substack{j \in \Omega \\ j \neq k}} (\hat{P}_{\text{buy } j,k}^t - P_{\text{sell } k,j}^t)^2 + \sum_{\substack{j \in \Omega \\ j \neq k}} (P_{\text{buy } k,j}^t - \hat{P}_{\text{sell } k,j}^t)^2 \right) \quad (3.30)$$

Equation (3.29) is obtained by the decomposition for each prosumer k of the Lagrangian, which incorporates OF (3.1) and constraints (3.2) multiplied by the relevant Lagrange multiplier λ_i^t , augmented by the squared norm of the same constraints multiplied by positive penalty parameter ρ and fixed scale factor m , as shown in (3.30).

OF_k can be seen as the summation of the costs of the energy bought by k from the utility grid at price π_{buy}^t and from each other prosumer j at price λ_j^t minus the sum of the revenues due to the energy sold by k to the utility grid at price π_{sell}^t and to the other prosumers at price λ_k^t . Once the procedure converges, ℓ_k^t is zero and the value OF for the entire system is the sum of the ones solved for each prosumer k :

$$OF = \sum_{k \in \Omega} OF_k \quad (3.31)$$

The optimization problem of prosumer k includes constraints (3.3) - (3.11) for $i=k$.

Moreover, the convergence of the ADMM procedure is improved if the following constraints are added starting from the second iteration:

$$P_{\text{sell } k,j}^t \leq \hat{P}_{\text{buy_Grid } j}^t + \sum_{\substack{i \in \Omega \\ i \neq j}} \hat{P}_{\text{buy } j,i}^t \quad t \in T, j \in \Omega \quad (3.32)$$

$$P_{\text{buy } k,j}^t \leq \hat{P}_{\text{sell_Grid } j}^t + \sum_{\substack{i \in \Omega \\ i \neq j}} \hat{P}_{\text{sell } j,i}^t \quad t \in T, j \in \Omega \quad (3.33)$$

At each iteration v , after the solution of all the optimization problems, one for each prosumer k , the ADMM includes the update of Lagrangian multipliers λ_k^t and of penalty parameter ρ .

Let r_k^v be the primal residual term for prosumer k , equal to the vector of dimension T with elements

$$r_k^t = \sum_{\substack{j \in \Omega \\ j \neq k}} P_{\text{buy } j,k}^t - \sum_{\substack{j \in \Omega \\ j \neq k}} P_{\text{sell } k,j}^t \quad (3.34)$$

the T dimensional vector of Lagrangian multipliers λ_k^v , with elements λ_k^t , is updated as:

$$\lambda_k^{v+1} = \lambda_k^v + 2m \cdot \rho \cdot r_k^v \quad \text{with} \quad |r_k^t| > \varepsilon \quad (3.35)$$

and the procedure is repeated until the absolute value of all residuals r_k^t is lower than tolerance ε (which is assumed to be 5 W in all the numerical tests of this chapter). At the beginning of the ADMM procedure, the prices λ_k^t are initialized to be equal to $1/2(\pi_{\text{buy}}^t + \pi_{\text{sell}}^t)$.

The penalty parameters are updated as follows (Boyd et al., 2011):

$$\rho^{v+1} = \begin{cases} 2\rho^v & \|r_k^v\|_2 > 10 \|s_k^v\|_2 \\ \rho^v / 2 & \|s_k^v\|_2 > 10 \|r_k^v\|_2 \\ \rho^v & \text{otherwise} \end{cases} \quad (3.36)$$

where $\| \cdot \|_2$ is the Euclidian norm and the T dimensional vector s_k^v is the dual residual term with elements

$$s_k^t = \rho^v \left[\left(\sum_{j \in \Omega} P_{\text{sell } k,j}^t \right)^v - \left(\sum_{j \in \Omega} P_{\text{sell } k,j}^t \right)^{v-1} + \left(\sum_{j \in \Omega} P_{\text{buy } k,j}^t \right)^v - \left(\sum_{j \in \Omega} P_{\text{buy } k,j}^t \right)^{v-1} \right]. \quad (3.37)$$

To accelerate the convergence, the initial value of m , which is equal to $5 \cdot 10^{-5}$, is multiplied by 10 when the maximum value of the total mismatch

$$r^v = \sum_k |r_k^v|, \quad (3.38)$$

becomes lower than 1 kW, and furtherly multiplied by 10 when $\max(|r_k^t|) < 100$ W.

3.3.2. Second stage: network with losses

The losses allocation follows the same rules and criteria described for the centralized approach. In order to avoid the introduction in the ADMM optimization model of constraints (3.13) and (3.26) - (3.28), which link the purchase and selling decision of all the prosumers, we introduce the calculation of the efficiencies of each energy transaction (between prosumer k and the grid or between k and j):

$$\eta_{\text{buy_Grid } k}^t = 1 - \frac{\sum_{b \in B} L_{\text{buy_Grid } b,k}^t}{P_{\text{buy_Grid } k}^t} \quad t \in T \quad (3.39)$$

$$\eta_{\text{sell_Grid } k}^t = 1 - \frac{\sum_{b \in B} L_{\text{sell_Grid } b,k}^t}{P_{\text{sell_Grid } k}^t} \quad t \in T \quad (3.40)$$

$$\eta_{\text{buy } k,j}^t = 1 - \frac{\sum_{b \in B} L_{\text{buy } b,k,j}^t}{P_{\text{buy } k,j}^t} \quad t \in T, j \in \Omega, j \neq k \quad (3.41)$$

where $L_{\text{buy_Grid } b,i}^t$, $L_{\text{sell_Grid } b,i}^t$, and $L_{\text{buy } b,j,i}^t$ are calculated at the end of the first stage, by using (3.22) - (3.24) and the values of L_b^t given by (3.12).

The efficiency parameters are included in the balance constraint of each prosumer k . Then constraints (3.21) become:

$$\begin{aligned}
P_{Gk}^t + P_{\text{BES_dis } k}^t + P_{\text{buy_Grid } k}^t \cdot \eta_{\text{buy_Grid } k}^t + \sum_{\substack{j \in \Omega \\ j \neq k}} P_{\text{buy } k, j}^t = \\
P_{Dk}^t + P_{\text{BES_ch } k}^t + \frac{P_{\text{sell_Grid } k}^t}{\eta_{\text{sell_Grid } k}^t} + \sum_{\substack{j \in \Omega \\ j \neq k}} \frac{P_{\text{sell } k, j}^t}{\eta_{\text{sell_Grid } k, j}^t}
\end{aligned} \quad t \in T, k \in \Omega \quad (3.42)$$

Also the models of the second stage of the ADMM procedure include constraints (3.25) for $k=i$ in order to prevent new energy transactions with respect to those of the first stage.

3.4. Implementation and test results

The models have been implemented in the AIMMS Developer modelling environment and tested by using the Cplex V12.8 solver on a 2-GHz Intel-i7 computer with 8 GB of RAM, running 64-bit Windows 10. The MILP solver is used for the centralized model and the MIQP (mixed integer quadratic programming) solver for the ADMM model.

All the calculations refer to a time window of 1 day, split in 96 periods of 15 min each.

The test system is composed of two LV feeders. Each feeder is composed by five lines, each with resistance $R_b = 189 \text{ m}\Omega$.

Five prosumers are connected to each feeder: prosumers 1-5 to a feeder and prosumers 6-10 to the other. Each prosumer is equipped with a PV system and a load. We repeat the calculations two times, once assuming the system without BES units and the other by assuming that each prosumer is also equipped with a BES unit. The load profiles adopted for each prosumer are shown in Figure 3-2. For the PV generation, we have assumed the same profile of the ratio between power production and panel surface for each prosumer shown in Figure 3-3. The area of the PV panel of each prosumer is given in Table 3-1.

Figure 3-3 also shows the profile of the price of the energy bought from the utility grid π_{buy}^t . We assume that the price of the energy sold by the LEC to the utility grid, i.e., π_{sell}^t , is half of π_{buy}^t . The sizes of the BES systems are reported in Table 3-2.

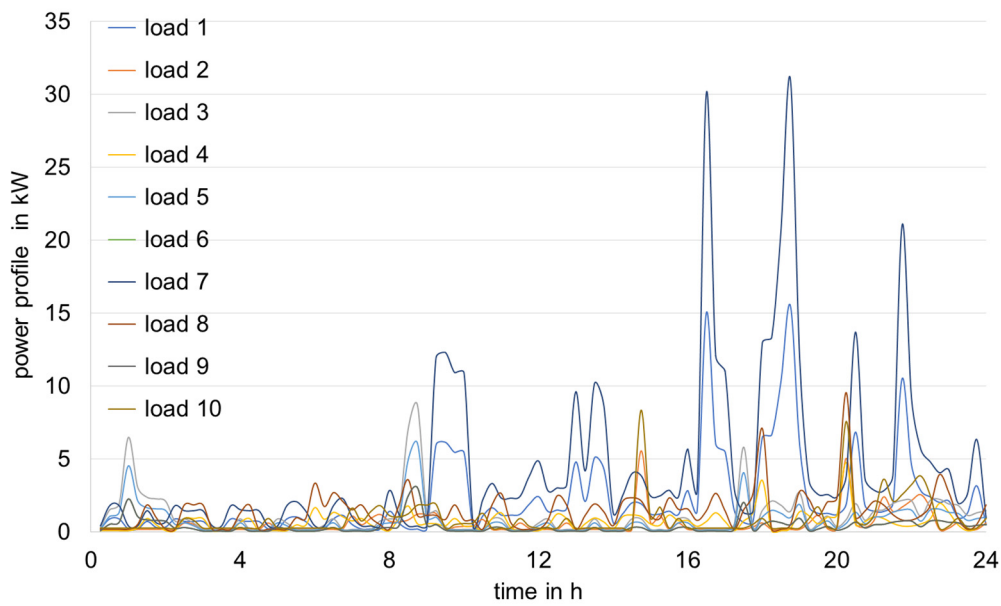


Figure 3-2. Load profile for each prosumer.

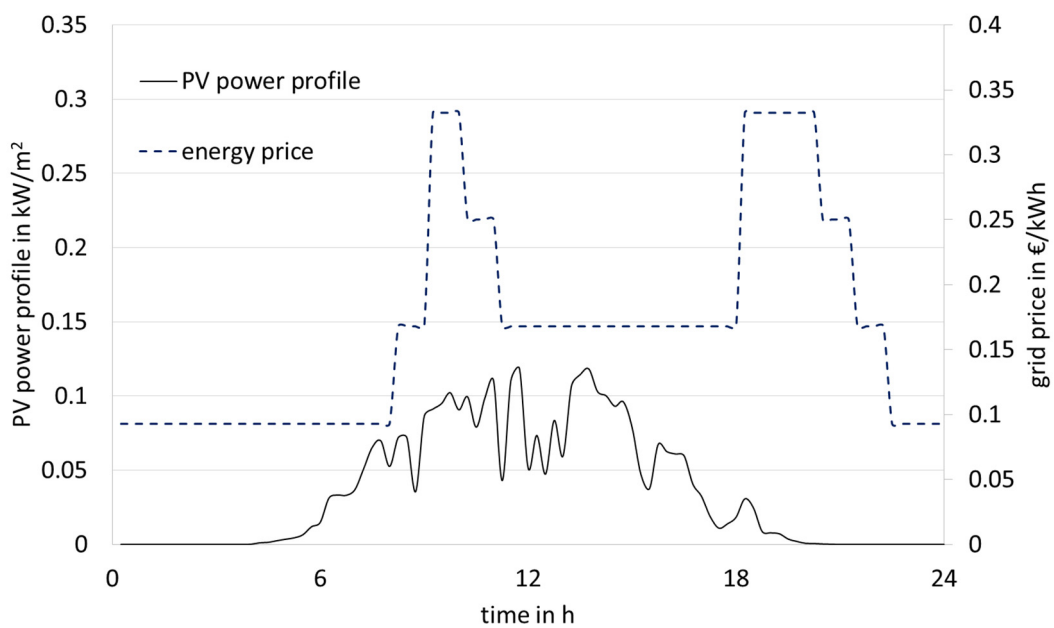


Figure 3-3. Profile of the PV production and grid purchase price.

TABLE 3-1 - PV PANEL SURFACE FOR EACH PROSUMER

Prosumer	1	2	3	4	5	6	7	8	9	10
PV surface (m ²)	32	14	21	32	28	14	42	32	14	42

TABLE 3-2 – SIZES OF THE BES UNITS

prosumer	1	2	3	4	5	6	7	8	9	10
Size (kWh)	5	3	4	2	3	1	2	2	2	6

3.4.1. Scenario 1: prosumers without batteries

Table 3-3 shows the values of OF for both stages and the total network losses in the 24 hours, for the centralized problem and the distributed one without BES units. The distributed model requires a solution time around 13 s / 12 iterations for stage 1 and 17 s / 9 iterations for stage 2. The solution of the centralized model without BES units needs around 0.5 s for each of both stages.

TABLE 3-3 - COMPARISON BETWEEN CENTRALIZED MODEL AND ADMM. SCENARIO 1

	OF (€)		Losses (kWh)
	stage 1	stage 2	stage 2
Centralized	26.58	27.06	2.66
ADMM	26.58	27.03	2.62

To illustrate the convergence behavior of the ADMM procedure, Figure 3-4 shows the average value of the primal residuals r_k^f denoted by R , the values of the augmented OF according to (3.31), and the value of the part of OF corresponding to the energy bought from and sold to the utility grid, i.e. (3.1), at each iteration.

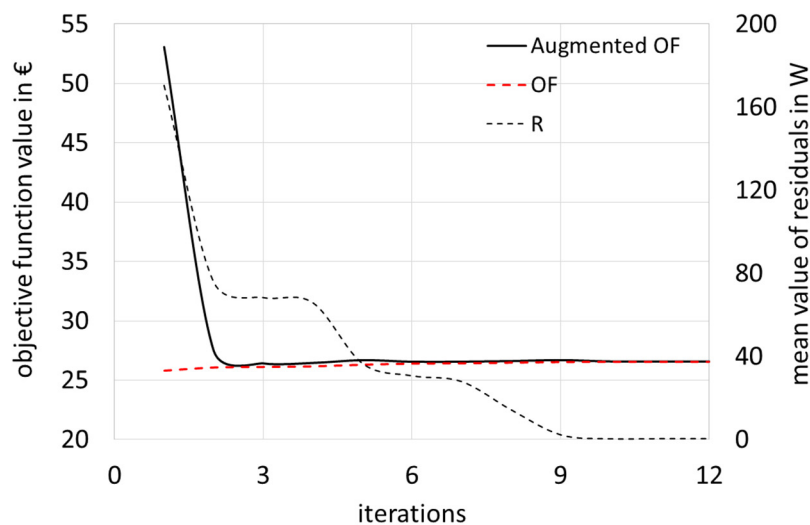


Figure 3-4. ADMM convergence in stage 1 for scenario 1: augmented OF , part of OF corresponding to the power exchanged with the utility grid, average of primal residuals at each iteration.

As shown in Figure 3-5 the profiles of the power exchanged by the LEC with the utility grid calculated by using the two approaches are quite similar.

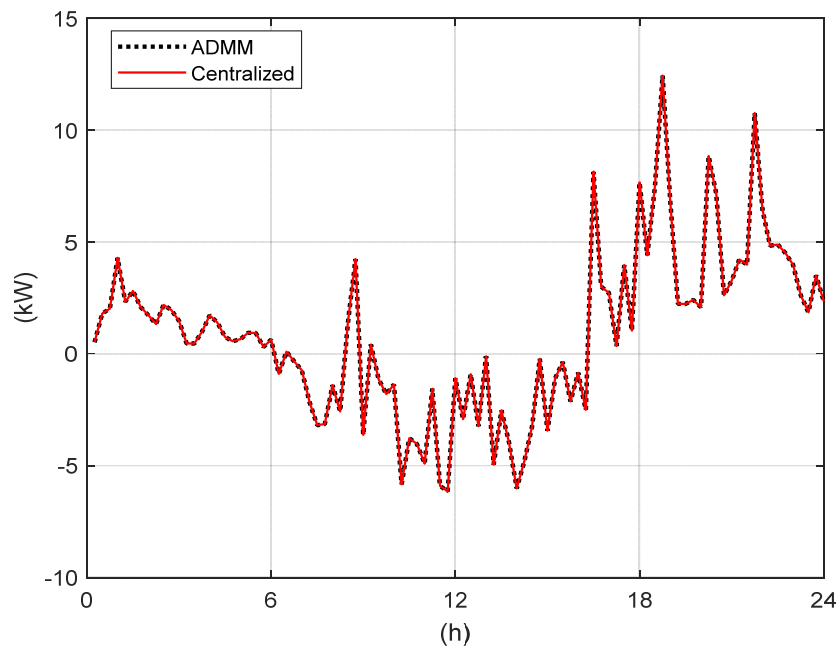


Figure 3-5. Comparison of the power flow exchanged with the utility grid (positive if consumed by the LEC) at the end of stage 2 (solid line: centralized model, dashed line: distributed model).

Figure 3-6, shows the energy sold by each prosumer to the others at the end of stage 2 calculated by using the centralized model and the ADMM approach.

The reasonable accuracy of the power loss representation in the second stage of both the centralized and distributed optimization models is confirmed by the limited values of the maximum percentage difference between the power loss calculated at the end of stage 2 for each period and the corresponding values obtained by (3.12): around 1.5% for the centralized procedure and 4% for the ADMM approach.

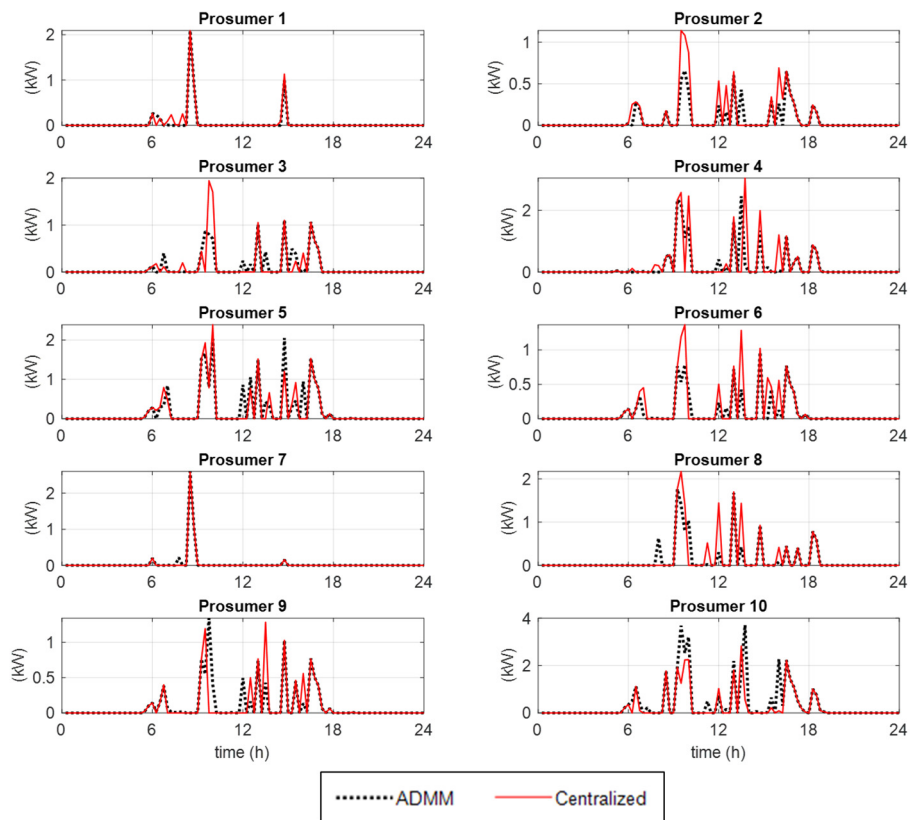


Figure 3-6. Comparison of the power flows from every prosumer when it sells to the others (excluding the utility grid) at the end of stage 2 for scenario 1 (solid line: centralized model, dashed line: distributed model).

3.4.2. Scenario 2: prosumers with batteries

Table 3-4 compares the results of *OF* for both stages and the total network losses in the 24 hours obtained by including the BES units in the models. The distributed model needs a solution time around 170 s / 26 iterations for stage 1 and 25 s / 13 iterations for stage 2. The solution of the centralized model needs around 5 s for stage 1 and around 8 s for stage 2.

TABLE 3-4 - COMPARISON BETWEEN CENTRALIZED MODEL AND ADMM. SCENARIO 2

	OF (€)		Losses (kWh)
	stage 1	stage 2	stage 2
Centralized	17.84	18.27	2.86
ADMM	17.98	18.36	3.06

The convergence performance of the ADMM procedure is illustrated in Figure 3-7.

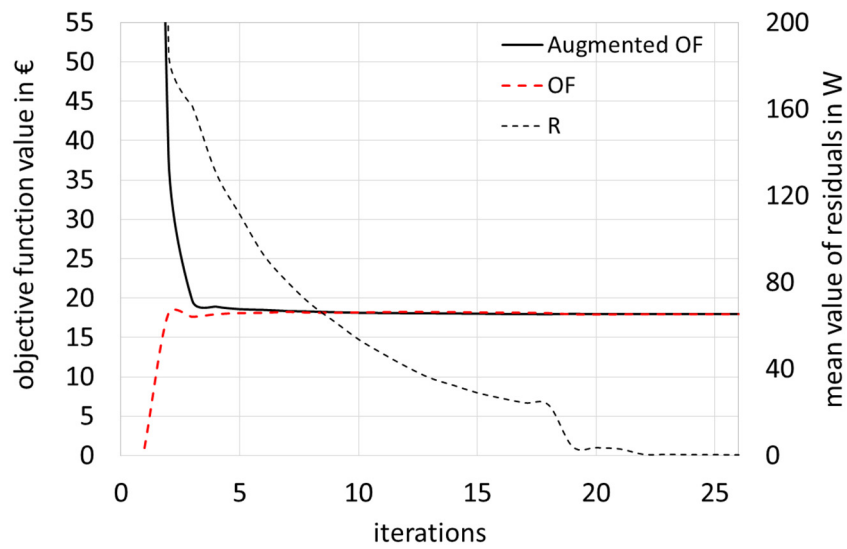


Figure 3-7. ADMM convergence in stage 1 for scenario 2: augmented *OF*, part of *OF* corresponding to the power exchanged with the utility grid, average of primal residuals at each iteration.

The total power exchanged by the LEC with the utility grid and the profiles of the energy sold between the various prosumers are reported in Figure 3-8 and Figure 3-9 for the centralized and ADMM approaches, respectively.

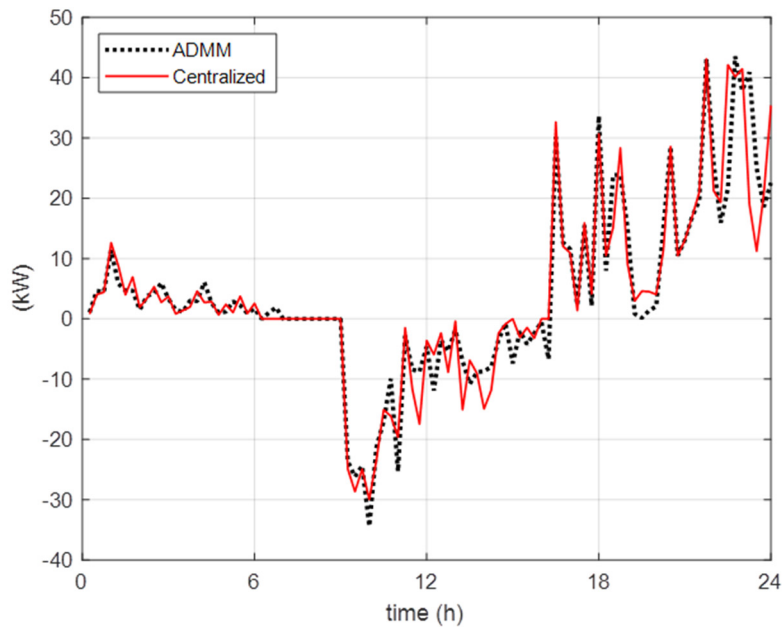


Figure 3-8. Comparison of the power flow exchanged with the utility grid (positive if consumed by the LEC) at the end of stage 2 (solid line: centralized model, dashed line: distributed model).

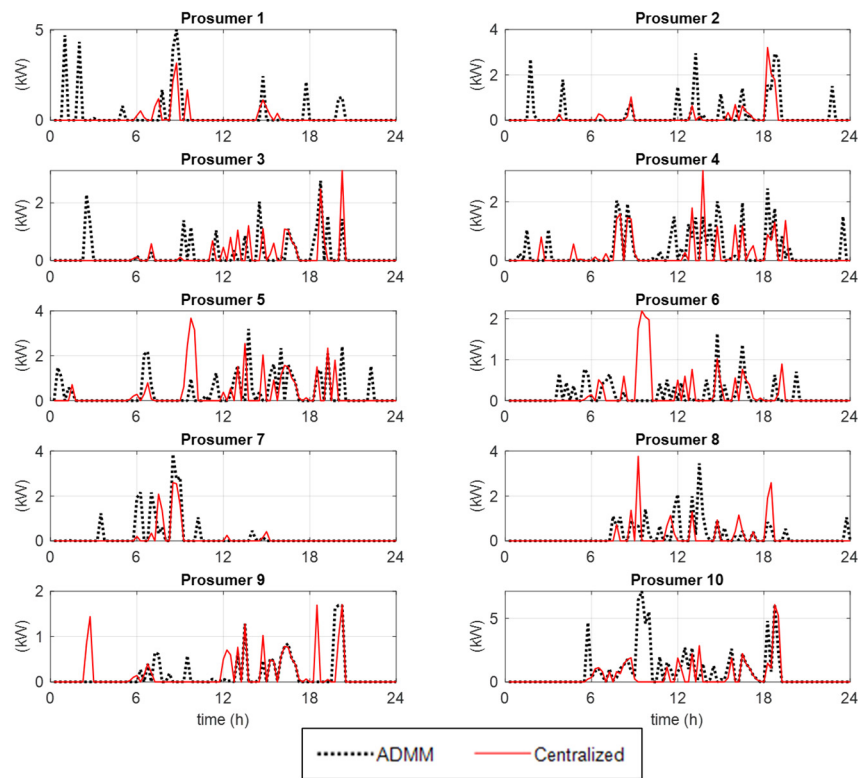


Figure 3-9. Comparison of the power flow from every prosumer when it sells to the others (excluding the utility grid) at the end of stage 2 for scenario 2 (solid line: centralized model, dashed line: distributed model).

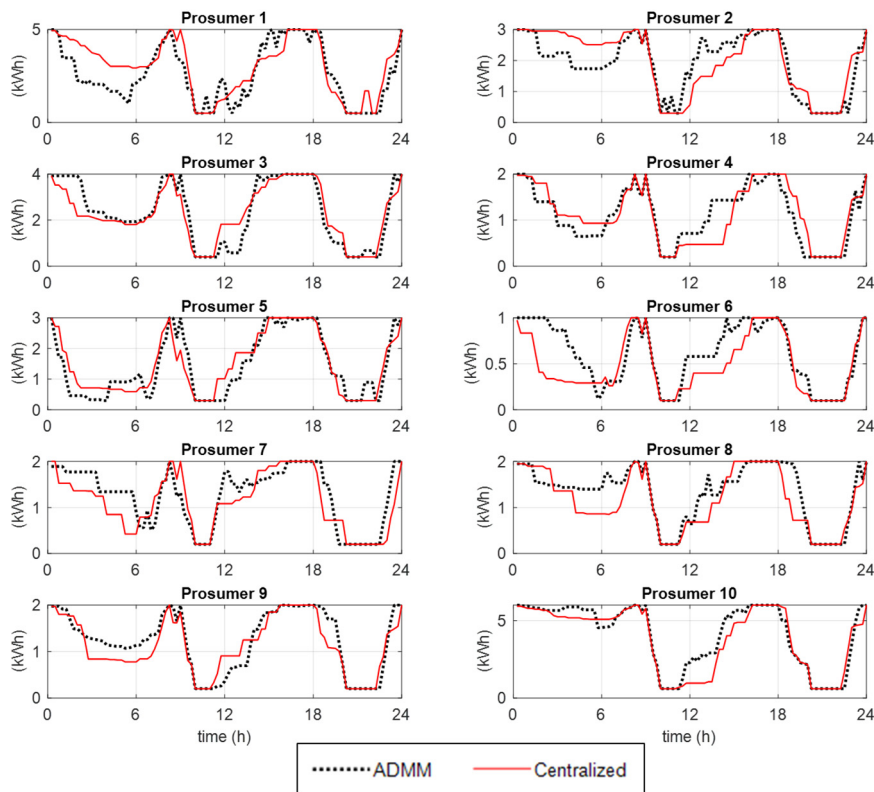


Figure 3-10. Battery SoE for each prosumer at the end of stage 2 for scenario 2 (solid line: centralized model, dashed line: distributed model).

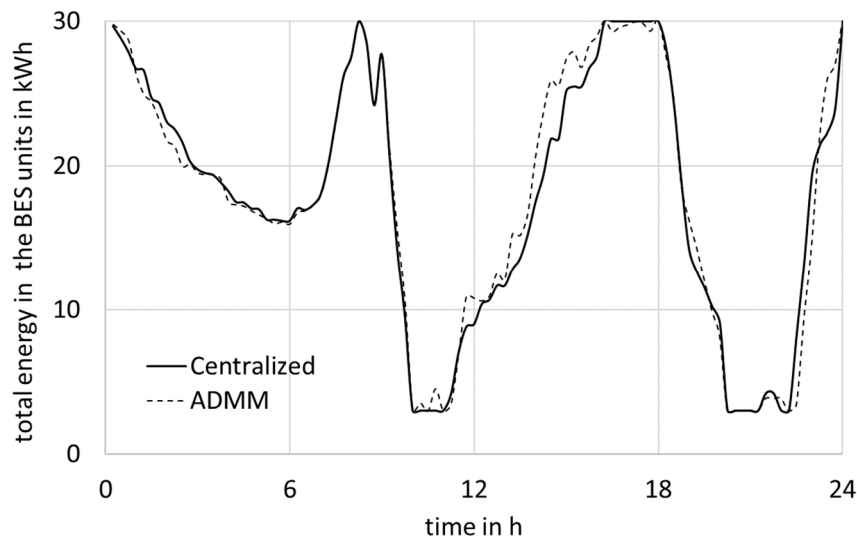


Figure 3-11. Comparison of the total energy in the batteries of the LEC obtained by the centralized and the distributed approach.

Figure 3-10 shows the profile of the SoE values of the BES units of all the prosumers in each period. Figure 3-11 shows the comparison between the profiles of the total energy contained in the BES units of the LEC as given by the centralized model and the distributed one.

As mentioned, the prices λ_i^t of each prosumer i that sells to other prosumers of the LEC are calculated in different ways in the two approaches. In the centralized MILP model, the prices are the Lagrangian multipliers of constraints (3.2). In the ADMM distributed procedure, the prices are updated at each iteration by (3.35). Although these differences, the profiles of the prices obtained by using the two models are similar for both the cases with and without the presence of BES units.

3.5. Conclusions of chapter 3

The chapter has presented a distributed optimization procedure for the day-ahead scheduling of a Local Energy Community with generation, loads and battery storage systems that incorporates the calculation of the losses and their allocation to each transaction.

The distributed approach is based on the ADMM algorithm and allows to limit the confidential information that each prosumer must provide to the other prosumers or a central coordinating unit.

The results obtained by using the proposed distributed procedure have been compared with those from a centralized approach based on a MILP model.

Both centralized and distributed approaches provide comparable results with an acceptable computation effort. The values of the objective function, the profiles of the power exchanged with the utility grid and the profiles of the energy stored in the batteries match.

The structure of the day-ahead scheduling procedures is consistent with the billing scheme and the metering units of the LEC.

Appendix C describes the developed algorithms.

4. Multi-stage stochastic optimization for the operation of local energy systems

4.1. Introduction

This part of the research deals with an electric local energy system with the presence of renewables, such as the power system of an industrial site or of a residential neighborhood. The considered system includes a PV unit capable to provide a significant part of the local energy consumption and it is also equipped with an energy storage unit to fully exploit the available renewable energy source even for the case of a limited capability of the external utility network to which the system is connected. The daily operation of the battery unit is addressed as an optimization problem with a 24h horizon, with the aim to minimize the electricity procurement cost. The inputs are the forecasting of the PV production and of the local loads.

In this chapter the stochastic optimization and the Monte Carlo approach are compared by using a mixed integer linear programming model of the local energy system, having the two following characteristics:

- 15 minutes time discretization, which appears more suitable for the energy management of the local system than the usual 1-hour time step;
- the use of the Kinetic Battery Model (KiBaM) for the representation of the battery state of charge, which is more detailed than the simple energy balance one.

In order to better adapt the day-ahead solution to the actual intraday operating conditions, the stochastic optimization problem is formulated as a multistage decision problem in which the battery output set points are decided at the beginning of the day and subsequently other three times during the day (every 6 hours). The five-stage stochastic optimization problem (where the decisions are taken at the beginning of each stage) needs a scenario tree model that is built by using the k -means clustering method.

The structure of the chapter is the following. Section 4.2 describes the linear programming model of the local energy system. Section 4.3 describes the multistage stochastic

programming (SP) procedure with the scenario generation and the construction of the scenario tree. Section 4.4 illustrates the test results and the comparison between the daily energy procurement costs calculated by using the five-stage stochastic optimization with those calculated by using the Monte Carlo solution (i.e., the average of the optimal decisions provided by the deterministic solution of each of the scenarios used for the construction of the tree). Section 4.5 concludes the chapter.

4.2. Model of the local energy system

We focus here on the solution of the day-ahead scheduling, which is in general associated with a real time control of the integrated PV-storage system, as dealt with in e.g., *Conte et al., 2017, Lilla et al., 2017*.

A typical aim of the energy management system is the minimization of the production costs associate with PV, storage units and the power exchange with the external network to feed the internal load in a time horizon T:

$$OF = \sum_{t \in T} (p_t^{imp} P_t^{imp} - p_t^{exp} P_t^{exp}) \Delta t \quad (4.1)$$

where:

- parameters p_t^{imp} and p_t^{exp} are the prices (in €/kWh) of the energy exchanged with the external grid (bought and sell, respectively);
- nonnegative variables P_t^{imp} and P_t^{exp} are the values of the power absorbed and injected into the external grid (in kW);
- parameter Δt is the 15-minutes time step (in h).

4.2.1. Model with a simple representation of the battery state of charge

The constraints of the model, to be described next, are the following for all the time intervals t .

$$P_t^{pv} - P_t^b + P_t^{grid} - P_t^{load} - L_t = 0 \quad (4.2)$$

$$P_t^b = P_t^c - P_t^d \quad (4.3)$$

$$P_t^c \leq (1 - u_t^b) M^b \text{ and } P_t^d \leq u_t^b M^b \quad (4.4)$$

$$-P_r^b \leq P_t^b \leq P_r^b \quad (4.5)$$

$$E_t^b = E_{\max} SOC_t \quad (4.6)$$

$$SOC_t = SOC_{t-1} + P_t^b \Delta t / E_{\max} \quad \forall t > 0 \quad (4.7)$$

$$SOC_{t=0} = SOC_0, SOC_{t=|T|} = SOC_{\text{end}} \quad (4.8)$$

$$SOC_{\min} \leq SOC_t \leq SOC_{\max} \quad (4.9)$$

$$L_t = L_t^d + L_t^c \quad (4.10)$$

$$L_t^c = \frac{1-\eta_c}{\eta_c} P_t^c \quad \text{and} \quad L_t^d = (1-\eta_d) P_t^d \quad (4.11)$$

$$P_t^{\text{grid}} = P_t^{\text{imp}} - P_t^{\text{exp}} \quad (4.12)$$

$$P_t^{\text{imp}} \leq (1 - u_t^{\text{grid}}) M^{\text{grid}} \quad \text{and} \quad P_t^{\text{exp}} \leq u_t^{\text{grid}} M^{\text{grid}} \quad (4.13)$$

$$-P_r^{\text{grid}} \leq P_t^{\text{grid}} \leq P_r^{\text{grid}} \quad (4.14)$$

where P_t^{pv} is the active power injected into the system by the PV unit, P_t^{load} is the power adsorbed by the internal loads; P_t^b is the battery power output (nonnegative P_t^c and P_t^d are the battery power outputs during charges and discharges, respectively); P_t^{grid} is the power exchanged with the external network (nonnegative P_t^{imp} and P_t^{exp} are the imported power and exported power, respectively), L_t are the losses of the battery converter (L_t^c and L_t^d are losses during charges and discharges); E_t^b is the energy level in the battery; SOC_t is the battery state of charge.

The definition of the parameters and, in parenthesis, the corresponding values adopted in the numerical tests are: P_r^b is the rated value of the battery output (630 kW), E_{\max} is the battery capacity (630 kWh); η_c and η_d are the converter efficiency factors for charges and discharges (0.95 and 0.97, respectively); P_r^{grid} is the maximum power that can be exchanged with the grid (1.5 MW), SOC_{\min} and SOC_{\max} are the minimum and maximum state of charge (0.1 and 1 p.u., respectively), SOC_0 and SOC_{end} are the initial value and the required final value of the state of charge (both assumed equal to 1 p.u. in the numerical tests).

The constraints represent: the power equilibrium (4.2); the power output of the battery with the big- M formulation in order to avoid concurrent charge and discharge (u_t^b is a binary variable and M_r^b is equal to P_r^b) (4.3)-(4.5); the energy stored and the state of charge of the battery (4.6)-(4.9); the losses in the battery converter (4.10)-(4.11); the exchange with the external grid (4.12)-(4.14), where u_t^{grid} is a binary variable and M^{grid} is equal to P_r^{grid} .

4.2.2. Model with the kinetic battery model

The refined model that includes the KiBaM replaces constraints (4.7) with the following constraints

$$E_t^b = q1_t + q2_t \quad (4.15)$$

$$q1_t = q1_{t-1} e^{-k \cdot \Delta t} + \frac{(k c E_{t-1}^b + P_t^b)(1 - e^{-k \cdot \Delta t})}{k} + \frac{k_{q1} P_t^b}{k} \quad (4.16)$$

$$q1_{t=0} = c SOC_0 E_{\max} \quad (4.17)$$

$$q2_t = q2_{t-1} e^{-k \cdot \Delta t} + E_{t-1}^b (1 - c)(1 - e^{-k \Delta t}) + \frac{k_{q2} P_t^b}{k} \quad (4.18)$$

$$P_t^c \leq \frac{1}{\eta_b} \frac{k c E_{\max} - k q1_t e^{-k \Delta t} - E_t^b k c (1 - e^{-k \Delta t})}{1 - e^{-k \Delta t} + k_{q1}} \quad (4.19)$$

$$P_t^c \leq \frac{1}{\eta_b} \frac{(1 - e^{-a \cdot \Delta t})(E_{\max} - E_t^b)}{\Delta t} \quad (4.20)$$

$$P_t^d \leq \eta_b \frac{q1_t k e^{-k \Delta t} + E_t^b k c (1 - e^{-k \Delta t})}{1 - e^{-k \Delta t} + k_{q1}} \quad (4.21)$$

where $k_{q1} = c(k \cdot \Delta t - 1 + e^{-k \Delta t})$, $k_{q2} = (1 - c)(k \Delta t - 1 + e^{-k \Delta t})$

The constraints represent: the definitions of readily available charge $q1_t$ and bound charge $q2_t$ (4.15)-(4.18); the battery power outputs limitations during charges and discharges phases (4.19)-(4.21). In Figure 4-1 the hydraulic equivalent scheme is represented.

The definition of the parameters and, in parenthesis, the corresponding values adopted in the numerical tests are the following: η_b is the batteries efficiency factor (p.u.) for charges and

discharges (0.9), k is the battery rate constant (9.51 h^{-1}), c is the battery capacity ratio (0.61), a is the battery maximum charge rate (2 A/Ah).

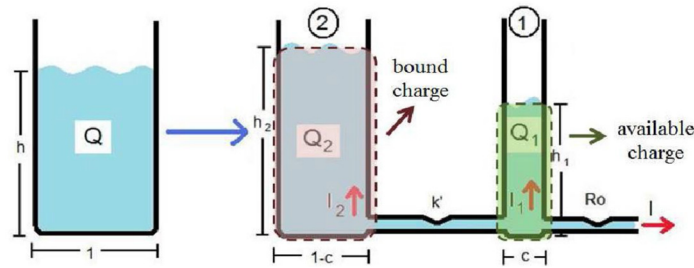


Figure 4-1. Kinetic Battery Model: hydraulic equivalent approach; adapted from Daniil *et al.*, 2015.

Figure 4-2 shows the results of a deterministic solution of the optimization problem for the considered test system, equipped with a 1 MW PV unit, a storage system of 630 kW and 630 kWh, and a local load with a power consumption of 1.5 MW.

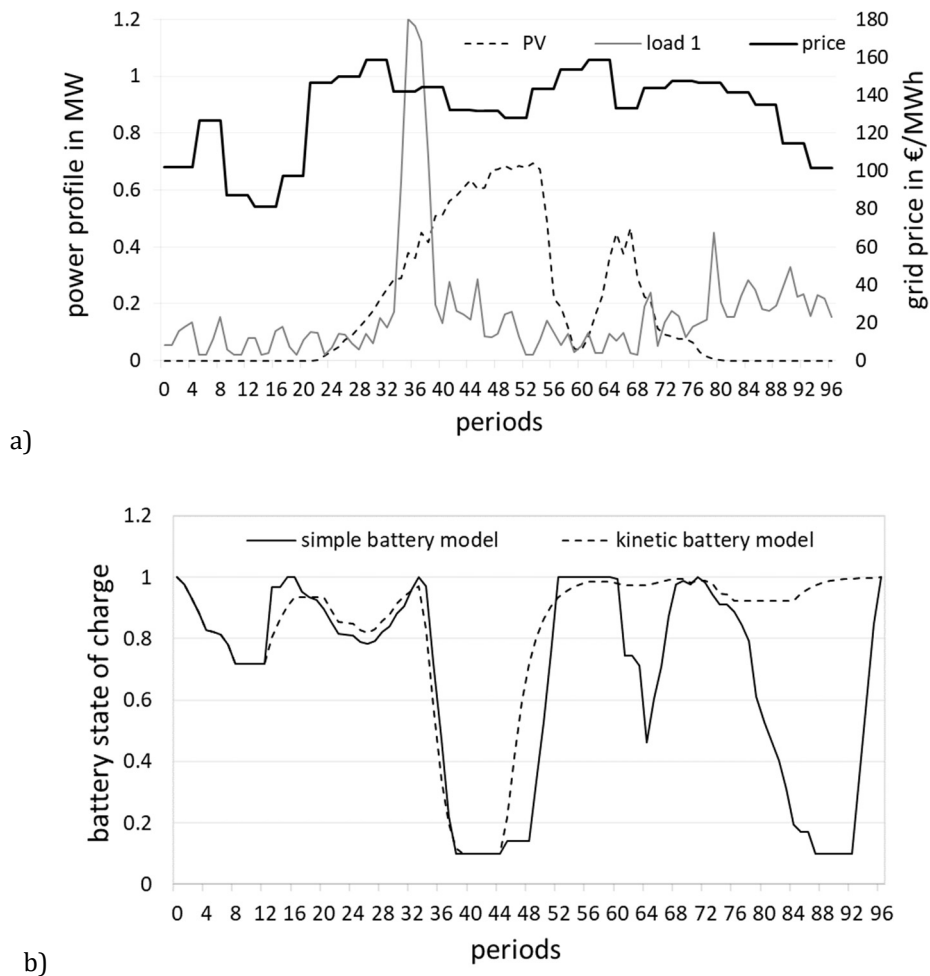


Figure 4-2. Deterministic solution: a) Profile of the PV production, load, and grid price; b) state of charge of the battery calculated by using the simple and kinetic model for profile load 1.

Figure 4-2 compares the results obtained by using the Kinetic energy model, which uses the parameters value indicated in *Bordin et al., 2017*, with those obtained by the simple battery model in which the state of charge is determined by the energy balance. The solution is completed by using Cplex in some tens of milliseconds for both models, with the OF values equal to € 36.70 for the simple model and equal to € 61.21 with the KiBaM.

4.3. Multi-stage stochastic optimization procedure

We assume that both the load profile and the PV generation are uncertain, whilst, to limit the complexity of the model, prices p_t^{imp} and p_t^{exp} are assumed known.

The decision variable is P_t^b . The decision is taken at the beginning of the day (which is the scheduling horizon) for all the periods of the first 6 hours and they are updated every 6 hours. The 6-hour periods represent the stages following the first one. The values of the other variables are calculated at the end of each stage, for all the periods of the stage.

Denoting the set of scenarios with Ω , the scenario index with ω , and the probability of scenario ω with π_ω , the deterministic equivalent of the multistage stochastic problem is the recourse model

$$\min_{P_t^b} \sum_{\omega \in \Omega} \pi_\omega \cdot OF_\omega \quad (4.22)$$

with constraints (4.2)-(4.14) for the simple battery model and with constraints (4.2)-(4.6) and (4.8)-(4.21) for the model that includes the KiBaM, other than the non-anticipativity constraints that represent the inability to anticipate the future by forcing the same decisions to be taken for scenarios with the same history.

In the following, we describe the procedures adopted for the generation of set Ω , for construction of the scenario tree that is used in the recourse model, and the intraday decision-making procedure to adapt the solution of the multistage stochastic problem to the actual PV generation and load request.

4.3.1. Generation of scenarios

In general, the number of scenarios for adequately describing this kind of stochastic process should be appropriately large. For the test, 200 scenarios are generated to limit the computational time required by the Monte Carlo method.

For the scenario generation, we have applied the procedure described in e.g. *Osório et al.*, 2015, which includes a Markov-process to represent the autocorrelation that exists between consecutive observations. Starting from the forecasted profiles P_t^{pv} and P_t^{load} , at first they are normalized by using the corresponding mean value and standard deviation; then, for each scenario ω , the normalized time series y_t^{pv} and y_t^{load} are given by

$$\begin{aligned} z_{\omega,t} &= x_{\omega,t} + y_t \\ x_{\omega,t} &= \phi \cdot x_{\omega,t-1} + \varepsilon_{\omega,t} \end{aligned} \quad (4.23)$$

where ϕ is the one-lag autocorrelation parameter, assumed to be equal to 0.999, and $\varepsilon_{\omega,t}$ is a Gaussian white noise with mean zero and standard deviation $\sqrt{1-\phi^2}$. The PV production and load profiles for each scenario ω ($P_{\omega,t}^{pv}$ and $P_{\omega,t}^{load}$) are obtained by applying the inverse transform method assuming a normal distribution, with the constraint that both profiles cannot be negative and that the difference between each profile and the corresponding forecast should not exceed 20% (in all the periods for the load and 75% of the periods for PV production).

Figure 4-3 shows the scenarios for the loads and the PV generated according to the above-mentioned criteria.

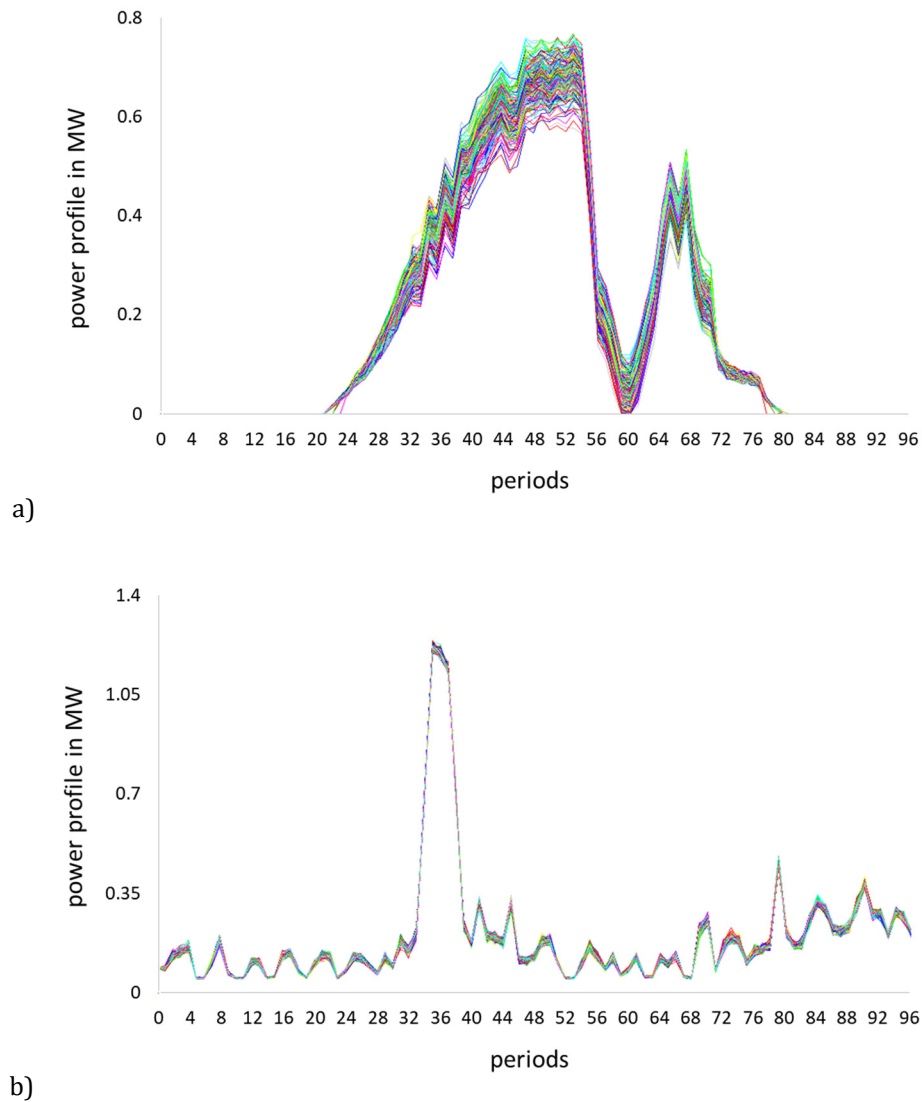


Figure 4-3. Scenarios: a) PV production; b) load.

4.3.2. Construction of the scenario tree

Each of the generated scenarios is assumed to be equiprobable and it is defined by the normalized difference between the PV production and the load:

$$\xi_{\omega,t} = \frac{P_{\omega,t}^{pv} - P_{\omega,t}^{load}}{P_t^{pv} - P_t^{load}} \tag{4.24}$$

The scenario tree is built by the consecutive application of the *k*-means clustering method, as described in e.g. *Pranevicius & Šutiene, 2007*. The main steps of this method are the following.

At stage $s=1$ (that includes only period $t=0$), all scenarios have the same value of parameter, i.e. $\xi_{\omega,t=0} = \xi_0$

At stage $s=2$ ($t=1\dots24$), the set of individual scenarios is divided in the predefined number K of desired clusters C_s^k (in the numerical tests, we compare the results obtained by using $K=3$ or $K=4$). At first, the initial K centers $\bar{\xi}_t^k$ are randomly selected; then each scenario $\xi_{\omega,t}$ is assigned to cluster C_s^k so to minimize the dissimilarity measure

$$d(\xi_{\omega,t}, \bar{\xi}_t^k) = \sum_{t \in T_s} \|\xi_{\omega,t} - \bar{\xi}_t^k\|_2 \quad \forall k = 1 \dots K \quad (4.25)$$

where $\|\cdot\|_2$ indicate the Euclidean distance and T_s is the set of periods in stage s . After, the center of each cluster is updated as the mean of all the scenarios assigned to the cluster and the procedure is repeated until the centers of the clusters are not modified in two consecutive iterations.

The probability of each cluster at the considered stage π_s^k is the sum of the probabilities of the individual scenarios belonging to the cluster. All the scenarios of the same cluster are replaced by the relevant center, i.e. $\xi_{\omega,t} = \bar{\xi}_t^k \quad \forall t \in T_s$ if $\xi_{\omega,t} \in C_s^k$.

At the stages following the second one, the k-means clustering algorithm is applied independently to each cluster defined in the previous stage.

The above-described procedure generates the scenario tree consisting, at each stage s , of nodes $\bar{\xi}_{t \in T_s}^k$ with the associated probabilities and the branches that connect nodes at different stages. The scenario tree used in the numerical tests for $K=3$ is shown in Figure 4-4.

The solution of the recourse model provides the optimal value of the decision variable in each node of the scenario tree at stage 1 (i.e. at $t=0$) and the beginning of each of the following stages from 2 to 5 (i.e., $t=24$, $t=48$, and $t=72$). The values of all other variables are calculated also at the end of each stage.

4.3.3. Intraday decision-making procedure

The solution of the recourse model provides multiple possible decisions at each stage following the first one (i.e., during the day). Therefore, for the actual operation, a decision-making procedure is needed for the choice of the most appropriate decision at each stage among those indicated by the stochastic problem solution, on the basis of the current PV generation and load.

At stage $s=2$, the decision-making procedure finds the scenario of the tree that is the most similar to the profile of the difference between PV generation and load in the previous 6 hours, on the basis of the Euclidean distance. Then it decides the set point values of the battery power output for each 15-minutes time intervals of the following 6-hours.

At stages $s=3$ and $s=4$, the decision-making procedure finds the scenario of the tree that is the most similar to the profile of the difference between PV generation and load in the previous 6 hours, only among those directly connected to the node chosen in the previous stage.

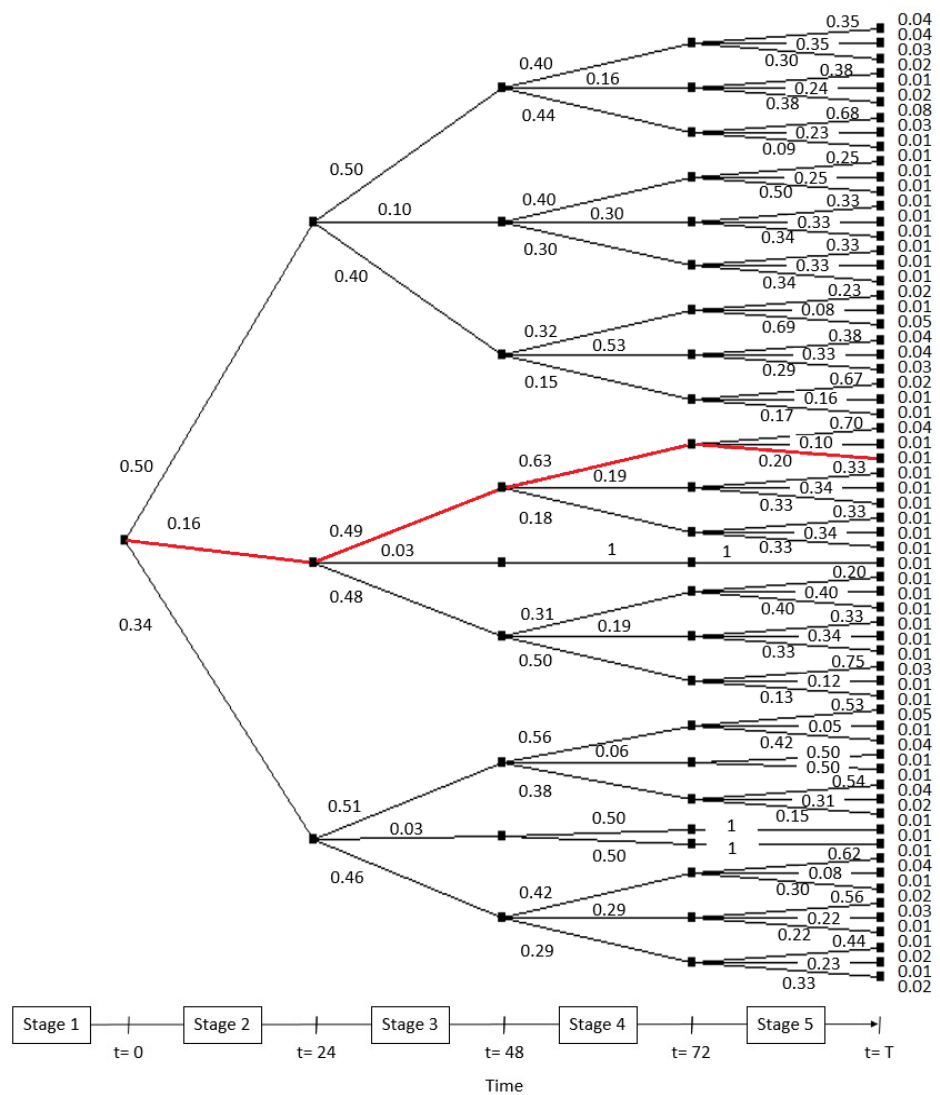


Figure 4-4. Scenario tree obtained for 200 initial scenarios and 3 centroids. In red, an example of the solution provided by the decision-making function.

4.4. Numerical tests

The optimization procedures have been implemented in AIMMS Developer and tested by using the Cplex V12.8 MIP solver on 2-GHz processors with 8 GB of RAM, running 64-b Windows.

Table 4-1 compares the OF values of the stochastic solution of the two models (the one simple battery representation and the one including the KiBaM) by using the scenarios trees obtained through the k -means clustering procedure (with 3 and 4 centroids) applied to 200 initial equiprobable PV generation and load profiles.

TABLE 4-1 – SP SOLUTIONS AND METRICS FOR THE CASE WITH A 630 KWH BATTERY.

Battery model	Simple		KiBaM	
	3	4	3	4
Number of centroids	3	4	3	4
OF (€)	38.02	38.25	61.67	61.80
VSS (€)	2.59	2.84	1.11	1.12
$EVPI$ (€)	0.85	1.08	0.47	0.56
Number of scenarios in the tree	64	139	64	139
Solution time (s)	1.54	2.97	3.47	8.26

Table 4-1 also shows the Value of Stochastic Solution (VSS) and the Expected Value of Perfect Information ($EVPI$), which are widely used metrics of the performance of using SP models (Escudero *et al.*, 2007).

VSS is the difference between the expected value solution (EEV) and the stochastic solution (i.e., the OF value). EEV is obtained by a two-step calculation: at first, the values of P_t^b for each t are given by the solution of the deterministic model obtained by replacing all random variables by their expected values; then, these P_t^b are set as a fixed parameters and EEV is given by the solution of the stochastic problem.

$EVPI$ is the difference between the stochastic solution and the wait and see (WS) solution. WS is the expected value of the deterministic solutions of each scenario in the tree.

As expected, the higher the number of centroids the longer the computational effort due to the enlargement of the tree, as shown by the comparison of the solution times and the number of scenarios in the trees reported by Table 4-1 for $K=3$ and $K=4$. However, a more detailed

clustering increases the *VSS*, even with an initial set of scenarios not very large with respect to the final dimensions of the tree.

Table 4-1 shows that the use of the more refined model of the battery increases both the *OF* values and the computation time, as expected.

We have performed the same calculations also for a smaller battery (315 kWh instead of 630 kWh). The results are summarized in Table 4-2 and, they show a significant increase of *OF* values, since the battery effect is less noticeable, and a decrease of both *VSS* and *EVPI*.

TABLE 4-2 – SP SOLUTIONS AND METRICS FOR THE CASE WITH A 315 KWH BATTERY.

Battery model	Simple		KiBaM	
Number of centroids	3	4	3	4
<i>OF</i> (€)	65.97	66.13	80.69	80.80
<i>VSS</i> (€)	1.95	2.09	0.98	0.98
<i>EVPI</i> (€)	0.48	0.63	0.43	0.52
Solution time (s)	1.17	3.47	2.97	7.39

As mentioned, we compare the SP approach with the Monte Carlo simulation technique, in which the deterministic model is solved for each initial scenario and then the P_t^b values are set equal to the average of the corresponding values obtained by the deterministic solutions.

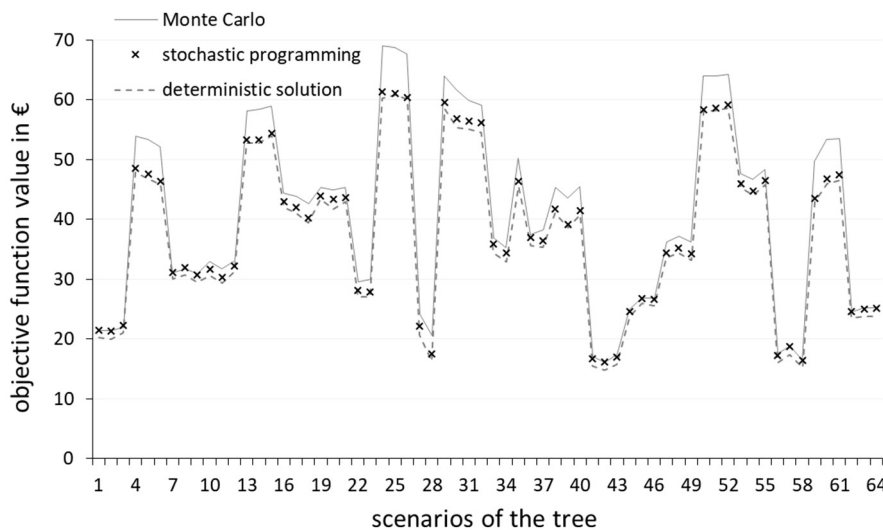


Figure 4-5. Comparison between the values of the objective function for each scenario of the tree obtained by applying the *k*-means clustering with 3 centroids (630 kWh battery).

Figure 4-5 shows, for each scenario in the tree obtained with 3 centroids, the comparison between the OF values calculated by using the Monte Carlo decisions and those given by the intraday decision-making procedure based on the SP solution. The figure also includes the OF values of the deterministic solutions. SP provides in general better results with respect to Monte Carlo and this is confirmed also by Figure 4-6 that shows the same comparison for 50 scenarios different from those included in the initial set. For the case of the small tree obtained by using 3 centroids the adoption of the SP approach needs also a shorter solution time, since the Monte Carlo simulations require around 5 s for the case of the simple battery model and 18 s if KiBaM is adopted, without parallel computing.

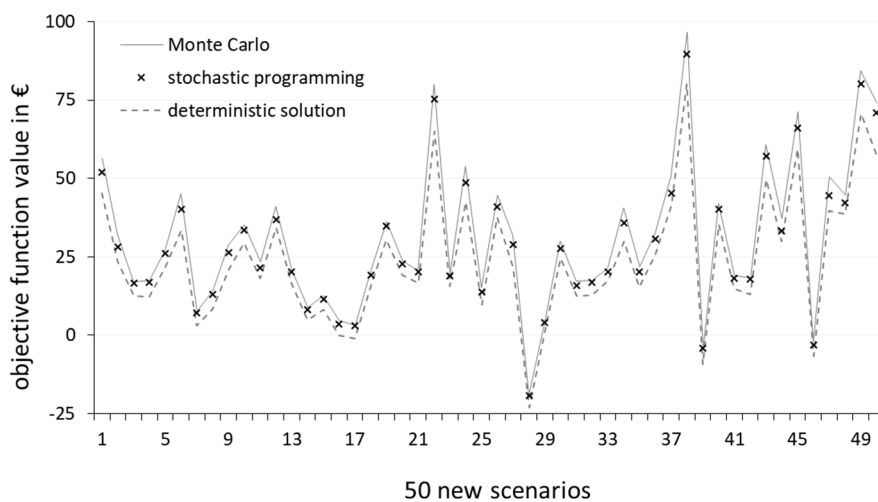


Figure 4-6. Comparison between the values of the objective function for 50 new scenarios (630 kWh battery).

Table 4-3 shows the average values of the following differences for the scenarios of the tree, for the initial set of 200 scenarios, and for 50 scenarios different from those of the previous set:

- SP-MC: difference between the OF values given by the intraday decision-making procedure and the Monte Carlo solution;
- SP-WS: difference between the OF values given by the intraday decision-making procedure and the deterministic solution.

The results of Table 4-3 show the advantage of using the SP and the benefit of a more accurate clustering procedure. We have repeated the comparisons also for the case of the 315-kWh battery and the results, shown in Table 4-4, confirm in general the advantages of using 4 centroids although the average differences are smaller than in Table 4-3.

TABLE 4-3 – COMPARISON BETWEEN SP AND MONTE CARLO SIMULATIONS AND BETWEEN SP AND DETERMINISTIC SOLUTIONS (630 KWH BATTERY).

Battery model		Simple		KiBaM	
Number of centroids		3	4	3	4
Scenarios tree	SP – MC (€)	-2.51	-2.55	-0.71	-0.69
	SP – WS (€)	0.97	1.13	0.55	0.60
Set of initial scenarios	SP – MC (€)	-2.05	-2.47	-0.23	-0.34
	SP – WS (€)	5.17	2.70	1.81	1.70
Set of new scenarios	SP – MC (€)	-2.28	-2.29	-0.26	-0.24
	SP – WS (€)	4.85	4.84	1.91	1.92

TABLE 4-4 – PERFORMANCE COMPARISON FOR THE BATTERY OF 315 KWH

Battery Model		Simple		KiBaM	
Number of Centroids		3	4	3	4
Scenarios Tree	SP – MC (€)	-1.61	-1.58	-0.60	-1.58
	SP – WS (€)	0.56	0.66	0.49	0.55
Set of initial Scenarios	SP – MC (€)	-1.13	-1.44	-0.26	-0.35
	SP – WS (€)	2.21	1.91	1.60	1.50
Set of New Scenarios	SP – MC (€)	-1.12	-1.14	-0.30	-1.14
	SP – WS (€)	2.81	2.79	1.67	2.79

Finally, in order to show the performance of the SP approach under different conditions, the results obtained by using a new set of load scenarios of Figure 4-7 (that replace those of Figure 4-3-b) are summarized in Table 4-5 (*OF* values and metrics) and Table 4-6 (comparison between SP and Monte Carlo simulations and between SP and deterministic solutions over several sets of scenarios).

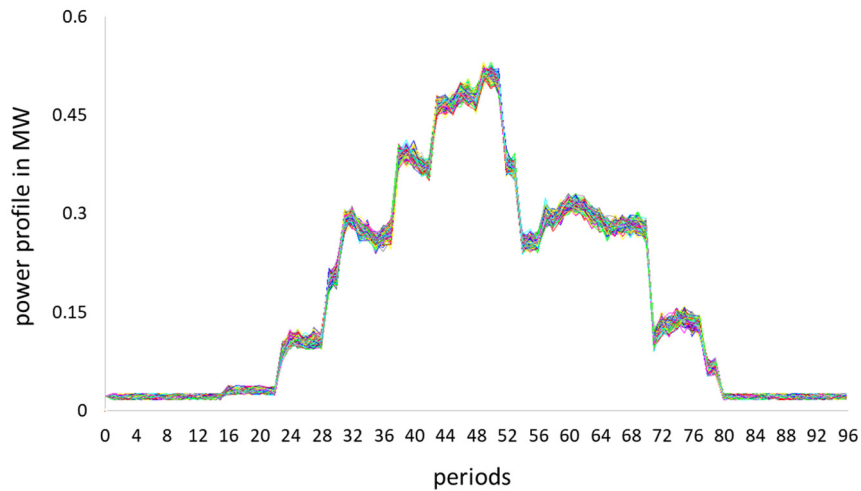


Figure 4-7. Scenarios obtained for a different load profile forecast.

Table 4-5 – SP solutions and metrics for the case with a 630 kWh battery and load scenarios of Figure 4-7.

Battery Model	Simple		KiBaM	
	3	4	3	4
Number of Centroids	3	4	3	4
<i>OF</i> (€)	-2.94	-2.33	9.54	9.84
<i>VSS</i> (€)	1.75	2.52	1.93	2.66
<i>EVPI</i> (€)	2.66	3.19	0.96	1.19
Number of scenarios in the tree	74	169	74	169
Solution time (s)	1.53	4.45	3.91	8.87

TABLE 4-6 – COMPARISON BETWEEN SP AND MONTE CARLO SIMULATIONS AND BETWEEN SP AND DETERMINISTIC SOLUTIONS (630 kWh BATTERY AND LOAD SCENARIOS OF FIGURE 4-7).

Battery Model		Simple		KiBaM	
Number of Centroids		3	4	3	4
Scenarios Tree	SP – MC (€)	-1.37	-1.84	-1.33	-1.94
	SP – WS (€)	3.71	3.37	1.29	1.14
Set of initial Scenarios	SP – MC (€)	-0.28	-1.06	-0.84	-1.40
	SP – WS (€)	7.19	6.41	4.45	3.89
Set of New Scenarios	SP – MC (€)	0.64	-0.39	-0.83	-1.30
	SP – WS (€)	9.35	8.33	4.50	4.03

The results confirm the advantages of the SP. Only in the case of the 50 new scenarios and the simple battery model using 3 Centroids, the average performance for the stochastic solution is higher than the one obtained by using the Monte Carlo solution. The use of 4 centroids

increases the VSS and allows to reach improved results with respect to the Monte Carlo technique.

4.5. Conclusions of chapter 4

Multistage SP represents an attractive method for the day ahead scheduling in local energy systems and provides improved results with respect to the application of the Monte Carlo method.

The construction of the scenario tree needs to be addressed properly. The k -means clustering provides appropriate results even with a limited number of centroids. The computational effort is reasonable for the considered five-stage SP problem.

The SP approach is also applicable to models that include a detailed representation of the battery under the assumption that the mixed integer linear programming characteristics of the model are preserved.

Appendix C describes the developed algorithms.

5. Conclusions

The thesis has dealt with EMS for MGs. Several models have been developed and implemented in the AIMMS software platform.

As described in chapter 2, a MILP model for the real time operation of a low voltage network, specifically developed to be computationally compatible with its use in energy management systems, has been presented and validated to be integrated in the EMS of the experimental network GridLab district of the HES-SO Valais-Wallis in Sion, Switzerland. The implementation of the developed optimization algorithm in the supervisory control and data acquisition (SCADA) architecture of the experimental system is included.

The model includes the characteristics of: power lines of the LV network, non-dispatchable loads and generators, dispatchable generators and storage units. Decision variables are:

- active and reactive power by the dispatchable generators and storage units,
- on-off state of generators and storage units with limited number of on-off operations.

The multi-objective function includes: costs associated with active/reactive energies absorbed and injected into the grid, costs associated with active/reactive energy production by dispatchable DG units and penalties associated with maximum and minimum voltage violations (first and second limit).

The MILP model represents single-phase and three-phase small loads, distributed generation units, and storage systems. It takes into account the unbalanced operation of the LV network and the presence of the neutral wire.

The comparison between the model results and the measurements gathered by means of the GridLab experimental network shows that the accuracy of the implemented model is reasonably adequate.

The day-ahead scheduling of a local energy community (LEC) with the optimization procedure in presence of local generation, loads and battery storage systems that includes the calculation of the losses and their allocation to each transaction is presented in chapter 3.

The results obtained by using a centralized approach based on a MILP model are compared with those of a distributed optimization procedure that avoids the presence of a central coordinator. The distributed approach is based on the ADMM algorithm and allows to minimize the private information that each prosumer is required to provide to the other prosumers.

For the typical number of prosumers in a LEC, both centralized and ADMM-based distributed approaches provides comparable results with an acceptable computation effort.

The structure of the day-ahead scheduling procedures is consistent with the billing scheme and the metering units of the LEC.

Chapter 4 has considered the uncertainty associated with the load and renewable generation forecasts. Multistage stochastic programming (SP) represents an attractive method for the day ahead scheduling in local energy systems and provides improved results with respect to the application of the Monte Carlo method.

The construction of the scenario tree needs has been properly addressed. The *k*-means clustering provides appropriate results even with a limited number of centroids. The computational effort is reasonable for the considered five-stage SP problem.

The SP approach is also applicable to models that include a detailed representation of the battery (KiBaM model) under the assumption that the MILP characteristics of the model are preserved.

It is worth mentioning that, since LV feeders may include not only non-dispatchable resources but also dispatchable ones (e.g., heat and power cogeneration units) the models described in chapter 3 and 4 can be extended to include dispatchable DG and also to take into account reactive power flows. This can be reasonably considered the subject for future work.

Furthermore, the SP approach (described in chapter 4) can be included in the distributed procedure, based on the ADMM method.

Another interesting investigation can be focused on the experimental validation of the consensus distributed approach by using low cost hardware technologies for the control and communication.

Appendix A : Energy storage systems in distribution networks

A.1. Introduction

Several type of Energy Storage System (ESS) are used in electrical power systems. The most common ones were examined by the IRENA agency (*IRENA, 2015*) and can be catalogued in:

- Pumped hydro storage;
- Compressed air energy storage;
- Flywheel energy storage;
- Lithium-ion batteries;
- Lead-acid batteries;
- Flow batteries;
- High temperature batteries.

Among the possibilities mentioned, the most evolving sector is certainly the one of the batteries. The speed at which stationary storage devices are improving will allow for a significant drop in prices to 2030 (more than halved compared to today's).

This cost-cutting will allow the batteries to compete with the pumping hydroelectric, the number one technology today in the world energy storage market and small-scale distributed applications could increase considerably, thereby producing a greater penetration into the renewable energy market (Figure A-1).

In this context, the most promising technologies on the market today are lithium-ion batteries, high-temperature batteries (based on sodium-sulfur cells and sodium-metal chlorides) and flow batteries. For these three categories, reductions in installation costs vary from 54% to 66% (Figure A-2).

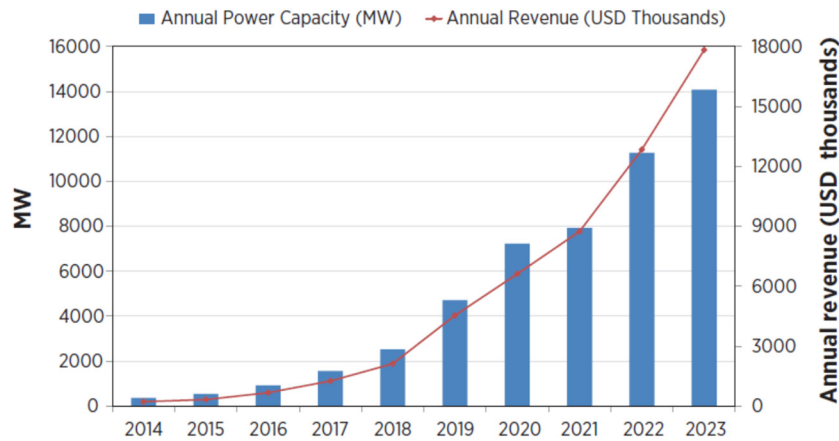


Figure A-1. Global capacity and revenues forecast for electro-chemical storage, utility scale applications. Adapted by IRENA, 2015.

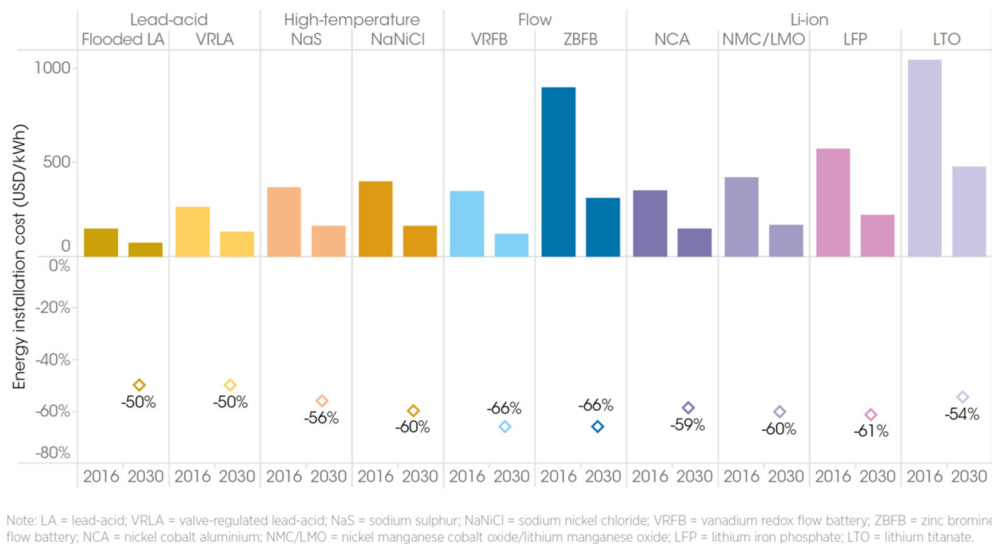


Figure A-2. Main types of battery, evolution costs. Adapted by IRENA, 2017.

The downward trend is clear already today, as evidenced by the case of lithium batteries. These devices, in the transportation sector, have visibly reduced prices in the space of 6 years (minus 76% from 2010 to 2016). Stationary storage downward trend has slower times than electric mobility, but development in the two compartments is inextricably linked. The growth in the use of lithium-ion batteries in electrical mobility (EV) and in the transportation sector in general in the next 10-15 years will help to reduce the cost of stationary applications (in particular electrical energy systems); the electric mobility will also open new opportunities for cars to provide services from vehicle to grid (V2G), helping to feed a virtuous circle renewable-storage.

It is estimated that by 2030 the life of lithium-ion devices will have been increased by 50 percent, raising the number of charge-discharge cycles by more than 90%. Consequently, the prices for these plants could fall below 200 dollars per kilowatt. For this reason, the stationary battery-based storage sector should move from 2 GW, currently installed worldwide, to over 175 GW by the end of the next decade, while at the same time pumping hydroelectric should reach 235 GW.

A.2. Technologies

A very important part in the ESS field is the electrochemical storage batteries. The most common technologies used in the production of batteries are the following:

- acid lead accumulators;
- lithium-ion battery;
- sodium-nickel chloride battery;
- sodium-sulphur battery;
- nickel-cadmium battery;
- electrolyte circulating Redox battery of vanadium (VRB).

In the following part, the scientific evolution of the technology in this sector is represented: some non-exhaustive insights will then be given, especially considering the rapid development of the segment.

A substantial cost reduction could be achieved by improving technologies based on less noble elements of lithium. In *Minah Lee, Jihyun Hong, Jeffrey Lopez, Yongming Sun, Dawei Feng, Kipil Lim, William C. Chueh, Michael F. Toney, 2017* a sodium device is proposed. The device can store the same amount of energy as the best lithium batteries and it is convenient for all those applications where the weight factor has little relevance (for example in stationary storage). In addition, this type of battery not requires the necessary lithium precautions, to avoid explosions or short circuits. There is an improvement in the production process by sodium and Mio-Inositol (the organic compound present in the salt) that allows the electrons flow and greatly increases the performance of the battery. The prototype of the built-in sodium battery has a reversible capacity of 484 mAh/g, an energy density of 726 Wh/kg, an energy efficiency of more than 87% and a good preservation of the cycle. Comparing lithium and sodium on the economic front, the latter would save up to 80 percent of the costs.

With regard to the technologies suitable both for stationary applications and electric-mobility (characterized by rapid recharge times and low specific weight) the Super Charge ion Battery (SCiB) technology based on lithium-ions (*Kobayashi, 2014*) is a promise. The device grants in the structure a titanate-lithium anode, almost inert material (as a substitute of graphite) and it is able to show good recharge performance and greater safety. For the positive electrode a titanium-niobium oxide is used. The process allows to organize this material in a crystalline structure able to store the lithium ions more efficiently. As indicated in the experimental results, SCiB would be able to keep more than 90% of its capacity after 5,000 charge-discharge cycles, with a fast charging time (six-minute).

An innovative type of electro-chemical battery for electric-mobility sector is the Li-Oxygen technology - Semi-Solid flow Li-O₂ battery (SFLOB) - (*Soavi et al., 2017*). The solid-flow battery can store up to five times the energy of a common battery type and combines the following technologies in the same device:

- high voltage operation (2, 5-3.0 V);
- exceptional high charge capacity (> 500 mAh/g total weight of cathode);
- high discharge rate;
- energy density from 5 to 10 times higher than conventional.

Potentially, the battery allows an electric car to reach the same autonomy of a conventional car; recharge of the battery can be done simply replacing the electrolyte fluid (which is also the cathode).

A.3. Applications

In the literature there are numerous studies and applications related to the integration of ESS in the distribution and transmission networks and in MGs with the presence of renewable sources.

The inclusion of a battery in a LV MG, including management algorithm for optimization of the network, is described in *Adinolfi et al., 2017*. It is carried out at the Department of Economics of the University of Genoa. The MG includes a 20 kWp PV system on the roof of the building and a 12 kWh ESS accumulator located in the MV/LV substation. The MILP optimization foresees the maximization of the production of the microgrid and, at the same time, the minimization of PV production curtailment, considering the PV forecast and the

measurements in the field for the real time operations. The program results are the active power of the MG and the *SoC* of the ESS; the algorithm is implemented in the Distribution Manager System installed on the MG.

In *Lilla et al., 2017* a distributed ESS combined with DG for each prosumer in a LV MG is represented. The MILP optimization model for the real time operation of the MG with various feeders provides for the connection of traditional users and consumer (with conventional generation, PV and batteries for each prosumer). The algorithm returns the dispatchable active and reactive power of each generator. The objective function to minimize is composed of various costs: active and reactive energy exchange with the DSO, the energy provided by DG and ESSs and the penalties for exceeding the voltage tolerance in two separate thresholds ($\pm 3\%$ and $\pm 10\%$ of V_n). The model allows to weigh the costs and the penalties in order to promote the minimization of one or more variables. Experimental validation was performed at the GridLab (University of Western Switzerland).

A relevant example of a ESS (lithium-titanium battery group with a capacity of 500 kWh) connected to the MV/LV substation, with power flows control in the MV feeders, is provided in *Sossan et al., 2016*. The model represents a method for the day-ahead scheduling (Dispatch plan). It is based on the control of the *SoC* with forecast of loads and PV as input and dispatching power as a decisional variable. For the real time operation, the dispatch plan is corrected using an MPC algorithm to recalculate the active power exchanged between ESS and MG.

The inclusion of an ESS in a transmission system would bring significant advantages. In *Fiorini et al., 2017* the optimum size of the storage in a transmission line (with high penetration of non-programmable renewable sources) is analyzed. Production costs are optimized in a 24-hour horizon. The study shows that an adequate size of the batteries can be a key step for a more flexible and smarter use of the storage in the transmission network. The analysis shows that the choice of the place of the storage does not have a significant influence on the duration of the overload of the lines. Furthermore, the introduction of the storage seems to reduce considerably the congestion of the critical corridors. The proposed method shows that the ESS placed near the generation from renewable source does not automatically imply an improvement in the overload of the lines. Better effects are achieved with a placement in the critical nodes.

In the field of the electric-mobility, *Barsali et al.*, 2016 analyzes the inclusion of a stationary storage in a vehicle service charging station, assuming that the recharge of the vehicles is excluded or included in the optimization system. The result is appreciable, especially when the vehicle recharging process is mainly concentrated during the hours of the day. Moreover, when the process is optimized by the charging station, the stationary storage contribution is abolished using the batteries installed on the vehicles.

No shortage studies on the ageing and wear of batteries, to understand both the adequacy of the main technologies for stationary uses, and to develop models that can preserve the investment to introduce the storage in the network.

In *Ceraolo et al.*, 2016 an experimental evaluation of "high power" and "super high power" lithium batteries, even in comparison with other types of storage such as supercapacitors, is performed. The study considers the charge and discharge speeds and the working temperatures of the battery. It is demonstrated that the capacity of these types of batteries remains unchanged during the execution of hundreds or thousands of micro-cycles, thus confirming the vocation of these devices for stationary power applications.

Considering the wear of the batteries in the network management model, in *Bordin et al.*, 2017 a MILP optimization model of an island microgrid is presented. The microgrid is composed of users, photovoltaic and Pb-Acid battery. The procedure is developed taking into account the wear of the battery in various models. As the wear cost increases, the models foresee the reduction of the discharge depth or the reduction of the charge-discharge cycles of the battery.

In *Foggo & Yu*, 2017 a realistic degradation of the battery cycle is used to examine the profitability of the storage and to try to increase profits by mitigating this phenomenon. An approximate linear degradation model is developed for the co-optimization, considering the ancillary services provided to the network. The simulation shows that 29% of the value of the storage system is lost due to the degradation phenomenon and with the co-optimization model the loss is reduced to 3.3% (corresponding to about one year more battery life).

Appendix B : GridLab

B.1. Configuration

GridLab experimental MG is composed of four feeders reproducing LV underground or overhead lines, 2-km-long each one (Figure 2-1). ABB ACS800 industrial drives emulate the three-phase controllable prosumers (12 in total). Electrical parameters of each prosumer and of each feeder are monitored by Siemens-Sicam P power meters. Each pair R_L - X_L is realized by actual resistors and inductors whose values shows in Table B-1 and reproduce the electrical equivalent of 500 m length of 95-mm² low-voltage line. More specifically, feeder A, C and D reproduce overhead lines (OH) whereas feeder B reproduces a buried line (UG). Each feeder is powered by a buried line and section 3x6 mm².

TABLE B-1 – MEASURED ELECTRICAL PARAMETERS OF THE FEEDERS.

Feeder	R_L , m Ω	X_L , m Ω	Section, mm ²	Lenght, m	Line Type
A	150	141.4	95	500	OH
B	150	40.2	95	500	UG
C	150	141.4	95	500	OH
D	150	141.4	95	500	OH

The MG system control is developed and assigned to a Python modular program. The standard for the communication between prosumers and central control is an Ethernet IEC 61850-90-7 MODBUS RTU.

B.2. Preliminary operation

The preliminary operation to validate the model has been carried out using a simplified configuration of the GridLab District, with a single feeder and without AVR, schematically illustrated in Figure B-1. The AIMMS optimization program model has been configured in term of buses and branches (with measured lines parameters, as shown in Table B-1).

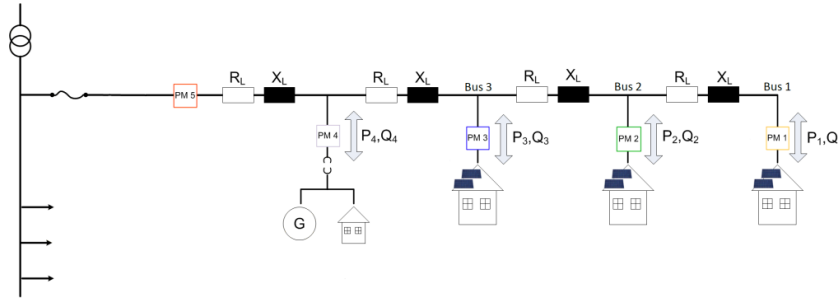


Figure B-1. Simplified topology used for preliminary operation.

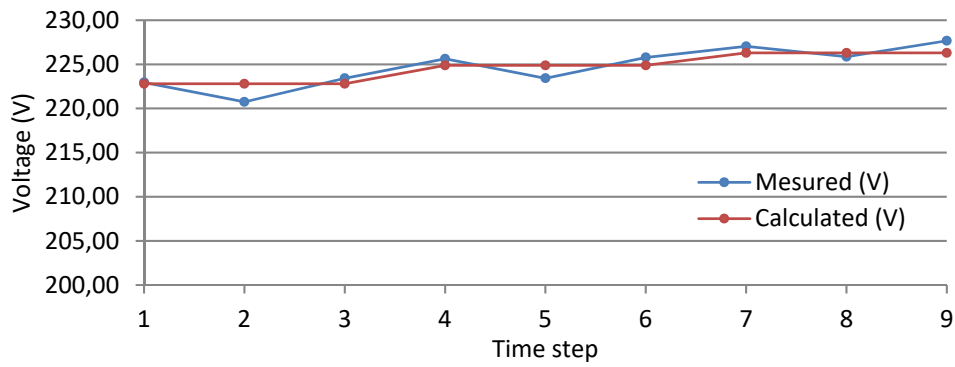


Figure B-2. Voltage profile in the feeder "B".

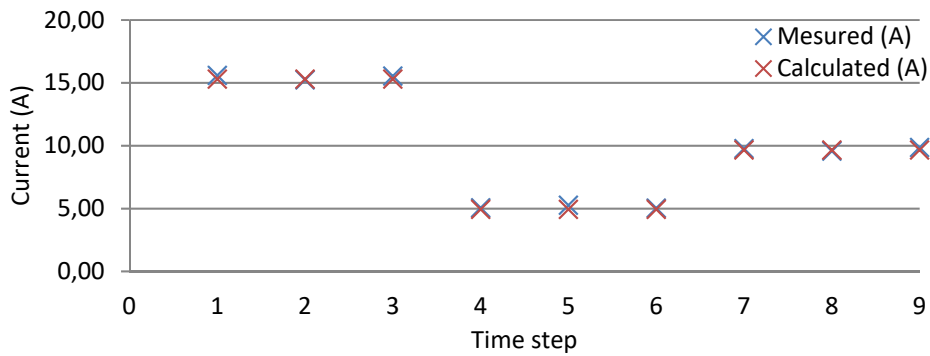


Figure B-3. Currents in the prosumers 1, 2 and 3, feeder "B".

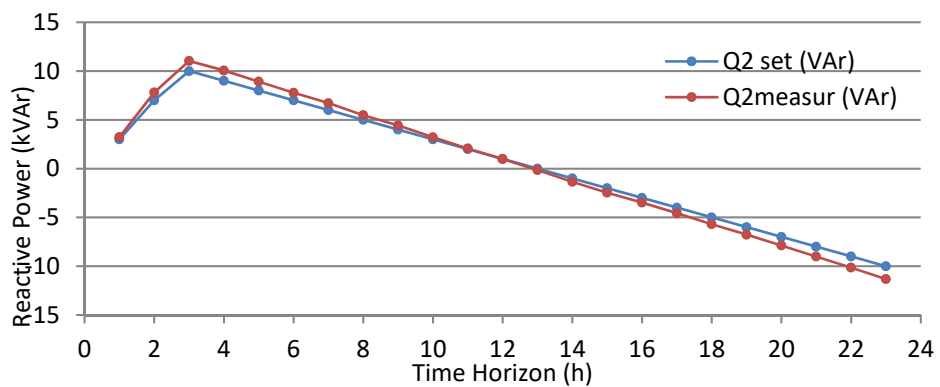


Figure B-4. Reactive power Q , set and measured values. Prosumer 2, feeder "D".

Some results of preliminary tests are reported in Figure B-2., Figure B-3. and Figure B-4. Voltage, current and power differences are very small, but significant differences in the currents were found for powers lower than 1 kW, due to the prevalence of reactive power exchanged with the grid. Background reactive current absorbed by the inverters leads high harmonic distortion (with consequent very high THD). As example, in Figure B-5. and Figure B-6. measurements by the oscilloscope are shown.

In order to further reduce differences between predefined power set-points sent by the control system to prosumers and actual magnitude of the power, we decided to introduce in the control system a software module, to pass from open chain control to feedback control with PID power regulator, in Python environment. In Figure B-7. the block diagram of the application is shown. The new set point to send to the prosumers is obtained by the sum of the set point and the output of the PID control. "C" block is the transduction module to allow a power measurement directly in W and VAR.

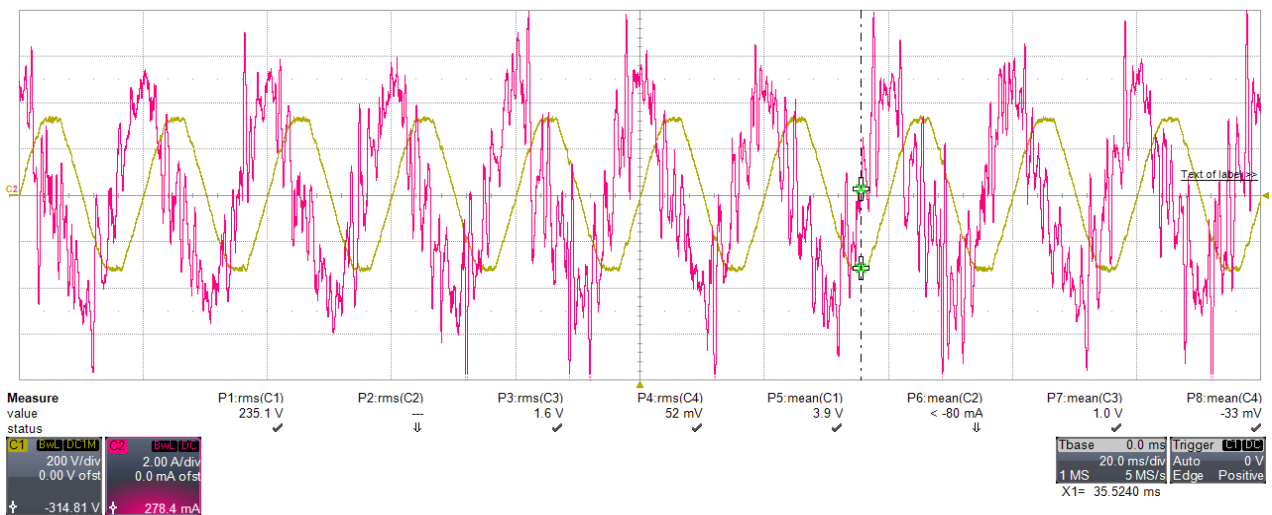


Figure B-5. Voltage (green) and current (red) trends; power set: $P=0$ W, $Q=700$ VAR.

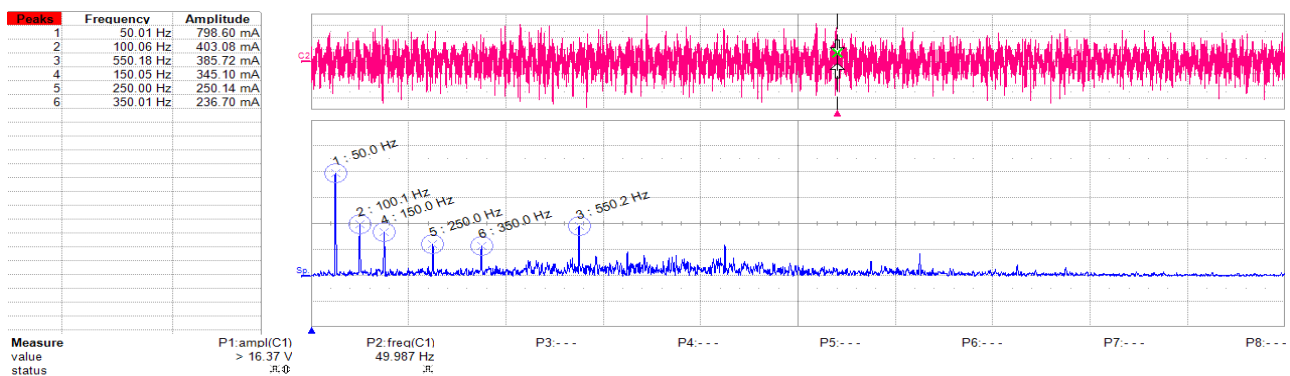


Figure B-6. Harmonic analysis; power set: $P=0$ W, $Q=0$ VAR.

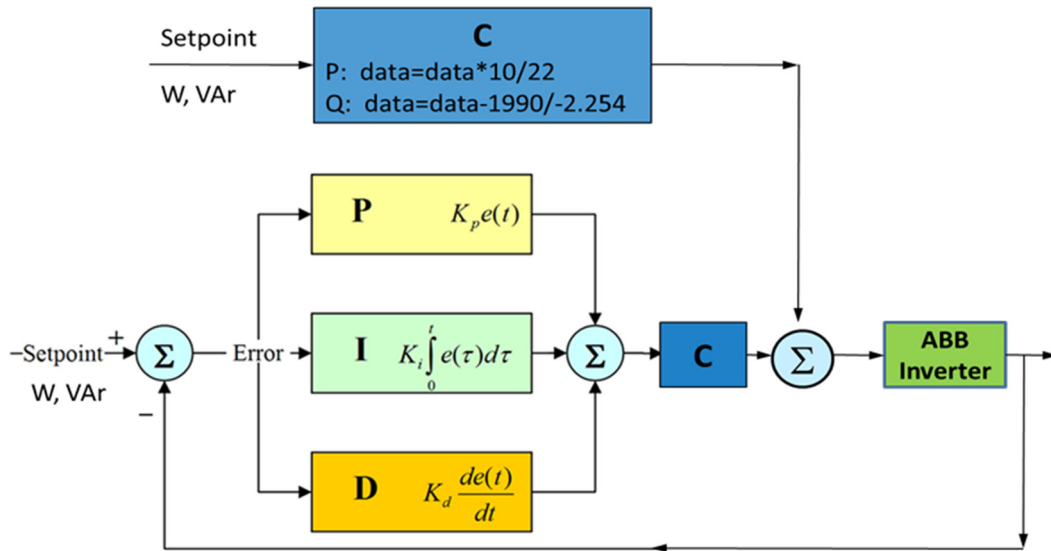


Figure B-7. P and Q feedback control. PID set parameters: $k_p=0.5$, $k_i=0.3$, $k_d=0.2$ and $dt=1$ S.

After preliminary checks and tuning of the MG with feedback control, several tests on the entire network are performed. With the introduction of PID regulation the average of the differences is reduced less than 3% for P and less than 4% for Q. A comparison between set values and measured values of reactive power is represented e.g. in Figure B-8..

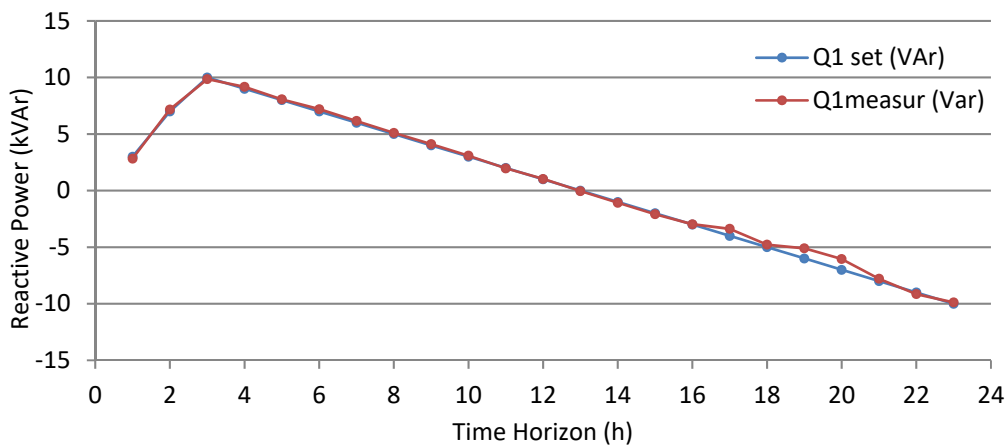


Figure B-8. Reactive power Q, set and measured values. Prosumer 1, feeder “D”, with PID control.

B.3. GridLab Laboratory

Some photos of the GridLab laboratory are shown below (Figure B-9., Figure B-10. and Figure B-11.).



Figure B-9. GridLab laboratory general overview.



Figure B-10. GridLab laboratory: drives and local control panels.

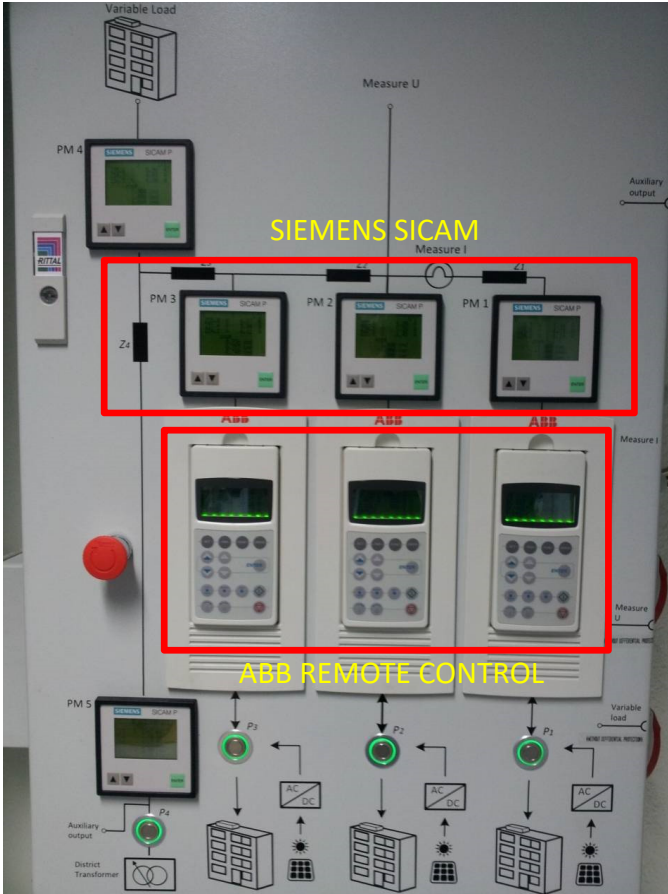


Figure B-11. GridLab laboratory: local control panel details.

Appendix C : Optimization Tools and Algorithms

C.1. AIMMS and the mathematical programming

The development of the models has been carried out by using the AIMMS (Advanced Interactive Multidimensional Modelling System) optimization environment, which is a well-known environment used in industry and universities for the solution of optimization and planning problems. It consists of an algebraic modelling language, an integrated development environment, and establishes a link with various solvers (CPLEX, Gurobi, MOSEK, CBC, and other ones). It can be easily expanded to incorporate other advanced commercial solvers. The AIMMS modeling language offers a sequence of advanced modeling concepts not found in other languages, as well as a complete graphical user interface for both Developers and End Users.

AIMMS supports a wide range of types of mathematical optimization problems: linear programming, quadratic programming, nonlinear programming, mixed-integer programming, mixed-integer nonlinear programming, global optimization, complementarity problems (MPECs), stochastic programming, robust optimization, constraint programming and it can take into account the uncertainties.

The models implemented are a MILP and MIQP. For their solution CPLEX MIP-MIQP solver has been used.

The following mathematical elements can be used to formulate a model:

- mathematical concepts such as sets, parameters, variables, constraints, etc.; variables are unknown quantities to be determined and can be either scalar or indexed, and their values can be restricted in several ways;
- operators such as unary operators (+, -, NOT), comparison operators (equal to, not equal to, etc.), algebraic operators (addition, subtraction, multiplication, etc.), logical operators (AND, OR, etc.), differential operators and integral operators;
- data: which links a model to a real-world situation.

From a practical point of view, after inserting sets, parameters, variables and constraints, the procedures for running the program must be written. All procedures and instructions to be executed are invoked in order of execution in the "*Main execution*", where the *solver* should be set. At least one procedure ("*Main Initialization*") is required to initialize all the parameters of the model, typically by reading one or more external files. For the output of the program, procedures can be set for the direct graphical display of the results or for writing external files that may be readable and able to be processed by Matlab or other programs.

More information about the environment are reported in the AIMMS manuals: language reference (LR), language reference stochastic programming (LRSP), function references (FR), optimization modeling (OM) and user's guide (UG).

C.2. Algorithms

The following tables show a schematic of the algorithms, the initial parameters and the network configuration parameters.

Table C-1- Execution procedure for P - Q convergence (dispatchable resources) described in Chapter 2

Algorithm
<p>1. Main Initialization: read parameters</p> <p style="padding-left: 20px;">Iteration = 1</p> $V_{re} = V_{re}^{nom}, V_{im} = V_{im}^{nom} \quad \forall phase, \forall bus$ <p>2. Solve Minimize OF (2.8)</p> <p>3. until $\Delta P_v^{max} , \Delta Q_v^{max} > \Delta P_v, \Delta Q_v \quad \forall phase, \forall bus$</p> $V_{re}^v = V_{re}^{v-1}, V_{im}^v = V_{im}^{v-1} \quad \forall phase, \forall bus$ $P_v = P_{v-1}, Q_v = Q_v \quad \forall phase, \forall bus$ <p style="padding-left: 20px;">Compute</p> $ \Delta P_v^{max} = \max(P_v - P_{v-1}) \quad \forall P \quad \forall phase, \forall bus$ $ \Delta Q_v^{max} = \max(Q_v - Q_v) \quad \forall Q \quad \forall phase, \forall bus$ $k_v = k_v + iteration \cdot k_v$ <p style="padding-left: 20px;">repeat Solve Minimize OF_iter (2.7), (2.9)</p> <p style="padding-left: 20px;">return the optimal solution</p> <p style="padding-left: 20px;">Iteration = Iteration + 1</p> <p>4. Write Results</p>

TABLE C-2 - SET AND PARAMETERS UPLOADED IN "MAIN INITIALIZATION" (CHAPTER 2).

Set, Parameter	Symbol - Value	Set, Parameter	Symbol - value
Time horizon set	$T = \{1...24\}$	Loads power rate	9 kVA
Step time	$dT = 1 \text{ h}$	Non-dispatchable DG power rate	10 kVA
Network branch set	$B = \{1...16\}$	Dispatchable DG power rate	12 kVA
Branch impedance	Table B-1	Batteries Capacity	8 kW / 8 kWh
Prosumer set	$k = \{1...12\}$	Network configuration	Table C-3
Voltage rate	$V_n = 230 \text{ V}$	Branch impedance configuration	Table B-1
Voltage first limit	$+3\%V_n \quad -6\%V_n$	Parameter	Price
Voltage second limit	$+10\%V_n \quad -15\%V_n$	Active energy imported	0.1 (€/kWh)
Min $\cos\phi$ at slack bus	0.8	Active energy exported	0.05 (€/kWh)
Battery efficiency factor	$\eta_{ch} = \eta_{dis} = 0.90$	Active energy by dispatchable DG and by batteries	0.08 (€/kWh)
Tolerance to end program	$\Delta P_v^{\max}, \Delta Q_v^{\max} = 10 \text{ W}$	Reactive energy by dispatchable DG and by batteries	0.08 (€/kWh)
Branch current limit	$I_{max} = 200 \text{ A}$	Voltage violation (second limit)	1 (€/V)
Initial k_v	0.1	Voltage violation (first limit)	0.1 (€/V)

TABLE C-3 - CONFIGURATION NETWORK (FIGURE. 2.1). TYPE 1: OH LINE - TYPE 2: UG BURIED LINE (CHAPTER 2).

Bus i	Bus j	Length (km)	Branch Type	I_{max} (A)
PCC	A5	0.01	type1	200
A5	A4	0.5	type1	200
A4	A3	0.5	type1	200
A3	A2	0.5	type1	200
A2	A1	0.5	type1	200
PCC	B5	0.01	type2	200
B5	B4	0.5	type2	200
B4	B3	0.5	type2	200
B3	B2	0.5	type2	200
B2	B1	0.5	type2	200
PCC	C5	0.01	type1	200
C5	C4	0.5	type1	200
C4	C3	0.5	type1	200
C3	C2	0.5	type1	200
C2	C1	0.5	type1	200
PCC	D5	0.01	type1	200
D5	D4	0.5	type1	200
D4	D3	0.5	type1	200
D3	D2	0.5	type1	200
D2	D1	0.5	type1	200

TABLE C-4- LINE PARAMETERS (FIGURE. 2.1). TYPE 1: OH OVERHEAD LINE - TYPE 2: UG BURIED LINE (CHAPTER 2).

$\Gamma_b(ph, ph, 'type1')$					$x_b(ph, ph, 'type1')$				
	A	B	C	N		A	B	C	N
A	0.300	0	0	0	A	0.2828	0	0	0
B	0	0.300	0	0	B	0	0.2828	0	0
C	0	0	0.300	0	C	0	0	0.2828	0
N	0	0	0	0.300	N	0	0	0	0.2828

$\Gamma_b(ph, ph, 'type2')$					$x_b(ph, ph, 'type2')$				
	A	B	C	N		A	B	C	N
A	0.300	0	0	0	A	0.0816	0	0	0
B	0	0.300	0	0	B	0	0.0816	0	0
C	0	0	0.300	0	C	0	0	0.0816	0
N	0	0	0	0.300	N	0	0	0	0.0816

TABLE C-5- EXECUTION PROCEDURE, CENTRALIZED AND DISTRIBUTED MODEL'S ALGORITHMS DESCRIBED IN CHAPTER 3.

Algorithm 1 – Centralized Model	Algorithm 2 – Distributed Model
<p><i>Stage 1: ideal network</i></p> <ol style="list-style-type: none"> 1. Main Initialization: read parameters 2. Solve MinCosts_OF (3.1) 3. Compute: <ul style="list-style-type: none"> Branches Power Flow, Branch Losses, Losses allocation for each power transaction Equations (3.13) -(3.20) 4. Write Results 	<p><i>Stage 1: ideal network</i></p> <ol style="list-style-type: none"> 1. Main Initialization: read parameters Iteration = 1 Price $\lambda(k,t) = \text{Utility grid price}(t)/2$ and $m = 10^{-5}$ 2. until $\text{Primal Residual}(k,t) > \epsilon \quad \forall \text{ prosumer } k, \forall t$ <ul style="list-style-type: none"> Compute primal residual(k,t) (3.34), dual residual(k,t) (3.37) Update ρ (3.36) Price $\lambda(k,t) = \text{Price } \lambda(k,t) + 2m \cdot \rho \cdot \text{Primal Residual}(k,t)$ (3.35) if (sum Primal Residual) < 1 kW (100 W) (3.38) <ul style="list-style-type: none"> $m = 10^{-4}$ (10^{-3}) endif repeat Solve MinCosts_OF $\forall \text{ prosumer } k, \forall t$ (3.29) return the optimal solution Iteration = Iteration + 1 3. Compute: <ul style="list-style-type: none"> Branches Power Flow, Branch Losses, (3.13)- (3.20) Losses allocation for each power transaction (3.22)- (3.24) Efficiency for each transaction, (3.39)- (3.41) 4. Write Results
<p><i>Stage 2: with network power losses</i></p> <ol style="list-style-type: none"> 1. Replace power balance constraints (considering the losses) (3.21) Read new constraints: <ul style="list-style-type: none"> - to avoid new energy transactions (3.25) - losses calculation (3.22)- (3.24) 2. Losses linearization procedure(3.26).(3.28) 3. Solve MinCosts_OF_losses (3.1) 4. Write Results 	<p><i>Stage 2: with network power losses</i></p> <ol style="list-style-type: none"> 1. Replace power balance constraints (with losses) (3.42) New constraints (3.32)- (3.33) New constraints to avoid new energy transactions (3.25) iteration = 1 Price $\lambda(k,t) = \text{Utility grid price}(t)/2$ and $m = 10^{-5}$ 2. until $\text{Primal Residual}(k,t) > \epsilon \quad \forall \text{ prosumer } k, \forall t$ <ul style="list-style-type: none"> Compute primal residual(k,t) (3.34), dual residual(k,t) (3.37) Update ρ (3.36) Price $\lambda(k,t) = \text{Price } \lambda(k,t) + 2m \cdot \rho \cdot \text{Primal Residual}(k,t)$ (3.35) if (sum Primal Residual) < 1 kW (100 W) (3.38) <ul style="list-style-type: none"> $m = 10^{-4}$ (10^{-3}) endif repeat Solve MinCosts_OF_Losses $\forall \text{ prosumer } k, \forall t$ (3.29) return the optimal solution Iteration = Iteration + 1 3. Write Results

TABLE C-9 – NETWORK CONFIGURATION MATRIX (FIGURE. 3.1 - FEEDER 1, BRANCH 3), PROSUMERS EXCHANGE (CHAPTER 3).

$A_{b,kj}$	Prosumer 1	Prosumer 2	Prosumer 3	Prosumer 4	Prosumer 5	Prosumer 6	Prosumer 7	Prosumer 8	Prosumer 9	Prosumer 10
Branch 3	-----	-----	-----	-----	-----	-----	-----	-----	-----	-----
prosumer1	0	0	-1	-1	-1	0	0	0	0	0
prosumer2	0	0	-1	-1	-1	0	0	0	0	0
prosumer3	1	1	0	0	0	1	1	1	1	1
prosumer4	1	1	0	0	0	1	1	1	1	1
prosumer5	1	1	0	0	0	1	1	1	1	1
prosumer6	0	0	-1	-1	-1	0	0	0	0	0
prosumer7	0	0	-1	-1	-1	0	0	0	0	0
prosumer8	0	0	-1	-1	-1	0	0	0	0	0
prosumer9	0	0	-1	-1	-1	0	0	0	0	0
prosumer10	0	0	-1	-1	-1	0	0	0	0	0

TABLE C-10 – NETWORK CONFIGURATION MATRIX (FIGURE. 3.1 - FEEDER 2, BRANCH 7), PROSUMERS EXCHANGE (CHAPTER 3).

$A_{b,kj}$	Prosumer 1	Prosumer 2	Prosumer 3	Prosumer 4	Prosumer 5	Prosumer 6	Prosumer 7	Prosumer 8	Prosumer 9	Prosumer 10
Branch 7	-----	-----	-----	-----	-----	-----	-----	-----	-----	-----
prosumer1	0	0	0	0	0	0	-1	-1	-1	-1
prosumer2	0	0	0	0	0	0	-1	-1	-1	-1
prosumer3	0	0	0	0	0	0	-1	-1	-1	-1
prosumer4	0	0	0	0	0	0	-1	-1	-1	-1
prosumer5	0	0	0	0	0	0	-1	-1	-1	-1
prosumer6	0	0	0	0	0	0	-1	-1	-1	-1
prosumer7	1	1	1	1	1	1	0	0	0	0
prosumer8	1	1	1	1	1	1	0	0	0	0
prosumer9	1	1	1	1	1	1	0	0	0	0
prosumer10	1	1	1	1	1	1	0	0	0	0

TABLE C-11 - EXECUTION PROCEDURE, STOCHASTIC OPTIMIZATION (CHAPTER 4).

Algorithm
<p>1. Main Initialization: read forecast and parameters</p> <p>2. Scenarios generation (Load and PV) procedure:</p> $\begin{cases} z_{\omega,t} = x_{\omega,t} + y_t \\ x_{\omega,t} = \phi \cdot x_{\omega,t-1} + \varepsilon_{\omega,t} \end{cases} \quad (4.23) \quad \text{St. deviation} = \sqrt{1 - \phi^2}$ <p>3. Solve procedure for simply battery model</p> <p>3.1 Solve deterministic model Minimize OF (4.1)</p> <p>3.2 Construction scenario tree k-means procedure:</p> <ol style="list-style-type: none"> 1. stage 1: all scenarios equiprobable 2. stage 2: merging scenarios in Clusters (3 or 4) based on Euclidian distance (4.24), (4.25): $d(\xi_{\omega,t}, \bar{\xi}_t^k) = \sum_{t \in T_s} \ \xi_{\omega,t} - \bar{\xi}_t^k\ _2 \quad \forall k = 1 \dots K$ <p>Intraday decision: comparison actual value with scenario tree and more similar scenario are choose for the next 6 hours.</p> <ol style="list-style-type: none"> 3. stage 3-4-5: repeat procedure for each stage independently of the previous. <p>Intraday decision: comparison actual value with scenario tree and more similar scenario are choose for the next 6 hours.</p> <p>3.3 Solve stochastic model Minimize Stoch_OF (4.22)</p> <p>3.4 Solve Monte Carlo method Minimize Stoch_OF (4.22)</p> <p>3.5 Solutions comparison and write Results</p> <p>4. Repeat procedure for kinetic battery model (KiBaM)</p> <p>4.1 Solutions comparison and write Results</p>

TABLE C-12 - SET AND PARAMETERS UPLOADED IN “MAIN INITIALIZATION”, STOCHASTIC OPTIMIZATION (CHAPTER 4).

Set, Parameter	Symbol - Value	Set, Parameter	Symbol - value
Time horizon set	$T = \{1 \dots 96\}$	Batteries Storage Capacity	$E_{max} = 315/630 \text{ kWh}$
Step time	$\Delta T = 0.25 \text{ h}$	Rated values of the battery converter	$P_b^r = 630 \text{ kW}$
Voltage rate	$V_n = 230 \text{ V}$	Battery rate constant	$k = 9.51 \text{ 1/h}$
Power demand forecast	$P_{load}(t,k) \text{ --> profiles}$	Battery capacity ratio	$c = 0.61$
Power PV generation forecast	$P_{pv}(t,k) \text{ --> profiles}$	Battery max. charge rate	$a = 2 \text{ A/Ah}$
Active energy imported price (23.00-7.00) - (7.00 - 23.00)	$p^{imp} = 0.131-0.172 \text{ (€/kWh)}$	State of charge min	$SoC_{min} = 0.1$
		State of charge max	$SoC_{max} = 1$
Active energy exported price	$p^{exp} = 0.5 p^{imp}$	Battery converter efficiency factor (charge, discharge)	$\eta_c = 0.95$ $\eta_d = 0.97$
Max. DSO power exchange	$P_{grid}^r = 6 \text{ MW}$	Battery efficiency factor (KiBaM)	$\eta_b = 0.90$
Confidence Interval PV - Load	$c.i. = 0.2 - 0.2$		

References

- Adinolfi, F., Conte, F., D'Agostino, F., Massucco, S., Saviozzi, M. & Silvestro, F. (2017). Mixed-integer algorithm for optimal dispatch of integrated PV-storage systems. *Conference Proceedings - 2017 17th IEEE International Conference on Environment and Electrical Engineering and 2017 1st IEEE Industrial and Commercial Power Systems Europe, IEEEIC / I and CPS Europe 2017*.
- Ahmad Khan, A., Naeem, M., Iqbal, M., Qaisar, S. & Anpalagan, A. (2016). A compendium of optimization objectives, constraints, tools and algorithms for energy management in microgrids. *Renewable and Sustainable Energy Reviews*. 58. p.pp. 1664–1683.
- Bahramirad, S. & Daneshi, H. (2012). Optimal sizing of smart grid storage management system in a microgrid. In: *2012 IEEE PES Innovative Smart Grid Technologies, ISGT 2012*. 2012.
- Barsali, S., Giglioli, R., Lutzemberger, G. & Poli, D. (2016). Optimal storage operation in EV charging stations delivering grid services. *IEEEIC 2016 - International Conference on Environment and Electrical Engineering*. p.pp. 0–5.
- Bennett, C.J., Stewart, R.A. & Lu, J.W. (2015). Development of a three-phase battery energy storage scheduling and operation system for low voltage distribution networks. *Applied Energy*. 146. p.pp. 122–134.
- Bordin, C., Oghenetejiri, H., Crossland, A., Lascurain, I., Dent, C.J. & Vigo, D. (2017). A linear programming approach for battery degradation analysis and optimization in offgrid power systems with solar energy integration. *Renewable Energy*. 101. p.pp. 417–430.
- Borghetti, A. (2012). A mixed-integer linear programming approach for the computation of the minimum-losses radial configuration of electrical distribution networks. *IEEE Transactions on Power Systems*. 27 (3). p.pp. 1264–1273.
- Borghetti, A. (2013). Using mixed integer programming for the volt/var optimization in distribution feeders. *Electric Power Systems Research*. 98. p.pp. 39–50.
- Borghetti, A., Napolitano, F. & Nucci, C.A. (2015). Volt/var optimization of unbalanced distribution feeders via mixed integer linear programming. *International Journal of Electrical Power & Energy Systems*. 72. p.pp. 40–47.
- Boyd, S., Parikh, N., Chu, E., Peleato, B. & Eckstein, J. (2011). *Distributed Optimization and Statistical Learning via the Alternating Direction Method of Multipliers*. Now Foundations and Trends.
- Caldon, R., Coppo, M. & Turri, R. (2014). Distributed voltage control strategy for LV networks with inverter-interfaced generators. *Electric Power Systems Research*. 107. p.pp. 85–92.
- Ceraolo, M., Lutzemberger, G. & Poli, D. (2016). Aging evaluation of high power lithium cells subjected to micro-cycles. *Journal of Energy Storage*. 6. p.pp. 116–124.

- Conejo, A.J., Arroyo, J.M., Alguacil, N. & Guijarro, A.L. (2002). Transmission Loss Allocation: A Comparison of Different Practical Algorithms. *IEEE Power Engineering Review*. 22 (5). p.p. 66.
- Conte, F., Massucco, S., Saviozzi, M. & Silvestro, F. (2017). A Stochastic Optimization Method for Planning and Real-Time Control of Integrated PV-Storage Systems: Design and Experimental Validation. *IEEE Transactions on Sustainable Energy*. 3029 (LV). p.pp. 1–10.
- Dabbagh, S.R., Mohammad Kazem, S.-E.-E. & Borghetti, A. (2016). Optimal operation of vehicle-to-grid and grid-to-vehicle systems integrated with renewables. *IEEE 19th Power Systems Computation Conference, PSCC 2016*. p.pp. 1–7.
- Daniil, N., Drury, D. & Mellor, P.H. (2015). Performance comparison of diffusion, circuit-based and kinetic battery models. *2015 IEEE Energy Conversion Congress and Exposition, ECCE 2015*. p.pp. 1382–1389.
- Escudero, L.F., Garín, A., Merino, M. & Pérez, G. (2007). The value of the stochastic solution in multistage problems. *Top*. 15 (1). p.pp. 48–64.
- European Commission (2017). *Study on “Residential Prosumers in the European Energy Union”*. (May).
- Fiorini, L., Pagani, G.A., Pelacchi, P., Poli, D. & Aiello, M. (2017). Sizing and Siting of Large-Scale Batteries in Transmission Grids to Optimize the Use of Renewables. *IEEE Journal on Emerging and Selected Topics in Circuits and Systems*. 7 (2). p.pp. 285–294.
- Foggo, B. & Yu, N. (2017). Improved Battery Storage Valuation Through Degradation Reduction. *IEEE Transactions on Smart Grid*. 3053 (c). p.pp. 1–1.
- Graditi, G., Ippolito, M.G., Telaretti, E. & Zizzo, G. (2016). Technical and economical assessment of distributed electrochemical storages for load shifting applications: An Italian case study. *Renewable and Sustainable Energy Reviews*. 57. p.pp. 515–523.
- Hossain, E., Kabalci, E., Bayindir, R. & Perez, R. (2014). Microgrid testbeds around the world: State of art. *Energy Conversion and Management*. 86. p.pp. 132–153.
- Ippolito, M.G., Di Silvestre, M.L., Riva Sanseverino, E., Zizzo, G. & Graditi, G. (2014). Multi-objective optimized management of electrical energy storage systems in an islanded network with renewable energy sources under different design scenarios. *Energy*. 64. p.pp. 648–662.
- IRENA (2015). *Battery Storage for Renewables : Market Status and Technology Outlook*.
- IRENA (2017). *Electricity storage and renewables: Costs and markets to 2030*.
- Jogunola, O., Ikpehai, A., Anoh, K., Adebisi, B., Hammoudeh, M., Son, S.-Y. & Harris, G. (2017). State-Of-The-Art and Prospects for Peer-To-Peer Transaction-Based Energy System. *Energies*. 10 (12). p.p. 2106.
- Katiraei, F. , Irvani, R., Hatziargyriou N., and Dimeas, A. (2008). IEEE may/june 2008. *IEEE Power and Energy Magazine*. p.pp. 54–65.
- Kobayashi, T. (2014). Power electronics technology in smart grid projects -Applications and experiences-. *2014 International Power Electronics Conference, IPEC-Hiroshima - ECCE Asia 2014*. p.pp. 1868–1873.

- Lazaroiu, G.C., Dumbrava, V., Balaban, G., Longo, M. & Zaninelli, D. (2016). Stochastic optimization of microgrids with renewable and storage energy systems. *EEEIC 2016 - International Conference on Environment and Electrical Engineering*.
- van Leeuwen, R., de Wit, J.B. & Smit, G.J.M. (2017). Energy scheduling model to optimize transition routes towards 100% renewable urban districts. *International Journal of Sustainable Energy Planning and Management*. 13. p.pp. 19–46.
- Lilla, S. (2015). *Auxiliary photovoltaic plant for generating energy*. p.p. Patent WO2015173742A1.
- Lilla, S., Borghetti, A., Napolitano, F., Tossani, F., Pavanello, D., Gabioud, D., Maret, Y. & Nucci, C.A. (2017). Mixed integer programming model for the operation of an experimental low-voltage network. *2017 IEEE Manchester PowerTech*.
- Liu, M., McLoone, S., Studli, S., Middleton, R., Shorten, R. & Braslavs, J. (2013). On-off based charging strategies for EVs connected to a Low Voltage distribution network. In: *Asia-Pacific Power and Energy Engineering Conference, APPEEC*. 2013.
- Liu, Y., Li, Y., Gooi, H.B., Ye, J., Xin, H., Jiang, X. & Pan, J. (2018). Distributed robust energy management of a multi-microgrid system in the real-time energy market. *IEEE Transactions on Sustainable Energy*. 3029 (vol. in print). p.pp. 1–11.
- Ma, W.J., Wang, J., Gupta, V. & Chen, C. (2018). Distributed energy management for networked microgrids using online ADMM with regret. *IEEE Transactions on Smart Grid*. 9 (2). p.pp. 847–856.
- Manwell, J.F. & McGowan, J.G. (1993). Lead acid battery storage model for hybrid energy systems. *Solar Energy*. 50 (5). p.pp. 399–405.
- Mengelkamp, E., Gärttner, J., Rock, K., Kessler, S., Orsini, L. & Weinhardt, C. (2018). Designing microgrid energy markets: A case study: The Brooklyn Microgrid. *Applied Energy*. 210. p.pp. 870–880.
- Minah Lee, Jihyun Hong, Jeffrey Lopez, Yongming Sun, Dawei Feng, Kipil Lim, William C. Chueh, Michael F. Toney, Y.C. & Z.B. (2017). 'High-performance sodium–organic battery by realizing four-sodium storage in disodium rhodizonate'. *Nature Energy*. p.p. 10.1038/s41560-017-0014-y.
- Musing, E., Mather, J. & Moura, S. (2017). Blockchains for decentralized optimization of energy resources in microgrid networks. *2017 IEEE Conference on Control Technology and Applications (CCTA)*. p.pp. 2164–2171.
- Olivares, D.E., Mehrizi-Sani, A., Etemadi, A.H., Cañizares, C.A., Iravani, R., Kazerani, M., Hajimiragha, A.H., Gomis-Bellmunt, O., Saeedifard, M., Palma-Behnke, R., Jiménez-Estévez, G.A. & Hatziargyriou, N.D. (2014). Trends in microgrid control. *IEEE Transactions on Smart Grid*. 5 (4). p.pp. 1905–1919.
- Orozco, C., Borghetti, A., Lilla, S., Pulazza, G. & Tossani, F. (2018). Comparison Between Multistage Stochastic Optimization Programming and Monte Carlo Simulations for the Operation of Local Energy Systems. *2018 IEEE International Conference on Environment and Electrical Engineering and 2018 IEEE Industrial and Commercial Power Systems Europe (EEEIC / I&CPS Europe), 12 -15 June, 2018*. 737434 (737434). p.pp. 1–6.

- Osório, G.J., Lujano-Rojas, J.M., Matias, J.C.O. & Catalão, J.P.S. (2015). A new scenario generation-based method to solve the unit commitment problem with high penetration of renewable energies. *International Journal of Electrical Power and Energy Systems*. 64. p.pp. 1063–1072.
- Pandzic, H. & Bobanac, V. (2018). An Accurate Charging Model of Battery Energy Storage. *IEEE Transactions on Power Systems*. 8950 (c). p.pp. 1–10.
- Parisio, A., Rikos, E. & Glielmo, L. (2014). A model predictive control approach to microgrid operation optimization. *IEEE Transactions on Control Systems Technology*. 22 (5). p.pp. 1813–1827.
- Pranevicius, H. & Štutienė, K. (2007). Scenario tree generation by clustering the simulated data paths. In: I. Zelinka, Z. Oplatková, & A. Orsoni (eds.). *Proceedings 21st European Conference on Modelling and Simulation ECMS 2007*. 2007, pp. 203–208.
- Ratnam, E.L., Weller, S.R. & Kellett, C.M. (2015a). An optimization-based approach to scheduling residential battery storage with solar PV: Assessing customer benefit. *Renewable Energy*. 75. p.pp. 123–134.
- Ratnam, E.L., Weller, S.R. & Kellett, C.M. (2015b). Scheduling residential battery storage with solar PV: Assessing the benefits of net metering. *Applied Energy*. 155. p.pp. 881–891.
- Reddy, S.S., Sandeep, V. & Jung, C.-M. (2017). Review of stochastic optimization methods for smart grid. *Frontiers in Energy*. 11 (2). p.pp. 197–209.
- Sakti, A., Gallagher, K.G., Sepulveda, N., Uckun, C., Vergara, C., de Sisternes, F.J., Dees, D.W. & Botterud, A. (2017). Enhanced representations of lithium-ion batteries in power systems models and their effect on the valuation of energy arbitrage applications. *Journal of Power Sources*. 342. p.pp. 279–291.
- Van Der Schoor, T. & Scholtens, B. (2015). Power to the people: Local community initiatives and the transition to sustainable energy. *Renewable and Sustainable Energy Reviews*. 43. p.pp. 666–675.
- Schweickardt, G., Alvarez, J.M.G. & Casanova, C. (2016). Metaheuristics approaches to solve combinatorial optimization problems in distribution power systems. An application to Phase Balancing in low voltage three-phase networks. *International Journal of Electrical Power and Energy Systems*. 76.
- Soavi, F., Arbizzani, C. & Ruggeri, I. (2017). *Semi-solid flow Li/O₂ battery*. p.p. Patent n. WO2017021840A1.
- Sossan, F., Namor, E., Cherkaoui, R. & Paolone, M. (2016). Achieving the Dispatchability of Distribution Feeders Through Prosumers Data Driven Forecasting and Model Predictive Control of Electrochemical Storage. *IEEE Transactions on Sustainable Energy*. 7 (4). p.pp. 1762–1777.
- Std. D-A-CH-CZ working group (2007). *Technical rules for the Assessment of Network Disturbances*.
- Std. EN 50438:2013/IS1 (2015). *Requirements for micro-generating plants to be connected in parallel with public low-voltage distribution networks 2015-05*.
- Teotia, F. & Bhakar, R. (2016). Local energy markets: Concept, design and operation. *2016 National Power Systems Conference (NPSC)*. p.pp. 1–6.
- Wang, Y., Mao, S. & Nelms, R.M. (2015). *Online Algorithms for Optimal Energy Distribution in Microgrids*. Springer (ed.).

- Williams, H.P. (1990). *Model building in mathematical programming*. 3rd ed. John Wiley & Sons, Chichester.
- Yuan, Y., Li, Q. & Wang, W. (2011). Optimal operation strategy of energy storage unit in wind power integration based on stochastic programming. *IET Renewable Power Generation*. 5 (2). p.p. 194.
- Zhao, B., Wang, X., Lin, D., Calvin, M., Morgan, J., Qin, R. & Wang, C. (2018a). Energy management of multiple-microgrids based on a system of systems architecture. *IEEE Transactions on Power Systems*. 33 (6). p.pp. 6410–6421.
- Zhao, Y., Yu, J., Ban, M., Liu, Y. & Li, Z. (2018b). Privacy-preserving economic dispatch for an active distribution network with multiple networked microgrids. *IEEE Access*. 6. p.pp. 38802–38819.
- Zheng, Y., Song, Y., Hill, D.J. & Zhang, Y. (2018). Multiagent system based microgrid energy management via asynchronous consensus ADMM. *IEEE Transactions on Energy Conversion*. 33 (2). p.pp. 886–888.
- Zhu, J., Chow, M.-Y. & Zhang, F. (1998). Phase balancing using mixed-integer programming. *IEEE Transactions on Power Systems*. 13 (4).
- Zizzo, G., Riva Sanseverino, E., Ippolito, M.G., Di Silvestre, M.L. & Gallo, P. (2018). A technical approach to P2P energy transactions in microgrids. *IEEE Transactions on Industrial Informatics*. 3203 (in print).

Acronyms

AC	Alternating Current
ADMM	Alternating Direction Method of Multipliers
AIMMS	Advanced Interactive Multidimensional Modelling System
AVR	Automatic Voltage Regulator
BES	Battery Energy System
DG	Distributed Generation
DSO	Distribution System Operator
EMS	Energy Management System
ESS	Energy Storage System
EV	Electric Vehicle
EVPI	Expected Value of Perfect Information
KiBaM	Kinetic Battery Model
LEC	Local Energy Community
LV	Low Voltage
MG	Micro-Grid
MILP	Mixed Integer Linear Programming
MIQP	Mixed Integer Quadratic Programming
MPC	Model Predictive Control
MV	Medium Voltage
OF	Objective Function
OH	Overhead Lines
PCC	Point of Common Coupling
PV	Photovoltaic
RES	Renewable Energy Sources
RTU	Remote Terminal Unit
SCADA	Supervisory Control and Data Acquisition
SG	Smart Grid
SoC	State of Charge
SoE	State of Energy
SP	Stochastic Programming
UG	Buried Line (Underground)
V2G	Vehicle to grid
VSS	Value of Stochastic Solution
WS	Wait and See